LIÈGE université
GIGA institute

PhD thesis

WOBBLE tRNA MODIFICATION SHAPES TUMOR ASSOCIATED NEUTROPHILS IN METASTATIC BREAST CANCER

PhD candidate: LOBNA OUESLATI

JUNE 22, 2026

THESIS SUBMITTED FOR THE DEGREE OF DOCTOR OF PHILOSOPHY

PROMOTERS : PR. PIERRE CLOSE & PR. CHRISTOPHE DESMET

To my parents, my backbone and the ones who gave me all the confidence and the power to be where I am now.

To the people who left us too soon, I hope that I made you proud.

Acknowledgements

I would like first to thank Pierre, for giving me his trust for this project, for being the mentor and the listener during rough moments. A source of inspiration for his dedication to research and for all the energy he gives to our lab. Thank you for the time and advice you gave during my PhD journey.

I also would like to thank Christophe for all the advice and the mentoring. I'm always impressed by his bioinformatics and immunology knowledge. You were the inspiration that pushed me to jump into the bioinformatics world.

I will be also thankful to Arnaud for his inputs during our lab meetings but also for guiding us through metabolomics and through experiments planification.

I also thank Francesca for all her input and advice for the whole project. You have been there since the first day of the ELP3 project in neutrophils.

Two magnificent people from Thomas Marichal lab crossed our path during this project: Domien and Margot thank you for your guidance during the start of this journey and for being our suppliers during our trials.

Jospeh, Glenn, Julien, Laurence from Christophe Desmet lab, thank you for all the help and the shared protocols.

I would like to thank also a lot of people from the lab, Raphael, Christian, Marine and Najla for all the help and suggestions.

The people who helped with science but not only and the people who made Liège feel like home: Debora, Miguel, Sharon, Rossana, Chunyan and my labmate Nil.

The power of the GIGA institute is our platforms members, so thank you to Raafat, Céline, Arnaud, Alice, Latifa, Manon and Alexandre for all the help with all our experiments and for all the time you spent with us.

I also would like to thank our proteomics platform adjusting the techniques to our requirements and for making us able to produce such a unique dataset for Tumor infiltrating neutrophils.

Thank you to our collaborators from the Luxembourg Institute of Health: Nathalie Legrave and Johannes Meiser for guiding us in the mystery world of metabolism. A special thanks goes to Oleg Chen for all his effort during the metabolomics and the seahorse and for spending long lab days with me.

Contents

Abstract 1

Introduction 3

I-Neutrophils 3

1. Presentation 3
2. Granulopoiesis 3
3. Neutrophil Life-span 4
4. Neutrophils recruitment 5
5. Neutrophils functions 7
   - 5.1. ROS release 7
   - 5.2. Degranulation 7
   - 5.3. Phagocytosis / Trogocytosis 8
   - 5.4. NETosis 8
6. Tumor Associated Neutrophils: Phenotype switching 9
7. Neutrophils metabolism 13

II- Breast cancer 17

1. Generalities 17
2. Molecular subtypes 18
3. Tumor immunity 19

III- mRNA translation and tRNA modifying enzymes 24

1. Generalities: mRNA translation 24
2. mRNA translation actors 25
   - 2.1. Ribosomes 25
   - 2.2. Transfer RNA 25
3. Translation process 26

4. Translation control 29
4.1. 5’ cap translation control 29
4.2. Poly-A tail translation control 30
4.3. eIF2 regulation 30
5. mRNA translation and cell plasticity 31
6. tRNA remodeling for translation control 33
7. U34 tRNA modifying enzymes in development, cancer and immune cells 38
Aim of the project 41
Materials and Methods 44
1.Mouse models 44
2. Neutrophil isolation from the bone marrow 44
3. RNAseq analysis 45
4. Single cell RNA-seq 45
5. Gene set enrichment analysis 47
6. Neutrophil viability assay 47
7. Neutrophil migration 47
8. Reactive oxygen species (ROS) measurement 47
9. Mitochondrial ROS assay 48
10. Intra-tumoral and blood neutrophils extraction 48
11. In Vivo Protein Synthesis Assay (OP-Puro Incorporation) 49
12. Hematoxylin and Eosin (H&E) Staining and Immunohistochemistry 49
13. Low-throughput proteomics 49
14. Proteomics data analysis 50
15. Secretome analysis 51
16. ELISA assay 51

17. Seahorse 51
18. Metabolomics 52
19. Data integration 53
Results 56
I. Tumor Infiltrating Neutrophil reprogramming in breast cancer ... 56
II. U34 tRNA modifying enzymes in neutrophils..... 59
1. Mouse model 59
2. Steady-state neutrophil homeostasis is preserved following ELP3 depletion..... 61
2.1. Neutrophil expansion 61
2.2. Neutrophils viability 61
2.3. ROS production in neutrophils..... 61
2.4. Neutrophils migration 62
III. Loss of ELP3 in tumor associated neutrophils in PyMT breast cancer model..... 64
1. Tumor initiation..... 64
2. Tumor progression 64
3. Tumor metastasis..... 65
4. Loss of ELP3 in neutrophils induces a delay of stage and impairs vasculature in primary tumors 66
5. ELP3 depletion in neutrophils does not alter the tumor immune landscape 68
5.1. Single cell RNA seq..... 68
6. Neutrophils undergo proteomic remodeling when infiltrating the tumor 78
7. Proteomic remodeling of ELP3 depleted neutrophils upon tumor infiltration 80

8. Proteomic analysis reveals mitochondrial pathway alterations in ELP3-deficient TINs 81

9. ELP3 depletion alters mitochondrial structure and metabolism in neutrophils..... 84

10. Investigation of ELP3 depleted neutrophils roles in vasculature regulation 89

11. Comparison of transcriptomic and proteomic profiles in ELP3 deficient tumor infiltrating neutrophils 90

Conclusions..... 94

Discussion 98

Supplementary materials 111

Bibliography.....106

List of figures

Figure 1: Neutrophil differentiation stages (adapted from Jaillon et al., 2020) 4
Figure 2: Neutrophil recruitment cascade (adapted from Kolaczkowska et Kubes, 2013). 6
Figure 3: Representation of different neutrophil's functions in the TME 13
Figure 4: Neutrophils metabolism 14
Figure 5: Krebs cycle 15
Figure 6:Glycolysis and oxidative and non-oxidative branches of pentose phosphate pathway 16
Figure 7: Mammary gland structure 18
Figure 8:Breast cancer subtypes 19
Figure 9: The central dogma of molecular biology: DNA to RNA to Proteins 24
Figure 10: Process of mRNA translation 28
Figure 11:tRNA structure 33
Figure 12: tRNA modifications (adapted from Suzuki, 2021) 34
Figure 13: Cytosolic tRNA modification impacting tumoral processes (Añazco-Guenkova et al., 2024) 35
Figure 14: Control of decoding by tRNA wobble modifications (adapted from Suzuki., 2021) 37
Figure 15: U34 modification enzymatic cascade (Rapino et al., 2021) 39
Figure 16: Tumor infiltrating neutrophils exhibit increased expression of tRNA modifying enzymes 58
Figure 17: Validation of ELP3 exon 2 deletion in sorted neutrophils and monocytes/macrophages 60
Figure 18: ELP3 is dispensable for steady state neutrophils integrity 63
Figure 19: ELP3 loss in neutrophils and its impact on tumor growth and metastasis 66
Figure 20: PyMT ELP3^{NEU} tumors show a lower grade of tumor progression and angiogenesis impairment 67
Figure 21: Single cell analysis at 10 Weeks Old 68
Figure 22: Single cell RNA seq analysis of the tumor microenvironment in PyMT ELP3^{CTR} and PyMT ELP3^{NEU} mice at 10WO 72
Figure 23: Single-cell transcriptomic analysis of T cell functional states in the tumor microenvironment 73
Figure 24: Subclustering analysis of the tumor-infiltrating T-cell compartment 75

Figure 25:Immune phenotyping at 10 weeks old PyMT ELP3 ^{CTR} and PyMT ELP3^{NEU}..... 77
Figure 26: Flow cytometry gating strategy for T cells..... 78
Figure 27: Proteomics analysis and protein synthesis flow cytometry analysis on PyMT Tumor infiltrating neutrophils and blood neutrophils at 12 weeks. 80
Figure 28:Proteomic remodeling of tumor infiltrating neutrophils in PyMT ELP3^{NEU} mice 81
Figure 29:Proteomics analysis and protein synthesis comparison between PyMT ELP3^{CTR} and PyMT ELP3^{NEU} tumor associated neutrophils at 12 weeks 83
Figure 30: Modulated proteins in Tumor infiltrating neutrophils PyMT ELP3^{CTR} and PyMT ELP3^{NEU} 84
Figure 31: Electron microscopy and Metabolomics analysis on Bone marrow ELP3^{CTR} and ELP3^{NEU} mice neutrophils at 12 weeks..... 86
Figure 32: OCR and ECAR measurement of 12 weeks ELP3^{CTR} and ELP3^{NEU} steady state bone marrow neutrophils..... 87
Figure 33: Mitochondrial ROS and membrane potential in Tumor associated neutrophils..... 88
Figure 34: Functional assessment of pro-angiogenic activities in neutrophils 90
Figure 35:Integrated transcriptomics and proteomics analysis in PyMT ELP3^{CTR} and PyMT ELP3^{NEU} TINs 92

Abbreviations

ADAT: Adenosine Deaminase Acting on tRNA

ALKBH8: AlkB Homolog 8

APC: Antigen Presenting Cell

ATP: Adenosine Triphosphate

BC: Breast Cancer

BV8: Prokineticin 2

CAF: Cancer Associated Fibroblast

CCL: Chemokine (C-C motif) Ligand

CCR: Chemokine Receptor

CMP: Common Myeloid Progenitor

CoA: Coenzyme A

CREB: cAMP Response Element-Binding Protein

CSF3R: Colony Stimulating Factor 3 Receptor

CTU1/2: Cytosolic Thiouridylase 1/2

DAMP: Damage-Associated Molecular Pattern

DNA: Deoxyribonucleic Acid

EIF / eIF: Eukaryotic Initiation Factor

ELP3: Elongator Complex Protein 3

EMT: Epithelial–Mesenchymal Transition

ER: Estrogen Receptor

ERK: Extracellular Signal-Regulated Kinase

FAO: Fatty Acid Oxidation

FMLP: Formyl-Methionyl-Leucyl-Phenylalanine

G-CSF: Granulocyte Colony-Stimulating Factor

GFI1: Growth Factor Independent 1

GLUT: Glucose Transporter

GMP: Granulocyte Monocyte Progenitor

HIF-1α: Hypoxia-Inducible Factor 1 Alpha

HER2: Human Epidermal Growth Factor Receptor 2

HLA: Human Leukocyte Antigen

HSPC: Hematopoietic Stem and Progenitor Cell

ICAM: Intercellular Adhesion Molecule

IFN: Interferon

IL: Interleukin

KAT: Lysine Acetyltransferase

LFA-1: Lymphocyte Function-Associated Antigen 1

MAC-1: Macrophage-1 Antigen

MDSC: Myeloid-Derived Suppressor Cell

MHC: Major Histocompatibility Complex

MMP: Matrix Metalloproteinase

mRNA: Messenger RNA

NAMPT: Nicotinamide Phosphoribosyltransferase

NET: Neutrophil Extracellular Trap

OCR: Oxygen Consumption Rate

OXPHOS: Oxidative Phosphorylation

PAMP: Pathogen-Associated Molecular Pattern

PD-1 / PD-L1: Programmed Death Receptor / Ligand

PI3K: Phosphoinositide 3-Kinase

PPP: Pentose Phosphate Pathway

PR: Progesterone Receptor

PRR: Pattern Recognition Receptor

RBP: RNA-Binding Protein

RNA: Ribonucleic Acid

RNA-seq: RNA sequencing

ROS: Reactive Oxygen Species

Sc-RNA seq: single-cell RNA sequencing

SG / GG / SV: Specific / Gelatinase Granules / Secretory Vesicles

STAT3: Signal Transducer and Activator of Transcription 3

TAM: Tumor-Associated Macrophage

TAN: Tumor-Associated Neutrophil

TCA: Tricarboxylic Acid Cycle

TIL: Tumor Infiltrating Lymphocyte

TIME: Tumor Immune Microenvironment

TIN: Tumor Infiltrating Neutrophils

TLR: Toll-Like Receptor

TNBC: Triple Negative Breast Cancer

TNF-α: Tumor Necrosis Factor Alpha

tRNA: Transfer RNA

U34-TM: Uridine 34 tRNA Modification

VEGF: Vascular Endothelial Growth Factor

Abstract

During cancer progression, neutrophils undergo extensive reprogramming, giving rise to tumor-associated neutrophils (TANs) with marked functional plasticity. Depending on the context, TANs can exert pro-tumoral activities by promoting tumor growth, angiogenesis and metastasis, or anti-tumoral functions by supporting anti-tumoral immune response and limiting tumor progression. In breast cancer, early neutrophilia correlates with poor clinical outcomes, and neutrophils have been shown to contribute to metastatic dissemination through the formation of a pre-metastatic niche, particularly in the lungs.

Recent evidence indicates that neutrophil plasticity extends beyond transcriptional changes and involves metabolic and translational adaptations.

Notably, our laboratory previously demonstrated that wobble uridine tRNA modifications (U34-TM) regulate context-specific translation programs driving tumorigenesis and metastasis. In line with this, we observed a coordinated upregulation of U34-TM enzymes, including ELP3, ALKBH8, and CTU1/2, in tumor-infiltrating neutrophils compared to circulating neutrophils.

Here, we hypothesized that U34-TM-mediated translational control contributes to neutrophil reprogramming during breast cancer progression. To address this, we generated a neutrophil-specific loss-of-function model by crossing *ELP3*$^{lox/lox}$ mice with the Mrp8-CRE strain and investigated tumor development in the MMTV-PyMT model. Strikingly, neutrophil-specific deletion of ELP3 resulted in a significant delay in primary tumor progression and a strong reduction in lung metastasis.

Mechanistically, proteomic and ultrastructural analyses revealed that tumor-infiltrating neutrophils undergo metabolic reprogramming characterized by increased mitochondrial activity, whereas ELP3 deficiency led to alterations in mitochondrial content and metabolic pathways specifically within the tumor microenvironment. These findings suggest that U34-dependent tRNA modifications contribute to the metabolic adaptation of neutrophils in cancer.

Collectively, our results identify U34-TM as a key regulator of neutrophil plasticity and reveal a previously unrecognized role for translational control in shaping neutrophil function during tumor progression. This work highlights tRNA-mediated regulation as a potential vulnerability that could be targeted to modulate neutrophil activity and limit metastatic breast cancer.

INTRODUCTION

Introduction

I-Neutrophils

1. Presentation

Neutrophils are the most abundant leukocytes in human peripheral blood and constitute a major component of the innate immune system. Approximately 100–200 billion neutrophils are generated daily in the bone marrow. To maintain homeostasis, neutrophils undergo tightly regulated production and rapid turnover, with inactive cells undergoing various forms of programmed cell death (Geering and Simon, 2011).
They represent the first line of cellular defense against invading pathogens. Under microscopic observation following hematoxylin and eosin staining, neutrophils appear neutral in color due to the limited affinity of their granules and cytoplasm for these dyes (Zhang *et al.*, 2024).

2. Granulopoiesis

Granulopoiesis in the bone marrow leads to the formation of neutrophils. Hematopoietic stem and progenitor cells (HSPCs) undergo several maturation steps that give rise to common myeloid progenitors (CMPs), which subsequently generate granulocyte monocyte progenitors (GMPs). This differentiation process is tightly regulated by the expression of transcription factors, including CCAAT/enhancer-binding protein-ε (C/EBPε) and growth factor independent 1 (GFI1) (Lawrence, Corriden and Nizet, 2018).

Granulocyte colony-stimulating factor (G-CSF) is the key cytokine driving granulopoiesis in mammalian species. Under its influence, GMPs progressively differentiate through several developmental stages: myeloblasts give rise to promyelocytes, which develop into myelocytes, metamyelocytes, band neutrophils, and finally mature neutrophils (Panopoulos and Watowich, 2008; Jaillon *et al.*, 2020).

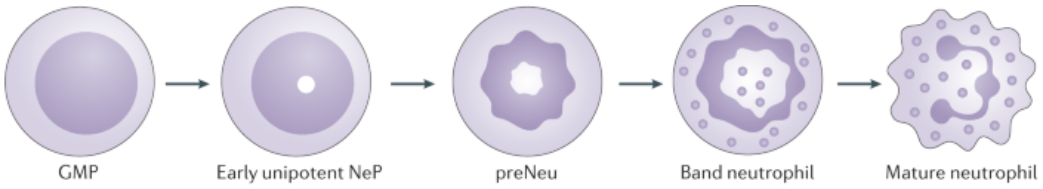

Human				
Lin$^-$, CD34$^+$, CD38$^+$, CD45RA$^+$, CXCR4$^+$, CXCR2$^-$	Lin$^-$, CD117$^+$, CD66b$^+$, CD38$^+$, CXCR4$^+$, CXCR2$^-$	Lin$^-$, CD117$^-$, Siglec8$^-$, CD15$^+$, CD34$^-$, CD66b$^+$, CD49d$^+$, CD101$^-$ CXCR4$^+$, CXCR2$^-$	CD66b$^+$, CD15$^+$, CD33^{mid}, CD49d$^-$, CD101^{mid}, CD10$^-$, CD16^{low}, CXCR4$^+$, CXCR2$^+$	CD66b$^+$, CD15$^+$, CD33^{mid}, CD49d$^-$, CD101^{mid}, CD10$^+$, CD16$^+$, CXCR4$^-$, CXCR2$^+$
Mouse				
Lin$^-$, IL-7R$^-$, CD117$^+$, Sca1$^-$, CD34$^+$, CD16/32$^+$, CXCR4$^+$, CXCR2$^-$	Lin$^-$, CD117$^+$, Sca1$^-$, Siglec-F$^-$, FcεRIα$^-$, CD16/32$^+$, Ly6B$^+$, CD11a$^+$, CD162^{low}, CD48^{low}, Ly6C^{low}, CD115$^-$, Ly6G$^-$, CXCR4$^+$, CXCR2$^-$	Lin$^-$, CD117^{mid}, CD115$^-$, Siglec-F$^-$, Gr1$^+$, CD11b$^+$, Ly6G^{low}, CXCR4^{high}, CXCR2$^-$	CD117$^-$, CD115$^-$, Siglec-F$^-$, Gr1$^+$, CD11b$^+$, CD101$^-$, Ly6G$^{low/mid}$, CXCR4$^+$, CXCR2$^-$	CD115$^-$, CD11b$^+$, Siglec-F$^-$, Gr1$^+$, CD101$^+$, Ly6G^{high}, CXCR4$^-$, CXCR2$^+$

Figure 1: Neutrophil differentiation stages (adapted from Jaillon et al., 2020) Neutrophils are generated in the bone marrow through granulopoiesis, a stepwise differentiation process from hematopoietic stem cells (HSCs) to common myeloid progenitors (CMPs) and granulocyte–monocyte progenitors (GMPs). Lineage commitment is regulated by transcription factors, with C/EBPε and GFI1 promoting neutrophil differentiation, while C/EBPα and PU.1 favor monocyte development. Under the control of cytokines such as G-CSF and GM-CSF, GMPs differentiate into myeloblasts, which sequentially mature into promyelocytes, myelocytes, metamyelocytes, band cells, and ultimately mature neutrophils. Recent advances using single-cell RNA sequencing and mass cytometry have refined this hierarchy by identifying intermediate populations, including early neutrophil progenitors (NePs) and pre-neutrophils (preNeus). At steady state, neutrophil production is highly dynamic, and in pathological conditions such as cancer, both immature and mature neutrophil populations can accumulate and acquire distinct functional properties.

3. Neutrophil Life-span

Circulating neutrophils have a relatively short half-life under homeostatic conditions, estimated to range from 4 to 18 hours. However, their lifespan can be extended in certain contexts, including within the tumor microenvironment. On the other hand, a study published in Blood in 2010 using in vivo labeling reported that neutrophils can reach a lifespan of up to 5.4 days under homeostatic conditions (Pillay *et al.*, 2010).

As the “body’s first responders,” neutrophils are highly effective at pathogen elimination. Their short lifespan is thought to limit tissue damage caused by the release of proteolytic enzymes and reactive oxygen species (ROS) (Carlos Silvestre-Roig, Andres Hidalgo, and Oliver Soehnlein, 2016). While prolonged neutrophil survival can support the activation of adaptive immune responses, excessive persistence of these cells has also been associated with increased disease severity and poorer clinical outcomes, for example in asthma, acute

coronary syndrome, severe COVID 19 infection and chronic inflammatory conditions (Kolaczkowska and Kubes, 2013; Veenith *et al.*, 2022).

Neutrophils exhibit a high degree of plasticity, allowing them to rapidly adapt to changes in their microenvironment. During inflammation, their lifespan can be extended through inhibition of apoptosis mediated by cytokines, pathogen-associated molecular patterns (PAMPs), and damage-associated molecular patterns (DAMPs) present at sites of tissue injury (Carlos Silvestre-Roig, Andres Hidalgo, and Oliver Soehnlein, 2016) . In addition to changes in survival, neutrophils can modulate their functional phenotype in response to inflammatory, hypoxic, or nutrient-deprived environments (Silvestre-Roig, Hidalgo and Soehnlein, 2016).

4. Neutrophils recruitment

Neutrophils are generally recruited in tissues following activation of endothelial cells triggered either by pathogen recognition through pattern-recognition receptors (PRRs) or by inflammatory signals released from sentinel leukocytes in contact with pathogens. This process leads to the release of pathogen-associated molecular patterns (PAMPs), chemoattractant molecules and growth factors that promote neutrophil recruitment. These granulocytes are highly sensitive to such stimuli and migrate along chemoattractant gradients toward sites of inflammation. Chemotaxis is orchestrated by several mediators, including lipids, N-formylated peptides, complement components, anaphylatoxins, and chemokines (Williams *et al.*, 2011; Petri and Sanz, 2018; Metzemaekers, Gouwy and Proost, 2020).

Neutrophils follow the classical recruitment cascade consisting of sequential steps: tethering, rolling, adhesion, crawling, and transmigration (Kolaczkowska and Kubes, 2013). However, the involvement of integrins and selectins in this process varies depending on the organ and the type of injury. For example, neutrophil recruitment to the skin involves cutaneous lymphocyte-associated antigen (CLA), E-selectin, and P-selectin, whereas recruitment to the liver can occur in a selectin-independent manner. In the lung, neutrophil recruitment largely depends on chemokine signaling. In fact, inhibition of CXCR2 has been shown to reduce acute lung injury in mice (Margraf, Ley and Zarbock, 2019).

Upon endothelial activation, pre-stored P-selectin and newly synthesized E-selectin bind to their respective ligands on circulating neutrophils, initiating the tethering process. Neutrophils subsequently roll along the vascular endothelium under blood flow, which facilitates their activation by immobilized

chemokines. Rolling is mediated by transient adhesive interactions between P-selectin and PSGL-1 that are continuously formed and dissociated as the cell moves along the vessel wall.

L-selectin can also contribute to neutrophil adhesion to the endothelium and their subsequent migration outside the vasculature. ELR-CXC chemokines, which contain a glutamate–leucine–arginine (ELR) motif preceding the CXC sequence, play a major role in neutrophil activation and adhesion through CXCR2 signaling. Neutrophils express integrins such as LFA-1 and MAC-1 that mediate binding to endothelial surface molecules including ICAM-1 and ICAM-2. The expression and activation state of these integrins are regulated by chemoattractant molecules, which promote their delocalization to the cell surface and induce conformational changes that increase their affinity for endothelial ligands (Muller, 2011; Kolaczkowska and Kubes, 2013; Zhang *et al.*, 2024).

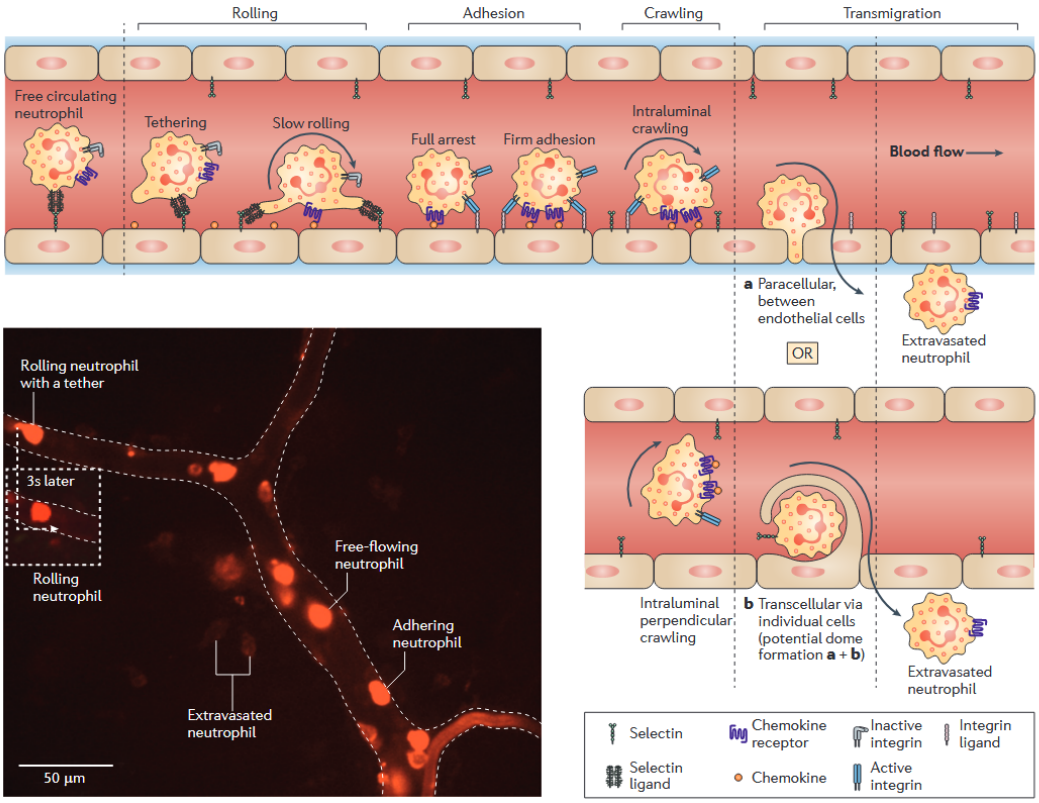

Figure 2: Neutrophil recruitment cascade (adapted from Kolaczkowska et Kubes, 2013) Neutrophil recruitment from the vasculature to tissues occurs through a multistep process involving rolling, adhesion, crawling, and transmigration. Rolling is primarily mediated by selectins, while firm adhesion, crawling, and transmigration depend on integrin interactions. Chemokines presented on the endothelial surface activate neutrophils, inducing integrin

conformational changes that enable stable adhesion and directional migration along the endothelium. Neutrophils can transmigrate either via a paracellular route (between endothelial cells) or a transcellular route (through endothelial cells). The intravital microscopy image illustrates neutrophils at different stages of this process, including circulating, rolling, adhering, and extravasated cells, following infection with Staphylococcus aureus.

5. Neutrophils functions

5.1. ROS release

Reactive oxygen species (ROS) production is a major effector function of the innate immune system and represents a powerful mechanism used by neutrophils to combat bacterial and fungal infections. Neutrophils generate ROS through the activity of the NADPH oxidase complex. These reactive molecules can be released extracellularly at sites of infection or intracellularly within the phagolysosome. In addition to their direct antimicrobial activity, ROS production also contributes to the amplification of antibacterial responses (Nguyen, Green and Mecsas, 2017; Belambri *et al.*, 2018; Veenith *et al.*, 2022).

5.2. Degranulation

During their development in the bone marrow, neutrophils progressively acquire their granule content, including azurophilic (primary) granules, specific (secondary) granules (SGs), gelatinase (tertiary) granules (GGs), and secretory vesicles (SVs) (Reiding *et al.*, 2021). Each granule type is characterized by its timing of formation and protein composition, which determine their specific functions. Azurophilic granules are the first to form during the promyelocyte stage and contain numerous antimicrobial proteins such as myeloperoxidase (MPO), lysozyme, and proteases. These primary granules are highly toxic, and studies have shown that they are typically the last to be released. Proteomic analyses have also revealed heterogeneity in their protein content, which may influence their ability to migrate to the cell membrane or fuse with phagosomes.

Secondary and tertiary granules share partially overlapping contents and functions. However, secondary granules are known to contain proteins such as lipocalin and lactoferrin but lack metalloproteinase 9 (MMP-9), which is present in tertiary granules. Tertiary granules express a subset of proteins and can be rapidly released upon activation by the chemoattractant formyl-Met-Leu-Phe (FMLP). Secretory vesicles are produced during the band and segmented stages through endocytosis. The release of proteins from SGs, GGs, and SVs primarily occurs at the plasma membrane and facilitates

neutrophil adhesion to activated endothelial cells. These granules therefore play an important role during the early steps of neutrophil trafficking to inflammation.

The degranulation process is regulated by activation of specific receptors that trigger signaling pathways targeting granule subsets. Despite the diversity of receptors and signaling mechanisms involved in granule release, these pathways can generally be grouped into two major signaling axes: Rac2 activation and intracellular calcium flux induction (Othman, Sekheri and Filep, 2022).

5.3. Phagocytosis / Trogocytosis

Neutrophils can engulf particles such as microbes, dead cells, and tissue debris through phagocytosis, a process accompanied by the fusion of intracellular granules with phagocytic vesicles. This process can occur through two distinct mechanisms. The first is the trigger mechanism, characterized by the formation of plasma membrane protrusions driven by actin polymerization in response to signals from the microenvironment. The second is the zipper mechanism, which is initiated when cell surface receptors bind to ligands on the target particle, leading to its progressive engulfment by the plasma membrane (Gierlikowska *et al.*, 2021).

In addition to phagocytosis, neutrophils can also perform trogocytosis, an antibody-dependent process involving the partial endocytosis of the plasma membrane of opsonized target cells. A study published in Cell Reports in 2018 demonstrated that neutrophils require CD18 integrin–mediated conjugate formation to perform trogocytosis. Using live-cell imaging, the authors showed that neutrophils can acquire fragments of the membrane from fluorescently labeled cancer cells (Matlung *et al.*, 2018).

5.4. NETosis

NETosis is a specialized form of cell death that leads to the formation of extracellular traps capable of capturing pathogens. Neutrophil extracellular traps (NETs) consist of a mixture of DNA and cellular components such as histones, granule proteins, and cytoplasmic proteins. The recognition of various signaling molecules can initiate this process which is followed by chromatin de-condensation.

The release of NETs contributes to the containment of infections by trapping pathogens and limiting their dissemination. However, excessive NET formation has also been associated with several pathological conditions. For

instance, impaired wound healing, particularly in diabetes, has been linked to excessive NET release, which can promote the activation of macrophages and the production of IL-1β, thereby amplifying local inflammation (Zhang *et al.*, 2024; Brambilla *et al.*, 2025).

It is also important to note that two distinct forms of NETosis have been described: suicidal NETosis and vital NETosis.

Suicidal NETosis is characterized by the release of web-like chromatin structures decorated with histones and neutrophil granule proteins, such as neutrophil elastase. This process is accompanied by chromatin decondensation, plasma membrane rupture, and ultimately neutrophil death. A variety of stimuli can induce suicidal NETosis, including phorbol 12-myristate 13-acetate (PMA), lipopolysaccharide (LPS), cytokines, and microbial products.

In contrast, vital NETosis occurs without neutrophil lysis and allows neutrophils to retain certain cellular functions after NET release. Upon stimulation through receptors such as Toll-like receptor 4 (TLR4), neutrophils can rapidly release mitochondrial or nuclear DNA into the extracellular space, generating NET-like structures while maintaining cell viability. Unlike suicidal NETosis, which generally occurs over several hours, vital NETosis is a rapid process that can take place within minutes (5–60 min) (Ravindran, Khan and Palaniyar, 2019; Buszka *et al.*, 2025).

Suicidal NETosis was initially considered to be strictly dependent on NADPH oxidase (NOX)-derived reactive oxygen species (ROS). However, subsequent studies demonstrated the existence of NOX-independent pathways involving calcium influx, mitochondrial ROS production, and peptidylarginine deiminase 4 (PAD4)-mediated chromatin decondensation. Similarly, vital NETosis can proceed through either NOX-dependent or NOX-independent mechanisms depending on the stimulus and the source of DNA released, highlighting the complexity and context-dependent regulation of NET formation (Ravindran, Khan and Palaniyar, 2019).

6. Tumor Associated Neutrophils: Phenotype switching

Neutrophils are a major component of the innate immune system and it has been shown that in multiple cancer types such as lung, colorectal, liver, bladder, pancreatic and breast, tumor cells produce G-CSF leading to neutrophilia that is often linked to a bad prognosis (Wculek and Malanchi,

2015; Moura *et al.*, 2025). During tumorigenesis, the installed chronic inflammation induced the premature egress of granulocytic progenitors into the blood stream, the tumor and extramedullary sites where the priming of pro-tumoral neutrophils occurs (Ioannis *et al.*, 2021; Ng *et al.*, 2024).

Analysis of neutrophil populations using an orthotopic pancreatic cancer model demonstrated that neutrophils undergo phenotypic reprogramming upon tumor infiltration. In this study (Ng *et al.*, 2024), integration of single-cell RNA sequencing datasets from healthy and tumor bearing mice revealed that neutrophil development in non-tumor tissues remains unchanged, following a conserved maturation trajectory. In contrast, immature and mature TANs formed a distinct cluster, clearly separated from both immature and mature neutrophils derived from bone marrow, spleen, and blood. This indicates that tumor infiltration induces a specific transcriptional program independent of developmental stage.

Chromatin accessibility analysis (ATAC-seq) further supported these findings, showing that TANs exhibit a unique epigenetic landscape enriched for genes associated with hypoxia, glycolysis, and angiogenesis.

Altogether, these results demonstrate that the tumor microenvironment reprograms neutrophils into a distinct functional state, irrespective of their maturation status.

It is important to note that neutrophils shouldn’t be considered as pro-tumoral cells or just classified into two different groups: Anti-tumorigenic neutrophils N1 and Pro-tumorigenic neutrophils N2. In fact, a Cell research paper published in 2024 showed that neutrophils across 17 types of cancer exhibited 10 different states. In this work, single cell RNA-sequencing analysis was performed on 225 samples collected from 143 patients and proved that neutrophil functions are broader than just anti and pro-tumoral. Moreover, tumor infiltration capacity of neutrophils varies according to the cancer type and stage and it has been shown that lung and kidney cancers had the highest neutrophil infiltration score. Hence, an antigen presenting cluster of neutrophils was detected across the different cancer types. This cluster was HLA-DR+CD74+ and showed a high enrichment in non-small cell lung cancer, bladder and ovarian cancer and a decreased enrichment in several other carcinomas. This cluster of neutrophils was generally linked to a better outcome (Wu *et al.*, 2024).

A study published in Blood 2017 (Vono *et al.*, 2017) demonstrates that the acquisition of MHC-II expression by neutrophils requires a combination of

signals, specifically the presence of cognate antigen together with antigen-specific $CD4^+$ T cells. In coculture systems using CMV pp65 (Cytomegalovirus antigen) or influenza HA antigens, neutrophils upregulated HLA-DR as well as co-stimulatory molecules such as CD40 and CD80 only when both antigen and antigen-specific memory T cells were present, whereas exposure to antigen or T cells alone was insufficient. In contrast, stimulation with TLR7/8 ligands induced a partial activation phenotype, characterized by increased expression of markers including CD80, CD83, CD11b, and CCR7, but failed to trigger HLA-DR expression. These findings indicate that inflammatory activation alone is not sufficient to confer antigen-presenting cell (APC)-like properties to neutrophils. Instead, MHC-II induction appears to be tightly regulated and dependent on interactions with antigen-specific T cells. Mechanistically, this process is likely mediated by T cell–derived signals, such as IFN-γ, which are known to promote MHC-II expression. Although cytokines like IFN-γ and GM-CSF can induce MHC-II in certain contexts, the study highlights that optimal induction in neutrophils requires antigen-specific cognate interactions with activated $CD4^+$ T cells.

It has also been demonstrated that IFN signaling promotes the polarization of anti-tumor neutrophils, characterized by elevated expression of TNF-α, CCL3, and ICAM-1, along with reduced arginase-1 activity. Moreover, IFN signaling inhibits pro-angiogenic factors production. These neutrophils exhibit cytotoxic effects against cancer cells (Andzinski *et al.*, 2016; Ozel *et al.*, 2022).

Conversely, a subset of TANs has been associated with poor prognosis. These neutrophils are $VEGFA^+$ and contribute to tumor angiogenesis. (Wu *et al.*, 2024) The role of neutrophils in angiogenesis was first described in 2006 by Nozawa et al. in a pancreatic cancer model, where they were identified as a major source of MMP-9 (Nozawa, Chiu and Hanahan, 2006a). In addition, these neutrophils, together with HIF-1α expressing neutrophils, were shown to be among the predominant infiltrating cells within tumors, promoting angiogenesis. Pro-angiogenic neutrophils secrete factors such as VEGF, BV8, MMP-9, and S100A8/S100A9, which stimulate endothelial cell proliferation and support angiogenesis (Coffelt, Wellenstein et de Visser, 2016; Ozel *et al.*, 2022). In vivo models of IFN-$\beta^{-/-}$ tumors have shown increased infiltration of pro-angiogenic neutrophils. The pro-angiogenic phenotype of these neutrophils can also be enhanced through activation of the nicotinamide phosphoribosyl transferase (NAMPT) signaling pathway, which acts downstream of CSF3R signaling triggered by the G-CSF receptor. Mechanistically, NAMPT promotes the tumorigenic activity of neutrophils via SIRT1 signaling, leading to increased production of pro-angiogenic factors.

Inhibition of NAMPT using the small molecule FK866 was shown to reduce this activity (Pylaeva *et al.*, 2019; Ozel *et al.*, 2022).

TANs also play an important role in tumor metastasis through the release of NETs. Beyond their well-established bactericidal functions, NETs can actively influence tumor progression and metastatic spread. In cancer, NET formation is triggered by tumor-derived signals, inflammatory cytokines, oxidative stress, and pro-angiogenic factors present within the tumor microenvironment and pre-metastatic niches.

NETs promote tumor cell proliferation and metastasis by trapping circulating tumor cells, enhancing their survival, and facilitating their adhesion and colonization at distant sites. In addition, proteases associated with NETs, such as elastase and matrix metalloproteinases (MMPs), contribute to extracellular matrix degradation and disruption of dormant cell niches. This can lead to the reactivation of dormant tumor cells and support metastatic outgrowth.

Furthermore, NETs contribute to immune evasion by physically shielding cancer cells, thereby limiting contact-dependent cytotoxicity mediated by $CD8^+$ T cells and natural killer (NK) cells. NETs have been detected in primary tumors, circulation, and metastatic lesions, and elevated NET levels are associated with advanced disease stages and increased metastatic burden across multiple cancer types (Brambilla *et al.*, 2025).

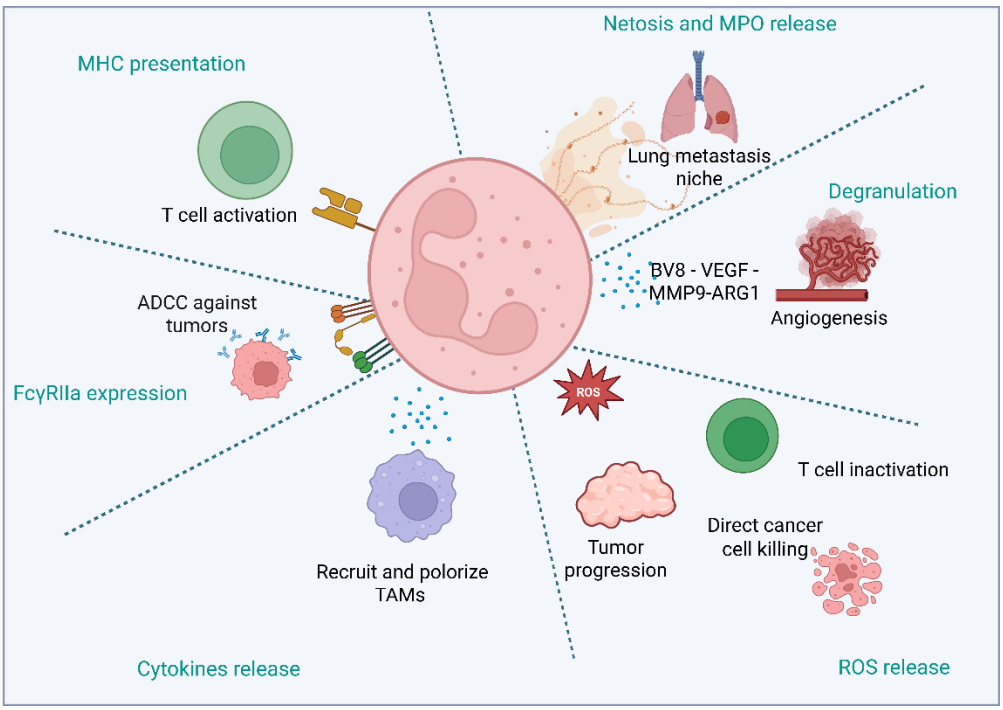

Figure 3: Representation of different neutrophil's functions in the TME (Figure created using Biorender): Tumor Associated Neutrophils can play anti-tumorigenic roles by activating T cells via antigen presentation, recruitment of other immune cells or playing a cytotoxic role against tumor cells. On the other hand, they can play pro-tumorigenic roles supporting cancer progression and metastasis by secreting pro-angiogenic factors, releasing NETs or inhibiting T cells

7. Neutrophils metabolism

From their resting state to activation, neutrophils modulate their metabolism to perform diverse functions while adapting to their environment. A study published in 2024 showed that primary human neutrophils use glycogen as a major nutrient source during their resting phase (Britt *et al.*, 2024). In this work, healthy volunteers received intravenous injections of labeled glucose tracer at a rate of 8g per hour, and ex vivo experiments conducted in the presence or absence of glucose confirmed these findings. In fact, when neutrophils were cultured, lactate production remained comparable between glucose-depleted and glucose-supplemented media. Glycogen stores in neutrophils were reduced by 60% after 4 hours of culture and by 95% after 12 hours in glucose-depleted conditions. Inhibition of glycogen phosphorylase further demonstrated that glycogen contributes to approximately 50% of the intermediates used in glycolysis. On the other hand, when stimulated using PMA, primary human neutrophils shifted toward using extracellular glucose,

reaching 80–90% labeled glycolytic intermediates compared with less than 50% under steady-state conditions. At the same time, neutrophils exhibited increased phosphorylation of glycogen phosphorylase, suggesting enhanced glycogen cycling in addition to the mobilization of intracellular glycogen stores [LO1.1] (Britt *et al.*, 2024).

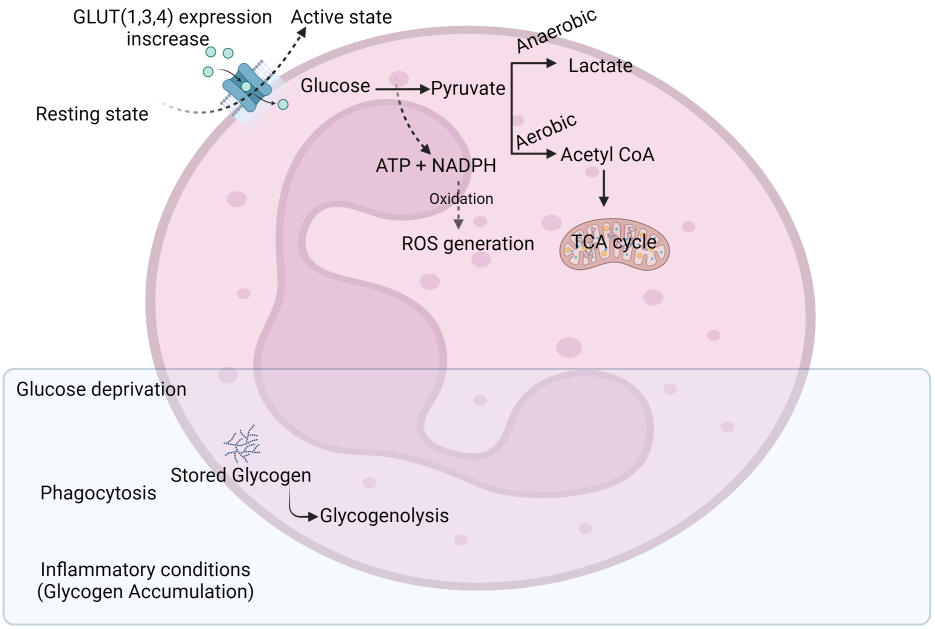

Figure 4: Neutrophils metabolism (Figure created by Biorender based on Jeon et al.*, 2020) Neutrophils primarily rely on glycolysis as their main source of energy. Upon activation, they increase glucose uptake through upregulation of glucose transporters (GLUT1, GLUT3, and GLUT4), supporting essential functions such as chemotaxis and effector responses. In addition, neutrophils store glycogen as an internal glucose reserve, which can be mobilized under conditions of glucose deprivation or hypoxia. Although mitochondria are present, they contribute minimally to ATP production and are thought to play regulatory roles rather than serving as the primary energy source. Under hypoxic conditions, neutrophils depend on anaerobic glycolysis, converting pyruvate to lactate, while glycogenolysis helps sustain their metabolic activity in nutrient-limited environments.*

At the molecular level, neutrophils express several glucose transporters (GLUTs), including GLUT1, GLUT3, and GLUT4, in the resting state, and their expression increases upon activation. Glucose, a major metabolic substrate for immune cells, is converted to pyruvate and subsequently to acetyl coenzyme A (CoA), which enters the tricarboxylic acid (TCA) cycle under normoxic conditions. In anaerobic conditions, however, neutrophils convert pyruvate into lactate instead of acetyl-CoA (Jeon *et al.*, 2020).

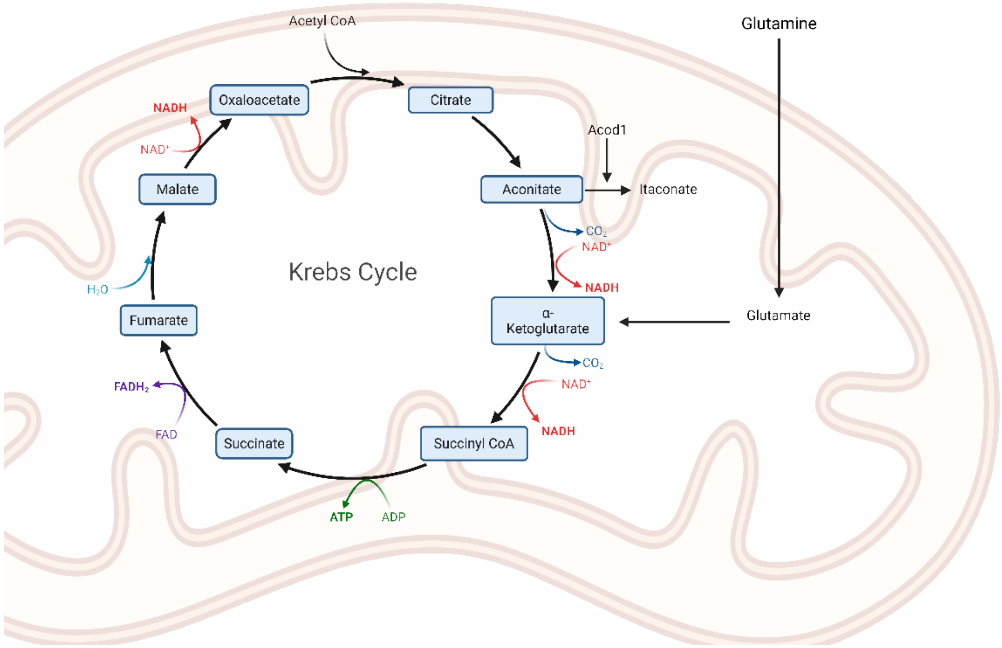

Figure 5: Krebs cycle (Figure created by Biorender Based on Martínez-Reyes et Chandel, 2020; Zhao et al.*, 2023). The tricarboxylic acid (TCA) cycle is fueled by multiple substrates, including glutamine, which enters mitochondria and is converted into glutamate and subsequently into α-ketoglutarate to feed the cycle. Through successive enzymatic reactions, the TCA cycle generates key reducing equivalents, notably NADH and $FADH_2$, which are used by the electron transport chain to drive oxidative phosphorylation and ATP production. In addition to ATP generation, this metabolic pathway also provides important intermediates that support cellular biosynthesis and metabolic flexibility.*

In parallel to glycolysis, the pentose phosphate pathway (PPP) oxidizes glucose to generate NADPH, ribose-5-phosphate, and pentoses, and has been described as a major driver of the neutrophil oxidative burst (Britt *et al.*, 2022; TeSlaa *et al.*, 2023).

ROS production is associated with an increase in NOX-dependent oxygen consumption and requires large amounts of NADPH, which are supplied by the oxidative branch of the PPP. To better understand the metabolic requirements of the oxidative burst, a study published in Nature Metabolism in 2022 compared the metabolic profiles of neutrophils stimulated with zymosan, TNF-α, PsA, or PMA with those treated with a NOX inhibitor. The results showed that oxidative burst was strongly coupled with the rewiring of the PPP rather than with glycolysis (Britt *et al.*, 2022).

Measurements of oxygen consumption rate (OCR) indicate that neutrophils display lower mitochondrial respiration compared with monocytes and other

immune cells. Nevertheless, mature neutrophils maintain mitochondrial membrane potential, and differences in mitochondrial abundance have been observed between immature and mature neutrophils. Immature neutrophils rely more strongly on oxidative phosphorylation (OXPHOS) and contain higher numbers of mitochondria. At this stage, fatty acid oxidation (FAO) also plays an important role, as immature neutrophils depend on lipophagy-mediated FAO for their differentiation (Jeon *et al.*, 2020).

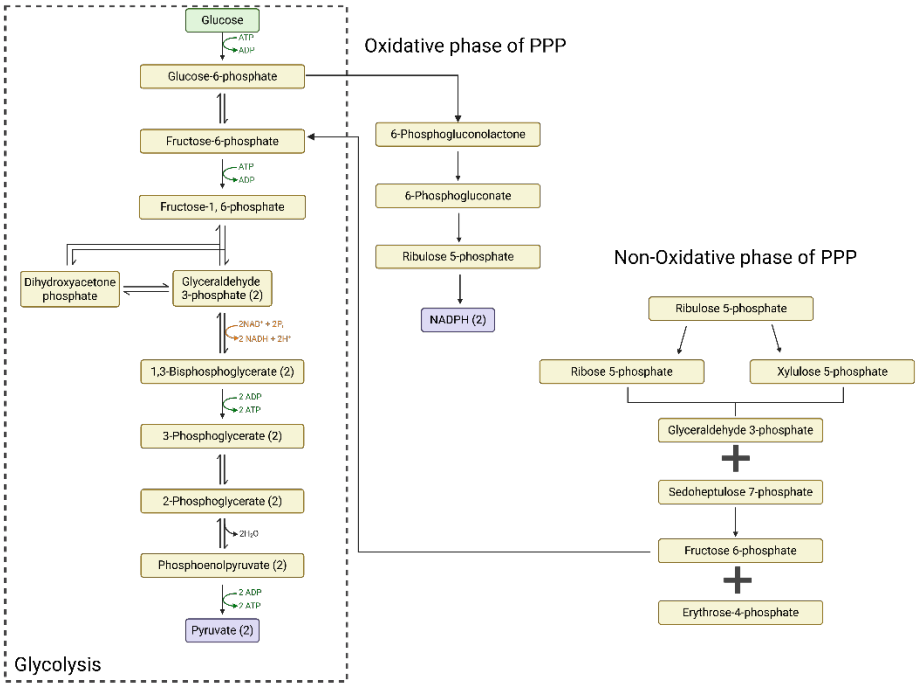

Figure 6:Glycolysis and oxidative and non-oxidative branches of pentose phosphate pathway (Figure created using Biorender based on: Britt. Et al., 2022, TeSlaa. Et al., 2023) In neutrophils, glycolysis represents the primary pathway for rapid ATP production, reflecting their limited reliance on mitochondrial respiration. Upon activation, glycolytic flux is partially redirected toward the pentose phosphate pathway (PPP) to support antimicrobial functions. The oxidative branch of the PPP converts glucose-6-phosphate into pentose phosphates while generating NADPH, a critical cofactor for NADPH oxidase–mediated reactive oxygen species (ROS) production during the oxidative burst. The non-oxidative branch recycles carbon intermediates, such as fructose-6-phosphate and glyceraldehyde-3-phosphate, back into glycolysis, enabling repeated cycling through the oxidative PPP and maximizing NADPH output. This metabolic rewiring, often referred to as the cyclic PPP, is essential for sustaining ROS production, pathogen killing, and other neutrophil effector functions, including NET formation.

Recent studies have highlighted the importance of lipid metabolism in neutrophil adaptation within the tumor microenvironment. Tumor infiltrating neutrophils have been shown to accumulate neutral lipid droplets, including triglycerides and cholesterol esters, in response to hypoxic conditions through

activation of HIF1α-dependent pathways. This lipid accumulation contributes to neutrophil functional reprogramming and has been associated with pro-tumoral activities, including metabolic interactions with cancer cells. These findings further support the concept that neutrophils exhibit a high degree of metabolic flexibility, enabling them to adapt to the nutrient-constrained tumor microenvironment (Gao *et al.*, 2026).

In the context of cancer, relatively few studies have characterized the metabolic adaptations of neutrophils. However, distinct neutrophil subsets appear to display specific metabolic signatures. Antigen-presenting neutrophils are enriched in amino acid metabolism pathways, whereas pro-angiogenic neutrophils exhibit activation of vitamin (i.e. Vitamin B1 (Thiamine), B2 (Riboflavin), B6 (Pantothenic acid)) and glycan metabolism. Further investigations using in vitro screening showed that leucine metabolism upregulated HLA-DR and costimulatory molecule expression and enhanced assembly of the MHC-II complex. Seahorse analysis demonstrated that leucine stimulation increased oxygen consumption rate (OCR), while transmission electron microscopy (TEM) revealed that leucine-treated neutrophils displayed elongated mitochondria and a higher number of membrane pseudopods (Wu *et al.*, 2024).

A study published in 2018 further demonstrated that splenic neutrophils isolated from 4T1 tumor-bearing mice exhibit enhanced mitochondrial fitness driven by c-Kit signaling. C-Kit was identified as a marker of immature neutrophils, confirmed by nuclear morphology showing myelocyte-like nuclei. Accordingly, c-Kit$^+$ neutrophils were more abundant in the bone marrow of steady-state mice and were also detected at higher levels in mammary tumors and in the circulation of tumor-bearing mice. In vitro analyses revealed that c-Kit$^+$ neutrophils displayed higher OCR rates and improved responses to mitochondrial inhibitors independently of glucose availability, suggesting that tumor-associated neutrophils engage mitochondrial metabolism to adapt to nutrient-limited environments (Rice *et al.*, 2018).

II- Breast cancer

1. Generalities

The World Health Organization (WHO) reported 2.3 million new breast cancer cases in 2022, leading to approximately 670,000 deaths. Epidemiological studies have also shown that breast cancer is a leading cause of cancer-

related death among women younger than 45 years. Despite advances in research and treatment, mortality associated with metastatic disease remains high, with a median survival of approximately 24 months. Breast cancer incidence is higher in developed countries and is expected to increase further in the coming decade. Although the mutational landscape of breast cancer remains complex, point mutations in TP53 and PIK3CA are detected in approximately 25% of cases (Anastasiadi *et al.*, 2017).

In parallel, a study conducted in North Carolina in 2009 identified a panel of 50 genes used to classify breast cancer. This work led to the development of the PAM50 (Prediction Analysis of Microarray 50) classifier, which is used to predict prognosis, relapse-free survival, and response to therapy (Parker *et al.*, 2009).

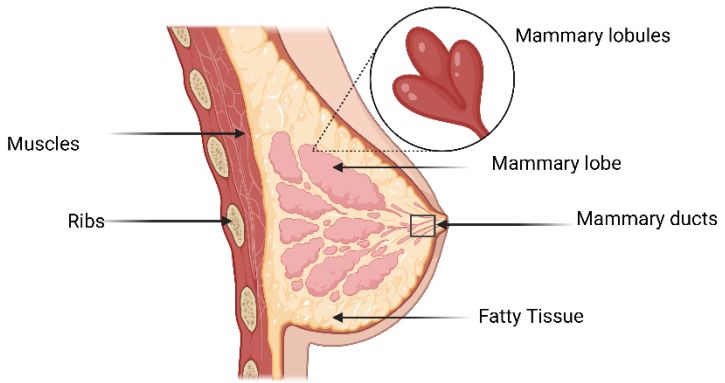

Figure 7: Mammary gland structure (Figure generated using Biorender)

2. Molecular subtypes

Breast cancer (BC) is a heterogeneous disease that can be classified into four major molecular subtypes based on molecular and histological characteristics. These classifications rely primarily on the expression of hormone receptors, including the estrogen receptor (ER), progesterone receptor (PR), and human epidermal growth factor receptor 2 (HER2).

Hormone receptor positive breast cancers include the Luminal A and Luminal B subtypes and account for approximately 60% of cases. HER2 enriched breast cancer represents 15–25% of cases, and HER2 status is an important determinant for therapeutic decisions. HER2 overexpression is considered an early event in breast cancer development and is associated with shorter disease-free survival.

The fourth subtype, triple negative breast cancer (TNBC), is characterized by the absence of ER, PR, and HER2 expression and is generally associated with a more aggressive clinical course. In addition, the proliferation marker Ki-67 is commonly used as a prognostic indicator to evaluate tumor aggressiveness and guide treatment strategies, as high Ki-67 expression correlates with poorer survival outcomes (Orrantia-Borunda *et al.*, 2022).

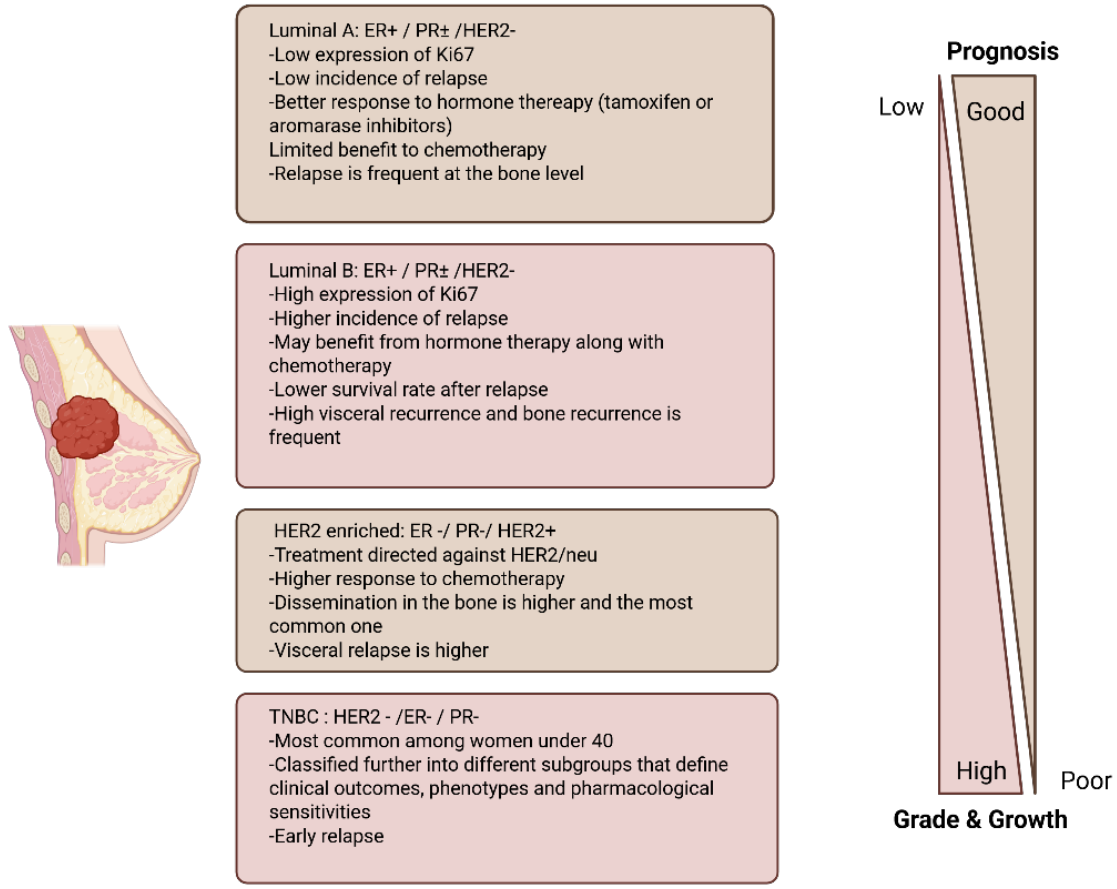

Figure 8:Breast cancer subtypes (Figure generated using Biorender)

3. Tumor immunity

Understanding the tumor microenvironment and the intrinsic characteristics of the tumor represents a critical step toward the development of effective therapies. The molecular heterogeneity of breast cancer (BC) influences tumor mutational burden (TMB), HLA expression, and tumor metabolism, ultimately leading to remodeling of the tumor immune microenvironment (TIME).

A study conducted on a large cohort of 3,969 breast cancer patients showed that higher TMB levels were observed in TNBC. Hormone receptor positive tumors presented lower TMB compared to HER2 enriched tumors. Although hypermutation can favor immune cell infiltration, it does not necessarily translate into increased tumor immunogenicity (Onkar *et al.*, 2023).

Antigen presentation through HLA class I expression represents a key mechanism regulating T cell interactions and immune infiltration. Tumor analyses revealed that $HR^{+}HER2^{-}$ tumors display lower levels of HLA class I expression. Both genetic and epigenetic alterations can affect MHC-I expression, and evidence suggests that in TNBC, HLA-A genes can be deleted or hypermethylated (Lee *et al.*, 2016; Han *et al.*, 2022).

In addition, cancer cells can express stimulatory or inhibitory ligands that regulate immune cell infiltration. TNBC displays the highest levels of PD-L1 expression, enabling tumor cells to evade immune surveillance (Barroso-Sousa *et al.*, 2020; Onkar *et al.*, 2023).

Tumor infiltrating lymphocytes (TILs) are particularly abundant in TNBC and HER2-enriched tumors. Myeloid cells, predominantly represented by tumor-associated macrophages (TAMs), also constitute a major immune compartment within tumors and support tumor progression through the secretion of pro-tumorigenic cytokines and growth factors. Dendritic cells and TAMs contribute to the interaction between innate and adaptive immunity through their antigen-presenting capacity. In addition, recent evidence highlights the role of cancer associated fibroblasts (CAFs) in remodeling the tumor microenvironment. These mesenchymal cells influence the extracellular matrix and regulate immune cell infiltration, including TILs and regulatory T cells.

The analysis of specific immune compartments also has clinical relevance. TILs are considered an important biomarker associated with better prognosis and can predict response to neoadjuvant chemotherapy in TNBC and HER2 enriched breast cancer. Early-stage TNBC patients with high TIL levels generally show improved survival outcomes. However, in luminal tumors, the relationship between TILs and survival remains variable and may even correlate with poorer outcomes. The localization of immune cells within tumors also plays an important role. Spatial transcriptomics studies have shown that tumors spatially distant from TILs tend to display higher levels of exhausted T cells. Conversely, tumors with a more homogeneous distribution of immune

cells show increased numbers of PD-1^{+}CD8^{+} T cells, and patients with this pattern tend to have improved survival (Dvir, Giordano and Leone, 2024).

Within the TIME, TAMs can represent up to 25% of immune cells in TNBC. These macrophages often display both pro-inflammatory and immunosuppressive characteristics. TAM populations originate from both tissue-resident macrophages and recruited monocytes and are frequently associated with poor clinical outcomes (Onkar *et al.*, 2023). A single cell proteomic analysis performed on 144 patient samples identified 19 distinct myeloid clusters that could be grouped into five major categories covering two functional axes: their inflammatory versus MDSC-like phenotype, and their migratory behavior versus tissue-resident status. This study also revealed that ER^{-} tumors and high-grade tumors show higher proportions of PD-L1 expressing TAMs (Wagner *et al.*, 2019).

The crosstalk between breast cancer cells and TAMs can also influence tumor metabolism and disease progression. Aerobic glycolysis drives lactate accumulation, creating an acidic and immunosuppressive microenvironment. Lactate promotes the activation of pro-tumorigenic TAMs through PKA/CREB and ERK/STAT3 signaling pathways, which further sustain the Warburg effect in breast cancer. In addition, lactic acid can activate the NOTCH pathway in macrophages and generate a feedback loop through CCL5 secretion (Lin *et al.*, 2017; Mu *et al.*, 2018).

Alterations in lipid and amino acid metabolism can also influence macrophage function. Elevated levels of saturated fatty acids are associated with invasive breast cancer phenotypes. Similarly, amino acids such as arginine, glutamine, and tryptophan are abundant in breast cancer and contribute to immunosuppressive mechanisms. For instance, glutamine depletion has been shown to promote pro-inflammatory TAM polarization (Liang *et al.*, 2023).

Overall, tumor metabolism plays a central role in shaping the tumor immune microenvironment by regulating nutrient availability and extracellular pH, thereby influencing immune cell function.

Beyond macrophages, other immunosuppressive myeloid populations such as myeloid-derived suppressor cells (MDSCs) also contribute to shaping the TIME. Polymorphonuclear MDSCs share phenotypic and functional characteristics with neutrophils, highlighting the potential role of tumor-associated neutrophils as key regulators of breast cancer immunity.

In several cancer types, changes in circulating neutrophil numbers have been reported. In the MMTV-PyMT mouse model of breast cancer, neutrophilia has been observed together with reduced expression of the L-selectin surface marker (CD62L). Similar observations were reported in patients with early hormone-negative breast cancer, but not in hormone-positive cases, suggesting that breast cancer subtypes may induce systemic changes in neutrophil populations (Ramessur *et al.*, 2023).

In this mouse model, neutrophils were found to play a key role in metastasis formation despite their relatively low numbers in primary tumors. Neutrophil frequency increased significantly in the lungs, where these cells accumulated and contributed to the establishment of the pre-metastatic niche. In G-CSF knockout MMTV-PyMT mice, neutrophils failed to accumulate in the lungs, leading to a marked reduction in metastasis. Similarly, time-controlled neutrophil depletion using anti Ly6G antibodies significantly reduced lung metastasis without affecting other immune compartments. Reduced metastasis was also observed in immunocompromised Rag1-null mice, indicating that neutrophils contribute to pre-metastatic niche formation independently of adaptive immunity through the secretion of multiple pro-metastatic factors (Wculek and Malanchi, 2015).

Recent evidence highlights a complex role for CXCR2 signaling in neutrophil-mediated control of breast cancer progression. CXCR2 ligands, including CXCL1, CXCL2, CXCL3, CXCL5, CXCL6, CXCL7, and CXCL8, are produced by multiple components of the tumor microenvironment, such as breast cancer cells, endothelial cells, mesenchymal stromal cells (MSCs), and cancer-associated fibroblasts (CAFs). Notably, expression of these chemokines is increased in the PyMT mammary tumor model.

Unexpectedly, genetic depletion of CXCR2 in the PyMT model resulted in enhanced primary tumor growth and metastatic dissemination. This phenotype was associated with reduced infiltration of tumor-associated macrophages (TAMs) and increased neutrophil accumulation within tumors. Functional analyses further revealed that CXCR2-deficient neutrophils displayed impaired anti-tumorigenic activity and acquired a transcriptional program enriched for pro-tumorigenic genes, suggesting that CXCR2 signaling contributes to maintaining anti-tumoral neutrophil functions (Timaxian *et al.*, 2021).

These observations were recently reinforced in the 4T1 triple-negative breast cancer (TNBC) model, where CXCR2 deficiency significantly increased metastatic burden. In this setting, loss of CXCR2 reduced neutrophil

recruitment to tumors, impaired anti-tumor immune responses, and promoted lung metastasis. Consistent with these experimental findings, clinical analyses in patients with basal-like breast cancer showed that high neutrophil infiltration associated with elevated CXCR2 expression and to a lesser extent CXCR1 expression correlated with improved prognosis. Together, these studies suggest that CXCR2 signaling plays a critical role in shaping neutrophil anti-tumor functions and restricting metastatic progression in breast cancer (Li *et al.*, 2026).

Moreover, a study analyzing 196 breast cancer biopsies collected in Japan between 2014 and 2021 reported a significant association between high tumor-associated neutrophil (TAN) infiltration and adverse clinicopathological characteristics, including higher histological grade, increased lymph node metastasis, advanced tumor stage, and particular intrinsic breast cancer subtypes. These observations further support the emerging role of TANs as potential drivers of tumor progression and poor clinical outcome in breast cancer (Kakumoto *et al.*, 2024).

Despite the increasing recognition of the role of neutrophils in tumor progression and metastasis, the molecular mechanisms that regulate their functional adaptation within the tumor microenvironment remain poorly understood. Tumor-associated neutrophils display a high degree of plasticity and can rapidly adjust their phenotype in response to environmental cues such as hypoxia, nutrient availability, and inflammatory signals. To support these adaptations, cells must dynamically regulate gene expression and protein synthesis in order to rapidly modify their functional programs (Jeon *et al.*, 2020).

While transcriptional regulation has been widely studied in immune cells, emerging evidence highlights the importance of post-transcriptional mechanisms in controlling cellular plasticity. Regulation of mRNA translation has recently emerged as a key layer of gene expression control that enables cells to respond rapidly to environmental changes.

Understanding how these translational regulatory mechanisms influence immune cell behavior may therefore provide new insights into the molecular processes that govern neutrophil function in cancer.

III- mRNA translation and tRNA modifying enzymes

In 1958, Francis Crick defined the central dogma as the transfer of sequential information from DNA to RNA and from RNA to protein, while stating that information cannot be transferred from protein to nucleic acids or to other proteins (Crick, 1970). Gene expression begins with the transcription of DNA into messenger RNA (mRNA) through the activity of RNA polymerase II. The resulting single-stranded mRNA molecule is then transported from the nucleus to the cytoplasm in eukaryotic cells, where it is translated into a protein. During translation, the mRNA sequence is read by the ribosome according to the genetic code, in which each codon composed of three nucleotides corresponds to a specific amino acid (*Translation: DNA to mRNA to Protein | Learn Science at Scitable*).

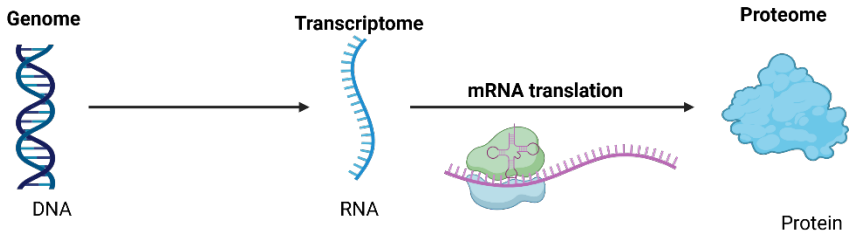

Figure 9: The central dogma of molecular biology: DNA to RNA to Proteins

1. Generalities: mRNA translation

Protein synthesis is a highly conserved biological process in which genetic information encoded in mRNA is translated into polypeptide chains. During this process, mRNA is decoded in the 5′ to 3′ direction, while the corresponding protein is synthesized from the amino (N-) terminus to the carboxy (C-) terminus. Each amino acid is determined by a three-nucleotide sequence, or codon, according to the nearly universal genetic code.

Translation is carried out by ribosomes and relies on transfer RNAs (tRNAs), which act as adaptors by matching codons on the mRNA with their corresponding amino acids. This process requires the coordinated interaction of multiple RNA species, including messenger RNA (mRNA), transfer RNA (tRNA), and ribosomal RNA (rRNA), along with a variety of protein factors that facilitate and regulate protein synthesis (Cooper, 2000).

2. mRNA translation actors

2.1. Ribosomes

Ribosomes are the cellular structures responsible for protein synthesis in both prokaryotic and eukaryotic organisms. They were initially identified as particles of cell lysates through ultracentrifugation and are classified based on their sedimentation coefficients, with bacterial ribosomes designated as 70S and the larger eukaryotic ribosomes as 80S. In both systems, ribosomes consist of two subunits composed of ribosomal RNAs (rRNAs) and associated proteins (rProteins). The abundance of ribosomes within cells reflects the essential role of protein synthesis in cellular function; for instance, Escherichia coli contains approximately 20,000 ribosomes, representing a substantial fraction of its cellular mass, while rapidly dividing mammalian cells may contain several million ribosomes (Rivalta *et al.*, 2025).

Although the overall architecture of ribosomes is conserved across species, structural differences exist between prokaryotic and eukaryotic complexes. In bacteria, the small 30S subunit contains a 16S rRNA and around 21 proteins, whereas the large 50S subunit is composed of 23S and 5S rRNAs along with approximately 34 proteins. In eukaryotes, ribosomes are larger and more complex: the 40S small subunit includes the 18S rRNA and about 30 proteins, while the 60S large subunit contains the 28S, 5.8S, and 5S rRNAs in association with roughly 45 proteins (Cooper, 2000).

Ribosomes perform two fundamental and closely linked functions in all cells: they decode the genetic information carried by mRNA sequences and catalyze the formation of peptide bonds between amino acids. These amino acids are delivered by tRNAs and are sequentially incorporated into the growing polypeptide chain according to the genetic code (Rivalta *et al.*, 2025).

2.2. Transfer RNA

During translation, each amino acid must be accurately matched to its corresponding codon on the mRNA. This process is mediated by tRNAs, which function as adaptor molecules that link specific amino acids to their respective codons. While all tRNAs share a common role in protein synthesis, they contain specific sequence elements that enable the accurate recognition and incorporation of the correct amino acid according to the genetic code. The first tRNA sequence to be determined was a 77-nucleotide alanine tRNA (tRNA-ALA) from yeast, identified by Holley et al in 1965 (*Structure of a Ribonucleic Acid*, 1965; Berg and Brandl, 2020).

tRNAs are small RNA molecules, typically 70–90 bases in length, and adopt a conserved secondary structure known as the cloverleaf, formed through intramolecular base pairing. At the tertiary level, they fold into a compact L-shaped conformation, which is essential for their interaction with the ribosome during translation. Functionally, tRNAs possess two key regions: the 3′ CCA terminus, where the amino acid is covalently attached, and the anticodon loop, which recognizes and binds complementary codons on the mRNA. Together, these features enable tRNAs to accurately translate genetic information into protein sequence (Suzuki, 2021).

The accurate incorporation of amino acids into proteins relies on both correct codon–anticodon pairing and the proper attachment of each amino acid to its corresponding tRNA. This incorporation step is catalyzed by a family of enzymes known as aminoacyl-tRNA synthetases. Each synthetase is highly specific, recognizing a particular amino acid as well as its corresponding tRNA(s).

The aminoacylation reaction occurs in two steps. First, the amino acid is activated through its reaction with ATP, forming an aminoacyl-AMP intermediate. In the second step, the activated amino acid is transferred to the 3′ end of the tRNA, specifically at the conserved CCA sequence.

Aminoacyl-tRNA synthetases exhibit a high degree of fidelity, ensuring accurate translation. This specificity arises from their ability to recognize both the chemical properties of amino acids and unique identity elements within tRNAs, often including sequences within the anticodon loop. In addition, some synthetases possess proofreading activity, allowing them to hydrolyze incorrectly activated amino acids before they are transferred to the tRNA, thereby preventing errors in protein synthesis (Cooper, 2000; Berg and Brandl, 2020).

3. Translation process

Translation is divided into three main stages: initiation, elongation, and termination. In both prokaryotic and eukaryotic cells, initiation begins with the association of the small ribosomal subunit with the mRNA and a specialized initiator methionyl tRNA. This is followed by the recruitment of the large ribosomal subunit, resulting in the formation of a functional ribosome capable of polypeptide elongation. Throughout this process, multiple non-ribosomal factors are required to regulate and coordinate the different steps of translation (Lin and Kuang, 2024).

Although the core mechanisms of translation are conserved between prokaryotic and eukaryotic cells, important differences exist in how translation initiation is regulated. In both systems, protein synthesis begins at specific initiation sites rather than directly at the 5′ end of the mRNA, leaving untranslated regions (UTRs) at both the 5′ and 3′ ends. While eukaryotic mRNAs are typically monocistronic and encode a single polypeptide, many prokaryotic mRNAs are polycistronic and contain multiple coding regions, each translated independently.

In all cases, translation is initiated with methionine, usually encoded by AUG, although alternative start codons can be used in bacteria. Notably, bacterial proteins are often initiated with a modified form of methionine (N-formylmethionine), whereas eukaryotic proteins begin with unmodified methionine (Cooper, 2000; Brito Querido, Díaz-López and Ramakrishnan, 2024).

Translation in eukaryotes is a highly regulated process that involves multiple initiation factors (eIFs). During initiation, the small 40S ribosomal subunit associates with initiator methionyl tRNA and several eIFs (eIF3, eIF1, eIF1A, and eIF5), while the mRNA is recruited through recognition of its 5′ cap structure by the eIF4 complex. Interactions between factors bound to the 5′ cap and the poly(A) tail promote mRNA circularization and enhance translation efficiency. The ribosomal complex then scans the mRNA until it encounters an AUG start codon, triggering GTP hydrolysis, release of initiation factors, and joining of the 60S subunit to form a functional 80S ribosome (Lin and Kuang, 2024).

Elongation proceeds through a cyclic process involving three ribosomal sites: the A (aminoacyl), P (peptidyl), and E (exit) sites. Aminoacyl-tRNAs are delivered to the A site by elongation factors in a GTP-dependent manner, allowing correct codon–anticodon pairing and providing a proofreading step that ensures translational fidelity. Peptide bond formation is catalyzed by the ribosome, followed by translocation of the ribosome along the mRNA, which shifts tRNAs between sites and prepares the complex for the next cycle.

Translation continues until a stop codon is reached, at which point release factors bind to the ribosome and promote the release of the newly synthesized polypeptide. The ribosomal subunits then dissociate and can be reused.

Finally, multiple ribosomes can simultaneously translate a single mRNA molecule, forming structures known as polysomes, which allow efficient protein production (Cooper, 2000).

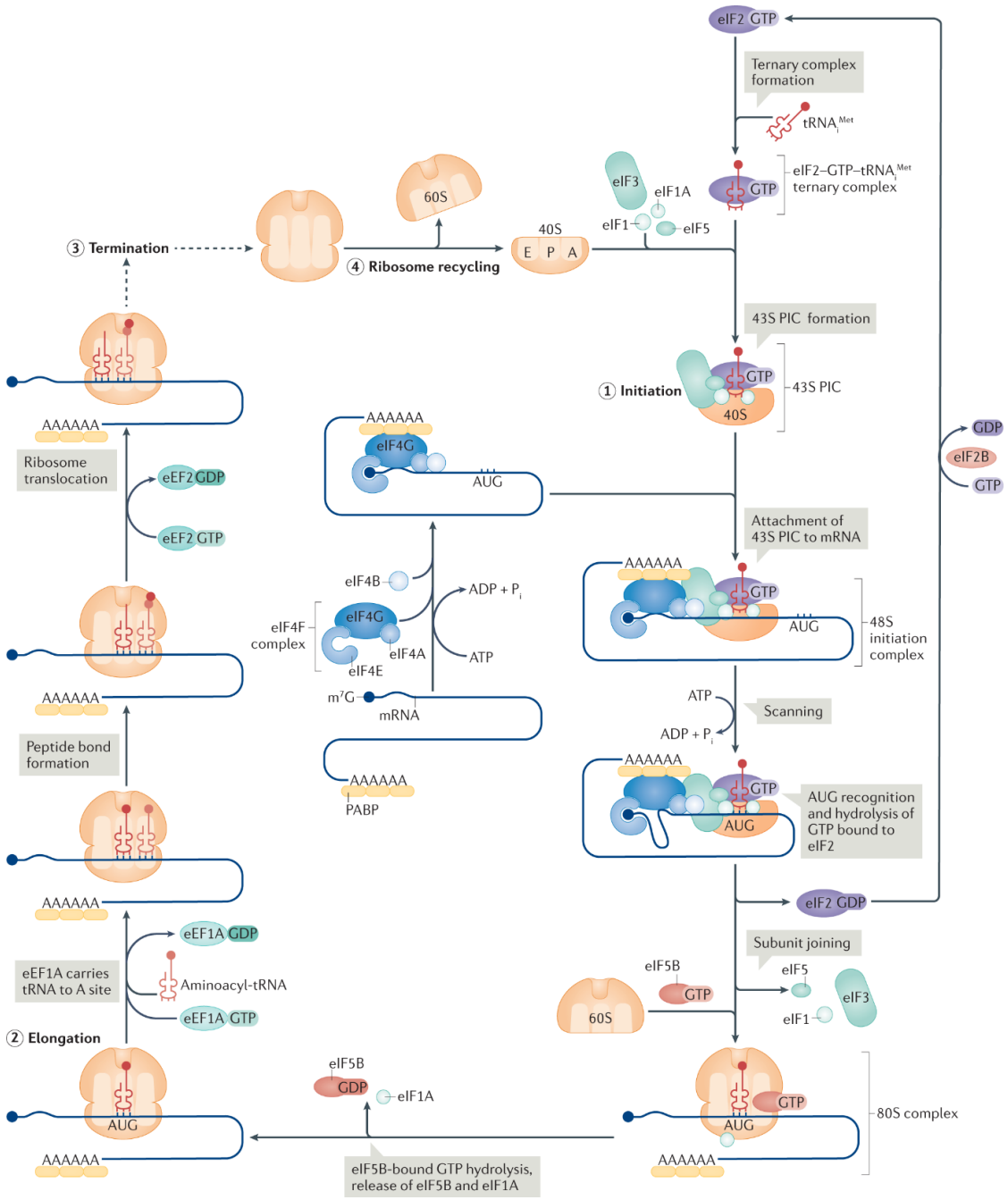

Figure 10: Process of mRNA translation (adapted from Fabbri et al.*, 2021)*. *mRNA translation occurs in four main steps: initiation, elongation, termination, and ribosome recycling. Regulation primarily takes place during initiation, which is typically cap-dependent and involves assembly of the pre-initiation complex and recruitment of the ribosome to the mRNA via the eIF4F complex. The ribosome scans the mRNA to identify the start codon, leading to formation of a functional 80S complex. During elongation, aminoacyl-tRNAs are sequentially delivered to the ribosome, allowing peptide bond formation and ribosome translocation. Translation continues*

until a stop codon is reached, triggering termination and release of the newly synthesized protein, followed by dissociation and recycling of ribosomal subunits.

4. Translation control

4.1. 5’ cap translation control

In eukaryotic cells, mRNAs are recruited by the 5' 7-methylguanosine (7mG) cap structure followed by the binding of initiation factors to allow the recruitment of the ribosome. This initiation step can be regulated by several mechanisms that will be detailed in this section (Kong and Lasko, 2012).

Translational initiation is tightly regulated by eIF4E-binding proteins (4EBPs), which act as key repressors of cap-dependent translation. 4EBPs bind to the initiation factor eIF4E and prevent its interaction with eIF4G, thereby blocking the assembly of the eIF4F complex required for ribosome recruitment. As a result, translation initiation is inhibited.

The activity of 4EBPs is controlled by phosphorylation. When 4EBPs are phosphorylated, their affinity for eIF4E decreases, allowing eIF4E to associate with eIF4G and promoting translation initiation. This mechanism is regulated by signaling pathways such as the mTORC1 pathway, which responds to nutrient availability and growth factor signals. Activation of mTORC1 leads to phosphorylation of 4EBPs and enhances translation of specific mRNAs involved in cell growth and proliferation (Nandagopal and Roux, 2015; Woodcock *et al.*, 2019).

In addition, 4EBPs can contribute to selective translation through interactions with RNA-binding proteins, thereby regulating specific subsets of mRNAs. This regulatory system plays an important role in processes such as cell cycle progression, metabolism, and cellular differentiation (Topisirovic *et al.*, 2011; Kong and Lasko, 2012).

Another alternative mechanism of translational repression at the mRNA cap involves the eIF4E homologous protein (4EHP). Although 4EHP can bind the 5′ cap structure, it does not interact with eIF4G and therefore prevents the formation of the eIF4F complex, ultimately inhibiting ribosome recruitment and translation initiation.

In contrast to global repression mediated by 4EBPs, 4EHP is often involved in selective translational control through its recruitment to specific mRNAs by RNA-binding proteins. This mechanism has been well characterized in developmental contexts, where 4EHP contributes to spatial regulation of

protein expression. For example, in *Drosophila*, 4EHP is recruited to target mRNAs by regulatory proteins, leading to localized translational repression and the establishment of protein gradients essential for embryonic patterning.

In mammalian systems, 4EHP has also been implicated in the regulation of specific transcripts involved in processes such as stem cell maintenance. Furthermore, its activity can be modulated by post-translational modifications, highlighting an additional layer of control in cap-dependent translational regulation (Morita *et al.*, 2012; Christie and Igreja, 2023).

4.2. Poly-A tail translation control

Translational control is also strongly influenced by the length of the poly(A) tail at the 3′ end of mRNAs. In general, longer poly(A) tails enhance translation efficiency, whereas shortening of the tail (deadenylation) leads to translational repression and often promotes mRNA decay. This regulatory mechanism is particularly important in processes requiring rapid and dynamic control of protein expression, such as germ cell development, neuronal plasticity, and cellular stress responses (Weill *et al.*, 2012).

Poly(A) tail length is determined by the balance between deadenylation and polyadenylation activities. Deadenylation is primarily mediated by the CCR4–NOT complex, which can be recruited to specific mRNAs by RNA-binding proteins, leading to reduced translation. Conversely, cytoplasmic poly(A) polymerases can extend poly(A) tails, thereby enhancing translation. Through this dynamic and reversible mechanism, cells can finely tune protein synthesis independently of mRNA abundance (Kong and Lasko, 2012; Weill *et al.*, 2012).

4.3. eIF2 regulation

The eukaryotic initiation factor eIF2 is a central regulator of translation initiation, acting as a key control point for ribosome recruitment. eIF2 forms a ternary complex with GTP and the initiator methionyl tRNA, enabling its delivery to the 40S ribosomal subunit. Following start codon recognition, GTP is hydrolyzed and eIF2 is released in its GDP-bound form, requiring recycling by the guanine nucleotide exchange factor eIF2B to initiate a new round of translation.

Regulation of eIF2 activity occurs primarily through phosphorylation of its α subunit (eIF2α) in response to cellular stress, such as amino acid deprivation, ER stress, or viral infection. Phosphorylated eIF2α inhibits eIF2B activity,

reducing the availability of active eIF2–GTP complexes and thereby globally decreasing translation initiation (Wek, 2018; Boye and Grallert, 2020).

5. mRNA translation and cell plasticity

Gene expression is not solely determined at the transcriptional level, as extensive post-transcriptional regulatory mechanisms modulate mRNA fate and protein output. In particular, translational control allows cells to promptly and dynamically adapt to environmental cues such as stress or growth signals. Importantly, mRNA abundance does not systematically correlate with protein levels, and multiple studies have highlighted frequent discrepancies between transcriptomic and proteomic profiles (Wang, 2008; Vélez-Bermúdez and Schmidt, 2014; (Fabbri *et al.*, 2021a), highlighting the importance of post-transcriptional regulation in shaping cellular phenotypes.

Among these mechanisms, regulation of poly(A) tail length plays a central role in controlling mRNA stability and translation efficiency. Poly(A) tails, together with poly(A)-binding proteins, promote translation and protect mRNAs from degradation, while deadenylation leads to translational repression and mRNA decay (Passmore and Coller, 2022). Beyond these canonical functions, poly(A)-mediated regulation is highly dynamic and contributes to fundamental biological processes, including stem cell maintenance, differentiation, and development (Miao and Hu, 2025). For instance, alternative polyadenylation can generate mRNA isoforms with distinct 3′UTRs, thereby modulating mRNA stability and translational efficiency, as illustrated by the regulation of pluripotency genes during embryonic stem cell self-renewal.

In parallel, RNA-binding proteins (RBPs) provide a major layer of mRNA-specific regulation by controlling transcript processing, localization, stability, and translation. Their activity is tightly regulated by environmental signals, allowing rapid adaptation to cellular stress or growth conditions. For example, oncogenic pathways such as PI3K/AKT/mTOR modulate RBP activity and epitranscriptomic regulators to enhance the translation of pro-survival and proliferative transcripts, whereas stress conditions promote RBP relocalization and mRNA sequestration in stress granules to transiently repress translation. Dysregulation of RBPs has been extensively linked to cancer progression, metabolic adaptation, and stem cell maintenance (Li, Deng and Chen, 2022). In addition, epitranscriptomic modifications such as m^{6}A further refine post-transcriptional regulation by modulating mRNA stability and translation. m^{6}A deposition by METTL3/14 promotes the translation of oncogenic transcripts, whereas its removal by demethylases such as FTO or ALKBH5 enhances

stemness-associated programs, highlighting the dynamic and reversible nature of this regulatory layer (Kang, Lee and Lee, 2020).

MicroRNAs represent another key mechanism of post-transcriptional control, acting through sequence-specific interactions to repress translation and promote mRNA degradation. Their expression is tightly regulated by signaling pathways and environmental cues, enabling fine-tuned control of gene expression programs. MicroRNAs play essential roles in immune cell function and plasticity, as illustrated by their requirement for T cell survival, differentiation, and regulatory T cell homeostasis. In fact, some miRNAs promote a specific subset and repress alternative lineages (e.g., miR-155 promotes Th1-like responses yet can also restrain IFN-γ signaling in certain contexts to avoid over-differentiation) (Baumjohann and Ansel, 2013). In cancer, microRNAs contribute to epithelial–mesenchymal plasticity by targeting key transcriptional regulators of EMT, thereby influencing invasion and metastatic potential (D'Amato, Howe and Richer, 2013).

Beyond these regulatory mechanisms, the translational machinery itself has emerged as an active contributor to gene expression control and cell plasticity. Ribosomes are no longer considered as uniform entities but can display compositional and functional heterogeneity, giving rise to "specialized ribosomes" that preferentially translate specific subsets of mRNAs. Variations in ribosomal protein composition, rRNA modifications, and associated factors can modulate translation efficiency, fidelity, and selectivity (Elhamamsy et al., 2022). Such ribosome remodeling has been linked to adaptive processes including stress responses, metabolic rewiring, and tumor progression. For example, epithelial-to-mesenchymal transition is associated with increased ribosome biogenesis, and inhibition of this process impairs cellular plasticity and metastasis (Elhamamsy et al., 2022; Rivalta et al., 2025). Similarly, recent multi-omics analyses have demonstrated that cancer cells exploit ribosome heterogeneity to selectively translate transcripts required for adaptation to hypoxia and therapeutic stress. In this context, hypoxia alters rRNA methylation and ribosome biogenesis, generating specialized ribosomes that preferentially support IRES-driven translation of pro-survival and pro-angiogenic factors (Ho *et al.*, 2020; Fabbri *et al.*, 2021).

Collectively, these mechanisms highlight that post-transcriptional regulation provides a highly dynamic and reversible layer of gene expression control, enabling rapid adaptation of the proteome to environmental and cellular demands. In this context, emerging evidence indicates that regulation of the translational machinery itself, including transfer RNAs, represents an

additional level of control. Indeed, tRNA abundance and modifications can fine-tune translation efficiency, codon decoding, and stress responses, thereby contributing to metabolic adaptation and cell plasticity (Suzuki, 2021). This highlights tRNA-dependent regulation as a critical component of translational control, which will be further explored in the following section.

6. tRNA remodeling for translation control

Transfer RNAs (tRNAs) are central components of the translational machinery and display a remarkable level of structural and functional complexity. The human genome encodes more than 420 potential tRNA genes, which fold into a conserved cloverleaf structure dictated by their nucleotide sequence composition. Notably, sequences with a high proportion (>50%) of mismatches fail to adopt this canonical structure. In addition, tRNAs sharing the same anticodon but differing in sequence or structure, termed “isodecoders,” further contribute to the diversity of the tRNA pool. Importantly, tRNA expression is not uniform across tissues, and specific subsets of tRNAs are selectively expressed depending on cellular context, highlighting a first level of regulation at the level of tRNA availability (Pan, 2018).

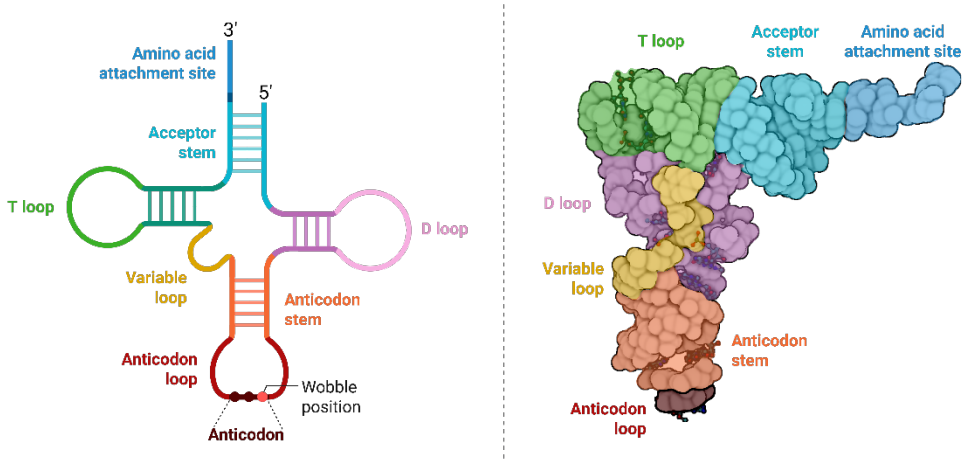

Figure 11:tRNA structure (adapted from the Biorender library). tRNAs adopt a conserved cloverleaf secondary structure composed of four main arms: the acceptor stem, D-loop, anticodon loop, and TΨC loop. This structure ensures proper folding, stability, and interaction with the translational machinery.

tRNAs are transcribed by RNA polymerase III and undergo a series of maturation steps, including removal of the 5′ leader sequence by RNase P,

processing of the 3′ trailer by RNases, addition of the CCA tail, and extensive chemical modifications required to generate fully functional molecules (Ren et al., 2023). Indeed, tRNAs are among the most heavily modified RNA species, with more than 100 distinct modifications identified to date. These modifications are distributed across the tRNA structure and play essential roles in maintaining structural stability, ensuring proper folding, and regulating interactions with the ribosome and the translational machinery. Modifications located within the tRNA body contribute to structural integrity and translational dynamics, whereas mitochondrial tRNAs typically harbor fewer modifications, reflecting differences in translational requirements (Suzuki, 2021).

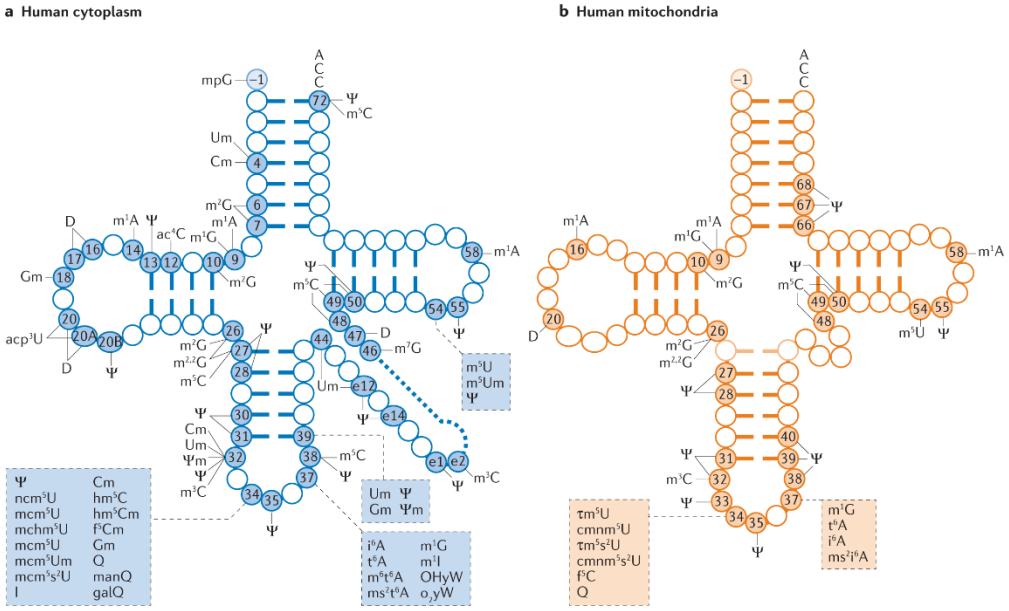

Figure 12: tRNA modifications (adapted from Suzuki, 2021). Overview of chemical modifications in human cytoplasmic and mitochondrial tRNAs, highlighting the diversity and positional distribution of modified nucleotides that contribute to tRNA stability, decoding capacity, and translational regulation.

A major hotspot for functional regulation is the anticodon loop, particularly positions 34 and 37. Position 34, known as the wobble position, is frequently modified to expand or restrict codon recognition, thereby modulating decoding capacity. Position 37, adjacent to the anticodon, plays a critical role in maintaining reading frame fidelity and accurate codon–anticodon interactions (Suzuki, 2021; Ren et al., 2023). Importantly, tRNA modifications are not static: many are only partially present under physiological conditions, suggesting that their levels can be dynamically tuned in response to cellular states. This variability enables a mechanism known as codon-biased translation, whereby

the selective modification or availability of specific tRNAs promotes preferential translation of mRNAs enriched in corresponding codons, thus reshaping the proteome according to cellular needs (Pan, 2018; Añazco-Guenkova *et al*., 2024).

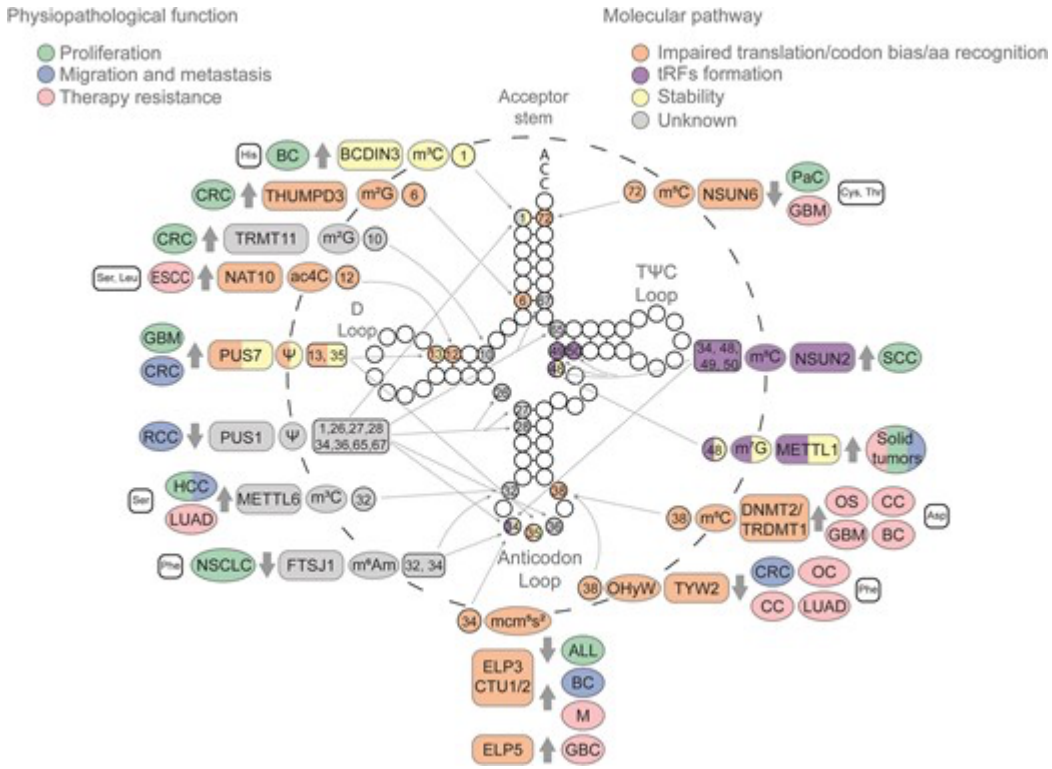

Figure 13: Cytosolic tRNA modification impacting tumoral processes (Añazco-Guenkova et al*., 2024). Epitranscriptomic marks deposited in cytosolic tRNAs have been implicated in various cancerous processes, including proliferation (green), migration and metastasis (blue), and therapy resistance (pink). These consequences arise from diverse molecular alterations such as impaired translation or codon bias (orange), the biogenesis of tRFs (purple), tRNA stability (yellow) or a still unknown mechanism (gray).*

Through these mechanisms, tRNA modifications emerge as key regulators of cellular plasticity, allowing rapid and reversible adaptation of protein synthesis in response to environmental and physiological cues. They contribute to diverse biological processes including development, immune activation, tumor progression, and metabolic reprogramming (Cui *et al.,* 2023; Añazco-Guenkova *et al.,* 2024).

For instance, the 7-methylguanosine (m7G) modification at position 46 enhances translation of oncogenic transcripts in a codon-dependent manner. In hepatocellular carcinoma, increased m7G levels correlate with tumor progression, and depletion of the methyltransferase METTL1 reduces

translation efficiency of mRNAs enriched in m7G-associated codons without significantly affecting mRNA levels, highlighting a direct translational control mechanism (Chen *et al.,* 2021; Ren *et al.,* 2023). Similarly, the methyltransferase METTL6, which modifies position 32 of tRNAs, has been implicated in cancer cell proliferation and response to chemotherapy, further supporting the role of tRNA modifications in tumor adaptation and drug resistance (Wang *et al.,* 2026).

Work published by our laboratory showed that modulation of tRNA modifications can directly influence immune responses. Disruption of N6-threonylcarbamoylation (t6A37) leads to accumulation of defective translation products that activate innate immune sensing pathways, promoting type I interferon responses and enhancing anti-tumor immunity (Dziagwa *et al.,* 2026).

Our lab also previously uncovered that tRNA-dependent translational control is also involved in adaptive resistance mechanisms. In a paper published in 2018 (Rapino *et al.*, 2018), we showed that U34 tRNA-modifying enzymes are upregulated in anti-BRAF-resistant melanoma cells, where they modulate HIF-1α expression in a codon-dependent manner. We also showed that valine aminoacyl-tRNA synthetase (VARS) drives codon-biased translational reprogramming in melanoma cells resistant to MAPK-targeted therapy, thereby promoting metabolic adaptation and survival (El-Hachem *et al.,* 2024). Collectively, these findings highlight that modulation of tRNA function, whether through chemical modification or aminoacylation dynamics, constitutes a powerful mechanism by which cells reprogram their proteome in response to stress, growth signals, or therapeutic pressure.

Beyond cancer, tRNA modifications also play critical roles in immune cell function. During T-cell activation, rapid translational upregulation is supported by increased expression of the TRMT6–TRMT61A complex, which catalyzes N1-methyladenosine (m1A58) modification and promotes MYC-dependent proliferation (Liu *et al.,* 2022). This modification is also essential for innate lymphoid cell function, contributing to intestinal homeostasis and antibacterial defense (Li et al., 2026).

Among the various modifications affecting the anticodon loop, those occurring at position 34 are of particular interest due to their direct impact on codon recognition. Adenosine at position 34 can be deaminated to inosine (I34), enabling recognition of multiple codons and expanding decoding capacity, a process mediated by the ADAT2–ADAT3 complex in humans (Suzuki, 2021). In parallel, uridine at position 34 undergoes complex modifications such as

mcm5s2U, generated through the coordinated action of the Elongator complex, ALKBH8, and thiouridylases CTU1 and CTU2 (Rapino *et al.*, 2017, Rapino *et al.,* 2021; Suzuki, 2021). These modifications fine-tune translation efficiency and codon usage preferences, thereby contributing to context-dependent translational programs. Given their central role in regulating gene expression at the translational level, U34-dependent modifications represent a critical regulatory node, which will be further explored in the following section.

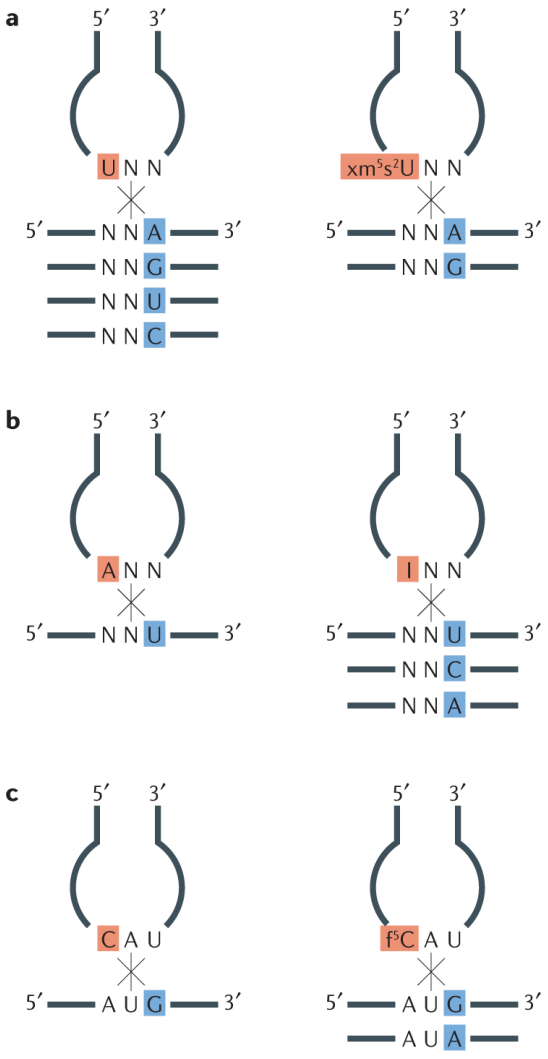

Figure 14: Control of decoding by tRNA wobble modifications (adapted from Suzuki., 2021): a. Restriction of codon recognition by 5-methyl-2-thiouridine derivative (xm5s2U)-type modifications. b. Expansion of codon recognition by inosine (I). c. Expansion of codon recognition by 5-formylcytidine (f5C).

7. U34 tRNA modifying enzymes in development, cancer and immune cells

Among tRNA modifications, those occurring at the wobble position 34 (U34) have emerged as key regulators of translational control due to their direct impact on codon recognition and decoding efficiency. U34 modifications are particularly important for the translation of AA-ending codons, including AAA, CAA, and GAA, which are enriched in specific subsets of transcripts. Importantly, codon usage alone is not sufficient to predict protein fate, as additional sequence features such as hydrophilic penta-motifs ([EKR]-[EKR]-[EKR]-R-[DEKR]) determine whether proteins undergo downregulation or aggregation upon loss of U34-modifying enzymes such as ELP3 or CTU2. Together, these features define a codon- and motif-dependent regulatory layer that contributes to proteome homeostasis (Rapino *et al.,* 2021).

The molecular basis of U34 modification relies on a conserved enzymatic cascade. The Elongator complex, composed of six subunits (ELP1–ELP6), plays a central role, with ELP3 acting as the catalytic subunit harboring both a radical S-adenosylmethionine (rSAM) domain and a lysine acetyltransferase (KAT) domain. This complex initiates the formation of modified uridines, including ncm^5U_{34} and mcm^5U_{34}, which can be further processed into $mcm^5s^2U_{34}$ through thiolation reactions mediated by CTU1 and CTU2 (Wang *et al.,* 2026). These modifications fine-tune codon–anticodon interactions and ensure efficient and accurate translation.

The dynamic nature of U34 modifications is first illustrated in yeast, where they function as adaptive regulators of stress responses. Under conditions such as heat shock, oxidative stress, or nutrient limitation, U34 modifications ($mcm^5s^2U_{34}$ and mcm^5U_{34}) are modulated to promote selective translation of stress-responsive transcripts enriched in AA-ending codons.

URM1-dependent thiolation is a conserved pathway in which the ubiquitin-like protein URM1 acts as a sulfur carrier to generate U34 tRNA modifications, thereby supporting translational fidelity and stress adaptation. Disruption of this pathway mildly reduces global translation, as evidenced by a decreased polysome-to-monosome ratio in URM1 depleted cells and increased sensitivity to translation inhibitors such as cycloheximide. These defects are detectable under basal conditions but become more pronounced under stress, including elevated temperature, highlighting the critical role of U34 thiolation in maintaining translational robustness (Damon, Pincus and Ploegh, 2015). In addition, stress-specific tRNA modifications can drive selective translation

programs, as shown by TRM4-dependent methylation of tRNALeu (CAA), which enhances translation of TTG-enriched transcripts such as RPL22A during oxidative stress, thereby promoting cellular adaptation (Chan *et al.,* 2012).

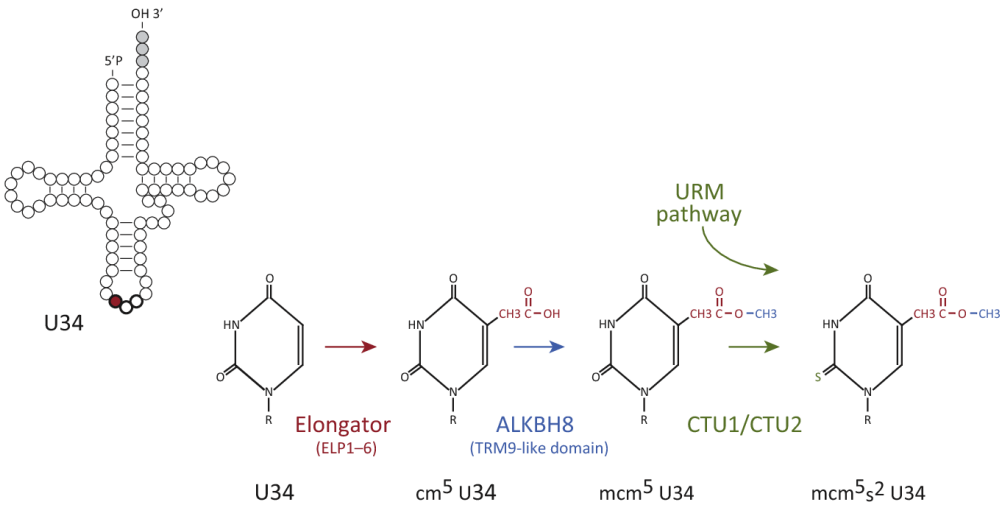

Figure 15: U34 modification enzymatic cascade (Rapino et al.*, 2021) U34 modification is established through a multistep enzymatic pathway in which the Elongator complex first catalyzes the formation of cm⁵U, which is subsequently methylated by ALKBH8 to generate mcm⁵U, and finally thiolated by CTU1/CTU2 to produce the fully modified mcm⁵s²U.*

In eukaryotes, U34 modifications are essential for development, particularly in the nervous system. They play critical roles in neuronal progenitor proliferation, migration, and proteostasis during cortical development, and their disruption leads to severe defects such as microcephaly through activation of unfolded protein response pathways and apoptosis (Creppe *et al.*, 2009; Laguesse *et al.*, 2015). Neurons, which rely heavily on local translation to rapidly adjust synaptic proteomes, are particularly sensitive to defects in codon decoding. U34 modifications prevent ribosome pausing and frameshifting on codon-biased transcripts, ensuring efficient synthesis of key synaptic proteins. Consistently, loss of U34-modifying enzymes such as ALKBH8 results in oxidative stress, synaptic abnormalities, and cognitive defects, and mutations in these pathways have been linked to neurodevelopmental disorders including intellectual disability and autism (Madhwani *et al.,* 2024; Guo, Russo and Tuorto, 2024).

In cancer, U34-dependent tRNA modifications have been shown to support tumor progression by enabling translational reprogramming. ELP3, the catalytic subunit of the elongator complex has been shown to be a driver of

Wnt-dependent cancer initiation in the intestine. In fact, ELP3 maintains specific pool of intestinal stem-like cells Lgr5+/Dclk1+/Sox9+ allowing tumor initiation (Ladang *et al.*, 2015). In colorectal cancer, the methyltransferase ALKBH8 regulates translation of the KRAS oncogene in a codon-dependent manner, and its deletion leads to reduced tumor formation and increased tumor cell death (Qian et al., 2025). On the other hand, in breast cancer, U34-modifying enzymes are upregulated and promote metastasis through enhanced translation of the oncoprotein DEK, which in turn activates IRES-dependent translation of LEF1 and drives WNT signaling (Delaunay et al., 2016,). Similarly, in melanoma, U34 enzymes contribute to oncogenic adaptation downstream of BRAFV600E mutation by promoting glycolytic reprogramming through HIF1α-dependent pathways (Rapino et al., 2018). These studies collectively highlight the role of U34 modifications in sustaining tumor growth, metabolic adaptation, and therapeutic resistance.

Beyond cancer, U34 modifications also play fundamental roles in hematopoiesis and immune cell function. In the myeloid lineage, loss of ELP3 induces a stress-like response characterized by activation of ATF4 and p53 signaling, leading to increased protein synthesis, impaired progenitor survival, and bone marrow failure (Rosu et al., 2021). In adaptive immunity, U34-modifying enzymes are dynamically regulated during T-cell activation, and ELP3 deficiency impairs T follicular helper cell responses by delaying cell cycle entry and limiting expansion (Lemaitre et al., 2021). In innate immunity, U34 modifications contribute to macrophage polarization, as ELP3 depletion disrupts metabolic reprogramming required for M2 polarization, including tricarboxylic acid cycle (TCA) activity and mitochondrial function (Chen et al., 2022).

Collectively, these findings demonstrate that tRNA-dependent translational regulation, and in particular U34 modifications, act as important drivers of cellular plasticity across diverse biological contexts. By linking codon usage to protein synthesis, metabolic adaptation, and stress responses, these mechanisms enable cells to dynamically reprogram their proteome. Importantly, this highlights post-transcriptional regulation as a rapid and efficient means for cells to respond to environmental changes. Given the high degree of functional and phenotypic plasticity exhibited by neutrophils within the tumor microenvironment, where they form distinct subsets associated with diverse roles, we sought to investigate whether tRNA remodeling contributes to shaping neutrophil adaptation in cancer.

Aim of the project

Metastatic breast cancer remains a leading cause of cancer related mortality as metastatic dissemination accounts for nearly 90% of breast cancer patient deaths and a 5-year survival rate of 30%. Tumor aggressiveness is driven by both intrinsic properties of cancer cells and extrinsic factors arising from the tumor microenvironment, among which immune cells play a central role. Particularly, neutrophils have emerged as key regulators of tumor progression, notably through their contribution to the formation of the pre-metastatic niche and their pro-tumoral functions. Tumor associated neutrophils exhibit a high degree of functional plasticity, displaying both pro- and anti-tumorigenic activities depending on environmental cues. While this plasticity has been extensively characterized at the transcriptional level, it remains poorly explored at the proteomic and translational levels.

The first aim of this work was therefore to characterize the proteomic remodeling occurring in neutrophils upon tumor infiltration, by comparing tumor infiltrating neutrophils and circulating neutrophils in the PyMT model using low-throughput proteomics.

This strategy will allow us to better understand how changes in protein expression may support neutrophils functional adaption within the tumor microenvironment.

In parallel, tumor infiltrated neutrophils exhibit higher expression of tRNA modifying enzymes. Importantly the previous work from our laboratory uncovered the importance of U34 tRNA-modifying enzymes as key regulators of cellular plasticity in both cancer and immune cells, indicating that tRNA mediated translational regulation may represent an additional layer controlling functional cell state transitions. Based on this, the second aim of this study was to determine whether U34-dependent tRNA modifications contribute to the functional reprogramming of tumor-infiltrated neutrophils.

To address this, we generated a mouse model with a conditional knockout of Elp3 gene in neutrophils. This model will allow us to investigate the importance of U34 tRNA modification in neutrophils in steady state conditions. We next crossed this model with the MMTV-PyMT metastatic breast cancer model. This model allows us to characterize the impact of ELP3 depleted neutrophils on the tumor development.

Next, we sought to investigate the role of ELP3 in the regulation of tumor - infiltrated neutrophil's function in breast cancer. We combined proteomics

analyses with functional and molecular approaches, including metabolomics, single-cell RNA sequencing. Altogether, this work aims to determine whether translational control through tRNA modifications constitutes a key mechanism driving neutrophil plasticity and shaping their contribution to tumor progression and metastasis.

Materials and Methods

Materials and Methods

1.Mouse models

Multiple mouse models were created to study breast cancer, however, the MMTV-PyMT model remains the most used one as it mimics the tyrosine kinases receptors signals that are activated in human BC. This model is used in the study of multiple facets of mammary tumors starting from their initiation, progression and metastasis. This model is also used to study the immune remodeling and the response to immunotherapies. This strain was produced using the murine mammary tumor virus long terminal repeat promoter (MMTV-LTR) to express the Polyomavirus Middle T antigen (PyMT) in the epithelium. This genetic insertion induces the formation of multifocal metastatic tumors. Tumorigenesis occurs in the luminal cells and evolves mimicking human ductal BC. PyMT BC tumors present an expression profile similar to the luminal B subtype in human and exhibit the loss of hormone receptors, an increase in the expression of ErbB2 and cyclin D1 at advances stages. Furthermore, the genetic background is fundamental. Notably, FVB/NJ MMTV-PyMT tumors evolve faster than in C57Bl/6J MMTV-PyMT (Attalla *et al.*, 2021).

For this project, 12-week-old and 10-week-old females FVB/N background MMTV-PyMT were used to characterize tumor associated neutrophils. Steady state mice $Elp3^{loxP/loxP}$ – MRP8-Cre ($ELP3^{CTR}$ and $ELP3^{NEU}$) were also used as organ donors to perform invitro and metabolomics characterization on neutrophils.

All experimental procedures, follow-up, and housing complied with the Belgian Council for Laboratory Animal Science guidelines. All animal experiments were approved by the Ethical Committee for Animal Experiments of university of Liège.

2. Neutrophil isolation from the bone marrow

Bone marrow cells were collected through the extraction of cells out of the tibia, femur and hip bones. The thicker edge of the bone was cut and placed in an extraction tube made in house. A 500µL tube pierced with an 18G syringe and inserted in a 2mL collection tube containing 180µL of PBS EDTA (pH=7.4). Bones are centrifuged at 5000g for 1min. Cells are after collected and placed in a falcon tube with 15mL PBS EDTA and incubated for 10 minutes on ice with 2 rounds of vortex to avoid cell aggregate.

Red blood cells lysis is performed using miltneyi red blood cell lysis solution 10X. The cell suspension is filtered using 70µm mesh nylon cell strainer. Neutrophils were enriched out of the bone marrow cell suspension using EasySep mouse neutrophil enrichment kit and following the manufacturer's protocol. This procedure was used for all experiments except for proteomics and experiments with flow cytometry readouts.

3. RNAseq analysis

Publicly available RNAseq dataset (GSE164766) was extracted from GEO datasets. Raw data was used following Deseq2 pipeline. Ensembl ID gene names were extracted from Ensembl website and merged to the data to have a full annotation of transcripts. The dataset displayed data of CXCR2 knockout neutrophils that were discarded and only bone marrow normal neutrophils and TINs samples were used. For statistical analysis WALD test was used as it is the one suggested in case of a comparison of 2 groups.

PCA analysis and figures were generated on R. DGE analysis figure was generated using GraphPad (8.4.3 version).

4. Single cell RNA-seq

CD45 immune cells were enriched at 10 weeks. Following the removal of red blood cell lysis, epithelial cells were stained using Epcam-FITC antibody and removed using Easy Sep FITC positive selection kit. As a last step, CD45 cells were enriched using Easy sep CD45 positive selection kit following manufacturer instructions.

For the whole tumor experiments, cells were processed after mechanical and enzymatical digestion followed by red blood cells removal.

Single cell analysis was performed using Seurat V5 R package. RPCA integration of CD45 enriched and whole tumor datasets was performed.

Only cells with a number of features between 500 and 3000 and mitochondrial genes lower than 10% were considered for the analysis. A trial without mitochondrial genes filtering layer was tested and no significant changes in the yield were detected.

Merged data were normalized following the SCT (SCTransform) (Lause, Berens and Kobak, 2021) to reduce the bias of technical factors including the sequencing depth. Merged normalized data were integrated using RPCA workflow (Reciprocal PCA). This integration method was used as we had

missing populations in one dataset compared to the other (CD45 enriched immune cells and whole tumor).

Unlike the standard canonical correlation analysis (CCA)-based integration approach, RPCA identifies integration anchors by projecting each dataset into the principal component space of the other dataset and retaining anchors that satisfy a mutual nearest-neighbor criterion. This strategy provides a computationally efficient and more conservative integration framework, reducing the risk of overcorrection and inappropriate alignment of cells in distinct biological states. RPCA-based integration is particularly well suited for datasets generated using the same experimental platform, datasets containing cell populations that are not fully shared across samples, and large-scale datasets comprising numerous cells or samples. Following anchor identification, datasets were integrated using the Seurat integration workflow to enable downstream comparative analyses while preserving biologically relevant variation.

Of note, single-cell RNA-seq analyses of CD45+ immune cells and whole tumors were performed at two distinct experimental time points. To assess the robustness of the results and exclude potential integration-related artifacts, each dataset was initially analyzed independently prior to integration. Comparable biological conclusions were obtained from the separate analyses, further supporting that the RPCA-based integration procedure did not introduce significant biases or alter the underlying biological signals.

For module score calculations for T cells, T cells cluster was isolated from the dataset. The defining list of genes for every signature was projected on the umap using addmodulescore function of the Seurat R package.

DGE (Differential gene expression) analysis was performed using findmarkers function and data was displayed using GraphPad. It is important to note that DGE analysis was performed using the raw count matrix rather than the integrated data. As integration procedures are intended for dimensionality reduction, clustering, and visualization, the use of raw counts preserves the original gene expression measurements and avoids potential biases introduced during dataset integration.

Each major cell cluster was isolated using the Seurat Subset() function and reanalyzed independently to investigate intracluster heterogeneity. For each subset, dimensionality reduction was followed by nearest-neighbor graph construction using FindNeighbors(), and subclusters were identified using the graph-based clustering algorithm implemented in FindClusters(). Differentially

expressed genes for each subcluster were identified using FindMarkers(), and cluster annotation was performed based on the expression of established cell-type and functional markers.

5. Gene set enrichment analysis

After DGE analysis, data are pre-ranked following the order of the Log2FC. An .rnk file is created by pasting gene names and Log2FC values. Available published pathways isolated from MitoCarta repository were used to generate .gmx signature files.

Gene Set Enrichment Analysis (GSEA) software is then used to perform enrichment analysis on the pre-ranked data.

Bubble plots are generated using R studio and chart bars and heatmaps were generated using GraphPad.

6. Neutrophil viability assay

Bone marrow neutrophils were enriched using stem cell kit (ref:19762) following manufacturer protocol. Neutrophils are placed in culture in 96 well plate (100000 cells per 100µL/well). 100µL of SARTORIUS RED cytotox dye (100µM) is added to each well to reach a final concentration of 500nM.

Cells were imaged using the IncuCyte live-cell imaging system, with images acquired in both phase contrast (brightfield) and red fluorescence channels at 1-hour intervals over a 48-hour period.

7. Neutrophil migration

Migration of neutrophils was tested using the 5µm Boyden transwell chambers and Fmlp (100nM) as a chemoattractant. In each well, 2 x 10^5 neutrophils resuspended in 100µL of HBSS were plated in the upper part of the chamber. In the lower part of the chamber 600µL of medium supplemented with FMLP was placed. The migration assay lasted for 2 hours at 37°C and migrated cells were counted by FACs using the counting beads.

8. Reactive oxygen species (ROS) measurement

Intracellular ROS assay was conducted using DHR 123 probe (KP06004). Cell permanent dye Dihydrodamine 123 is oxidized by ROS and releases fluorescence captured on a channel going from 500nm to 536nm (equivalent to FITC fluorochrome). 1µL of the probe working reagent is diluted in 999µL

of PBS to make the working solution. After optimization, 100µL of the working solution was used to test the ROS production in 1x 10^6 of cells and an incubation time of 15 minutes at 37°C.

For this assay 1x 10^6 of cells/mL total bone marrow cell suspension was put in culture in IMDM complete medium (1%P/S, 20% FBS, 1% of glutamine and 0.1 % of β-mercaptoethanol). Cells were cultured in normal control condition and in stimulation condition using PMA (100nM) for 45 minutes before washing with PBS and adding the probe working solution.

Membrane markers staining is performed on ice after 30 minutes of incubation in the dark and the results are analyzed immediately to avoid any excess staining with the probe.

9. Mitochondrial ROS assay

MitoSox Red (Invitrogen: M36007) is a dye that is oxidized only by superoxide and this makes it specific to mitochondrial respiration. The dye is used at a concentration of 1µM and 3x 10^6 of cells/mL are used for this analysis as it was performed on TINs after cell culture at 37°C for 30 minutes. Membrane markers staining is performed after cell washing following the usual protocol (30 minutes of staining on ice and in the dark).

10. Intra-tumoral and blood neutrophils extraction

Neutrophils were cell sorted using the SONY MA-900 using. Prior to sacrifice, biotin CD45 anti mouse antibody was injected intra-orbitally. Mice were sacrificed after 7 minutes to ensure the staining of all the immune cells in circulation. Blood was collected out of the retro-orbital sinus of sedated mice. Tumors were isolated out of sacrificed mice. Tumors were digested in the gentle macs. Dissociator, using 30µL of DNAse I (Roche, ref: 04716728001) and 180µL collagenaseA (50mg/mL) (Roche, ref: 10103586001) diluted in 3mL of HBSS supplemented with 5% FBS.

Cells were stained using anti-biotin antibody, CD45-BV421 anti-mouse (for total immune cell staining), Ly6G-APC Cy-7 and CD11b-APC. Intra-tumoral neutrophils (CD45-BV421 +, CD45 biotin -, Ly6G+, CD11b+) and blood neutrophils (CD45-BV421 +, CD45 biotin +, Ly6G+, CD11b+) were cell sorted and conserved for proteomics.

11. In Vivo Protein Synthesis Assay (OP-Puro Incorporation)

In vivo protein synthesis was assessed using O-propargyl-puromycin (OP-Puro, Thermo Fisher Scientific). Mice received a single intraperitoneal injection of OP-Puro (1 mg per mouse) and were sacrificed one hour later. Blood was collected immediately prior to sacrifice, and bone marrow and tumor tissues were subsequently harvested. Single-cell suspensions were prepared from the collected samples and processed according to the manufacturer's instructions. OP-Puro incorporation was detected using the Click-iT™ chemistry-based staining protocol (Thermo Fisher Scientific) and analyzed by flow cytometry as a measure of nascent protein synthesis.

12. Hematoxylin and Eosin (H&E) Staining and Immunohistochemistry

Hematoxylin and eosin (H&E) staining was performed by the Histology Platform. Briefly, paraffin-embedded tissue sections underwent xylene-based deparaffinization followed by progressive rehydration through graded ethanol solutions. Sections were subsequently stained with hematoxylin and eosin, dehydrated, and mounted for histological examination.

For CD31 immunohistochemistry, paraffin-embedded tumor sections were deparaffinized in xylene followed by graded ethanol rehydration. Antigen retrieval was performed in citrate buffer at 98°C for 30 minutes. Endogenous peroxidase activity was blocked using hydrogen peroxide, and non-specific binding sites were blocked using a solution containing 5% BSA, 10% donkey serum, 10% milk, and 0.5% Triton X-100 in TBST. Sections were incubated overnight at 4°C with an anti-CD31 primary antibody (clone SZ31, DIA-310; dilution 1:20). Following washing steps, slides were incubated with an HRP-conjugated anti-rat secondary antibody (ImmPRESS, Vector Laboratories) for 1 hour at room temperature. Signal detection was performed using DAB chromogen for 5 minutes, followed by hematoxylin counterstaining. Sections were subsequently dehydrated through graded ethanol and xylene baths and mounted using Mountex mounting medium.

13. Low-throughput proteomics

Cell sorting was performed on digested-tumor cell suspension and blood cell suspension to isolate neutrophils. Each sample contained 1000 sorted cells.

The peptides were analyzed using TIMS TOF SCP spectrometer from Bruker using the parallel accumulation-serial fragmentation (PASEF). The tims ramp voltages ranged from 0.75V to 1.25V with a ramp time of 150ms at a 100% duty cycle. The proteins were reduced using dithiothreitol (DTT, 5mM, 30min at 56°C), alkylated with iodoacetamide (10mM, 30 min at RT). The samples were then digested with trypsin (Pierce, Thermo Scientific) overnight at 37°C (50 ng of tryspin). At the end of the digestion, each sample was spiked with a commercial mixture of protein digest standards originated from non-human biological material: the MassPREP™ Digestion Standards (Waters), at 0.2 fmol of ADH per injection. Each sample was injected into the Waters Symmetry C18 5µm (180µmx20mm) trap column followed by the analytical column IonOptiks Aurora 15cm CSI (75µmx150mm). The total run time was 60 minutes with 28 minutes effective linear gradient (300 nL/min total flow rate, trap refocusing elution mode). Sample injection order on Acquity M-Class UPLC (Waters)-timsToF SCP (Bruker) was randomized and equivalent of 20 ng of protein digest were injected per sample (9 µL injection volume).

Data were processed using DIA-NN software version 1.8.2 beta 11. Oxidation of methionine and acetylation of protein N-term were set as variable modifications (maximum number of modifications per peptide set to 2), carbamidomethylation of cysteines was set as fixed modification. Charge states were fixed between 1 and 4 for precursors and m/z range from 300 to 1800. The minimal peptide length was set to 7 amino acids. The database SwissProt restricted to Mus Musculus taxonomy (17527 sequences, January 2022, the 4 proteins of MPDSMix standard were added to the fasta file) was used for interrogation. Output have been filtered at 0.01 FDR.

14. Proteomics data analysis

Protein abundance was calculated using the LFQ (label free quantification) algorithm on MaxQuant software.

Proteomics data were analyzed using Perseus software (Version 2.1.3.0) and the resulting figures were generated using GraphPad prism (Version 8.4.3).

Prior to statistical analysis, LFQ intensities were processed in Perseus. Log2 transformed LFQ intensities were analyzed using the two-sample welch test with a permutation based false discovery rate (FDR) of 0.05 and a number of randomizations of 250 and a minimum 3 valid values in at least one group.

15. Secretome analysis

After cell enrichment, bone marrow neutrophils are put in culture for 2 hours in serum free medium. 500,000 neutrophils are resuspended in 200µL of medium and cultures in 96wells cell suspension plate. At the end of the experiment, medium is collected, and supernatant is transferred to a new tube after centrifugation at 380G for 5 minutes. Secretome is saved at -20°C for the ELISA assay.

16. ELISA assay

After set up, samples were diluted 20 times in assay diluent and the protocol used was following the manufacturer instructions (RAB0373 Mouse pro-MMP-9 ELISA Kit from sigma-aldrich).

17. Seahorse

Neutrophils were enriched out of bone marrow cell suspension using stem cell kit. The oxygen consumption rate (OCR) and Extracellular acidification rate (ECAR) of isolated neutrophils were determined by Agilent Seahorse XFe96 Extracellular Flux Analyzer using XF Cell Mito Stress Test kit (Agilent Technologies, USA) according to the manufacturer's instructions. Sensor cartridge hydration was prepared a day before by adding 200ul of XF Calibrant Solution (Agilent Technologies, USA) to each well and placed in non-CO2 incubator for overnight. Isolated cells were seeded in Cell-Tak coated Seahorse XF-96 plates at density 2×10^5/well and spinned down at 200g for 3 min. Before the analysis, plates were coated with Cell-Tak solution at final concentration 0.5µg/well for cell attachment. Five to six technical replicates for each condition were plated. Cells were incubated in CO2-free incubator for 45 minutes in XF RPMI Medium pH 7.4 without FBS for stabilization before the measurement as recommended by Agilent Technologies. At the same time, each of the following compounds was loaded into the corresponding ports on a Seahorse cartridge and calibrated in the XF96 instrument: port A – Oligomycin (2 µM); port B – CCCP (15 µM); port C – Rotenone (2 µM) and Antimycin A (1 µM). The drugs were subsequently injected to reveal the key parameters showing mitochondrial function. Finally, basal respiration, ATP production, maximal respiration, spare capacity and proton leak were calculated.

18. Metabolomics

Stable isotope tracing experiments were performed as described in Kiweler, 2022. Briefly, [U-13C]-Glutamine (Cambridge Isotope Laboratories, CLM-1822) tracing was performed in DMEM medium (Thermo Fisher Scientific, A1443001) with 4 mM Glutamine, 25 mM Glucose and 10% FBS. For tracing, 1 million of freshly isolated neutrophils were washed with PBS and seeded in [U-13C] Glutamine DMEM medium in 24-well plates for 2hrs in duplicates. Identical extra wells per condition were counted to assess cell number for normalization. Cells were incubated for the indicated times (3 hours) and triplicate wells was used for metabolite extraction. Cells were washed with 500µl cold PBS by centrifugation and extracted with 100µl extraction solvent (MeOH/Acetonitrile/H2O, 50/30/20) with internal standards for 5 min at 4°C under agitation. Extraction solvent was centrifuged full speed 16000g for 10 min at 4°C and supernatant was submitted for LC-MS analysis.

Metabolite analyses were performed using a Thermo Vanquish Flex Quaternary LC coupled to a Thermo Q Exactive HF mass spectrometer. Chromatography was carried out with a SeQuant ZIC-pHILIC 5 µm polymer (150 × 2.1 mm) column connected to the corresponding SeQuant ZIC-pHILIC Guard (20 × 2.1 mm) pre-column. Column temperature was maintained at 45°C. The flow rate was set to 0.2mL/min and the mobile phases consisted of 20mmol/L ammonium carbonate in water, pH 9.2 (Eluent A) and Acetonitrile (Eluent B). The gradient was: 0 min, 80% B; 2 min, 80% B; 17 min, 20% B; 18 min 20% B; 19 min 80 % B; 20 min 80% B (0.4 mL/min); 24 min 80% B (0.4 mL/min); 24.5 min 80% B. The injection volume was 5µL. All MS experiments were performed using electrospray ionization with polarity switching enabled (+ESI/-ESI). The source parameters were applied as follows: sheath gas flow rate, 25; aux gas flow rate, 15; sweep gas flow rate, 0; spray voltage, 4.5 kV (+) / 3.5 kV (–); capillary temperature,325°C; S-lense RF level, 50; aux gas heater temperature, 50°C. The Orbitrap mass analyzer was operated at a resolving power of 30,000 in full-scan mode (scan range: m/z 75…1000; automatic gain control target: 1e6; maximum injection time: 250 ms). Data were acquired with Thermo Xcalibur software (Version 4.3.73.11) and analyzed with TraceFinder (Version 5.1). Subsequent data analysis for normalization and natural isotope subtraction was performed using Metabolite AutoPlotter (Pietzke, 2020).

19. Data integration

To compare transcriptomic and proteomic alterations associated with ELP3 deletion in neutrophils, single-cell RNA-seq data from the neutrophil cluster and low-input proteomics data obtained from PyMT ELP3^{NEU} and PyMT ELP3^{CTR} samples were integrated. Genes detected in both datasets were matched based on gene symbols and classified according to their differential expression between conditions. Low-input proteomic analysis identified approximately 3,000 proteins, resulting in a total of 3,155 genes shared between the proteomic and transcriptomic datasets. To identify discordant regulation between RNA and protein abundance, genes were categorized based on their log2 fold-change (log2FC) values. Genes were considered candidates for post-transcriptional regulation when protein abundance was decreased (log2FCprotein [PyMTELP3^{NEU}/PyMTELP3^{CTR}] < -0.5) while transcript levels were unchanged or increased (log2FCRNA ≥ 0). Conversely, genes were also selected when protein abundance was increased (log2FCprotein > 0.5) while transcript levels were unchanged or decreased (log2FCRNA ≤ 0). These criteria enabled the identification of genes displaying opposing trends at the transcript and protein levels. Correlation analyses were performed using GraphPad Prism. Both Pearson's correlation coefficient and Spearman's rank correlation coefficient were calculated to assess the relationship between transcriptomic and proteomic fold-change values across genes shared between the two datasets.

Product	Manufacturer	Reference
Ly6G-APC-Cy7	BD-Pharmingen	560600
CD11b-APC	INVITROGEN	17-0112-82
CD45-BV421	BIOLGEND	1031134
CD45-Biotin	BD	553078
FITC-VD	Biolegend	565802
7AAD -VD	BD-Pharmingen	559925
Zombie VD	BD	423107
CD127_CY7	BIOLEGEND	158209
CD19CY5.5	BIOLEGEND	B354914
FOXP3_PE	BIOLEGEND	118903
GDTCR BV421	BD HORIZON	562892
CD63PE	BD-Pharmingen	564222
NKP46_BUV737	BD HORIZON	612805
Red blood cell lysis	Miltenyi	130-094-183
Mouse neutrophil enrichment kit	Stemcell	19762A
CD45 enrichment kit	Stemcell	18945
Seahorse XFe96/XF Pro FluxPak Mini	Agilent	103793-100
Corning® Cell-Tak(TM) Cell and Tissue Adhesive	Sigma	CLS354240
ELISA-VEGF	Sigma	RAB0509-1KT
ELISA-MMP9	Sigma	RAB0373-1KT
DHR123-Cellular ROS	BQC	KP06004

Results

Results

I. Tumor Infiltrating Neutrophil reprogramming in breast cancer

Neutrophils undergo extensive transcriptional reprogramming upon infiltration into the tumor microenvironment, driven by local signals such as cytokines, hypoxia, and cellular interactions. This remodeling reshapes gene regulatory networks and activates distinct effector programs that underpin the specialized functions of tumor infiltrating neutrophils, distinguishing them from normal neutrophils.

We investigated the gene expression remodeling taking place in tumor infiltrating neutrophils (TINs) in murine breast cancer from a publicly available RNA-seq dataset (GSE164766) (Timaxian *et al.*, 2021). This dataset displays gene expression profiles of TINs (i.e. PyMT TINs) isolated from the MMTV-PyMT mouse model compared to bone marrow normal neutrophils (i.e. BM NN) from healthy mice.

Raw count data were processed using the DESeq2 pipeline in R-studio, and differential gene expression (DGE) analysis was performed using the Wald test. Principal component analysis (PCA) was conducted as part of quality assessment and revealed clear segregation between TIN samples and bone marrow neutrophils (Fig 16-c), indicating distinct global transcriptional profiles.

As described in figure 16-a, DGE analysis identified extensive transcriptional changes in TINs relative to bone marrow neutrophils, with 6,999 genes significantly upregulated and 5,137 genes significantly downregulated.

To gain functional insight into these transcriptional modifications, Gene Set Enrichment Analysis (GSEA) was performed. Multiple pathways were significantly modulated in TINs, indicating broad transcriptional reprogramming upon tumor infiltration (Fig 16-b), potentially linked to specific functions of TINs.

The transcriptional profile of tumor-infiltrating neutrophils was characterized by enrichment of TNFα/NF-κB and inflammatory response gene sets, supporting a model in which exposure to tumor derived cytokines and inflammatory mediators rewires neutrophil regulatory networks toward a tumor adapted state. Such programs are consistent with previous reports describing

tumor associated neutrophils as key amplifiers of local inflammation and as active participants in immunomodulatory and pro-tumoral signaling pathways. In addition, the enrichment of an estrogen response signature suggests that, in this tumor context, neutrophil reprogramming may also be shaped by hormone dependent microenvironmental signals. This observation is particularly plausible in mammary tumors, where estrogen has been shown to influence neutrophil recruitment and pro-tumoral activity (Rae & Lippman, J Clin invest, 2021).

While translational regulation has been described in neutrophils, it remains comparatively less well characterized than transcriptional control. Notably, we observed differential expression of tRNA modifying enzymes, suggesting that tumor infiltrating neutrophils may undergo remodeling of the translational machinery itself. Such changes could influence codon dependent translation efficiency and selectively regulate protein synthesis downstream of mRNA abundance. In a volcano plot, we highlighted the changes observed in tRNA modifying enzymes expression (in green), with enzymes associated with wobble urine (U34) tRNA modification specifically indicated (in red). Of note, most of the genes (ELP2-ELP6, CTU1-CTU2, ALKBH8) defining the U34 tRNA modification pathway (Rapino et al., Nature, 2018) were upregulated in TINs compared to bone marrow neutrophils (Fig 16-d).

A focused visualization using a heatmap of $\log_2$ fold change values comparing TINs to normal neutrophils confirmed coordinated upregulation of U34 regulating enzymes, except for ELP1 (Fig 16-f). These findings indicate that components of the U34 tRNA modification pathway are transcriptionally upregulated in tumor infiltrating neutrophils.

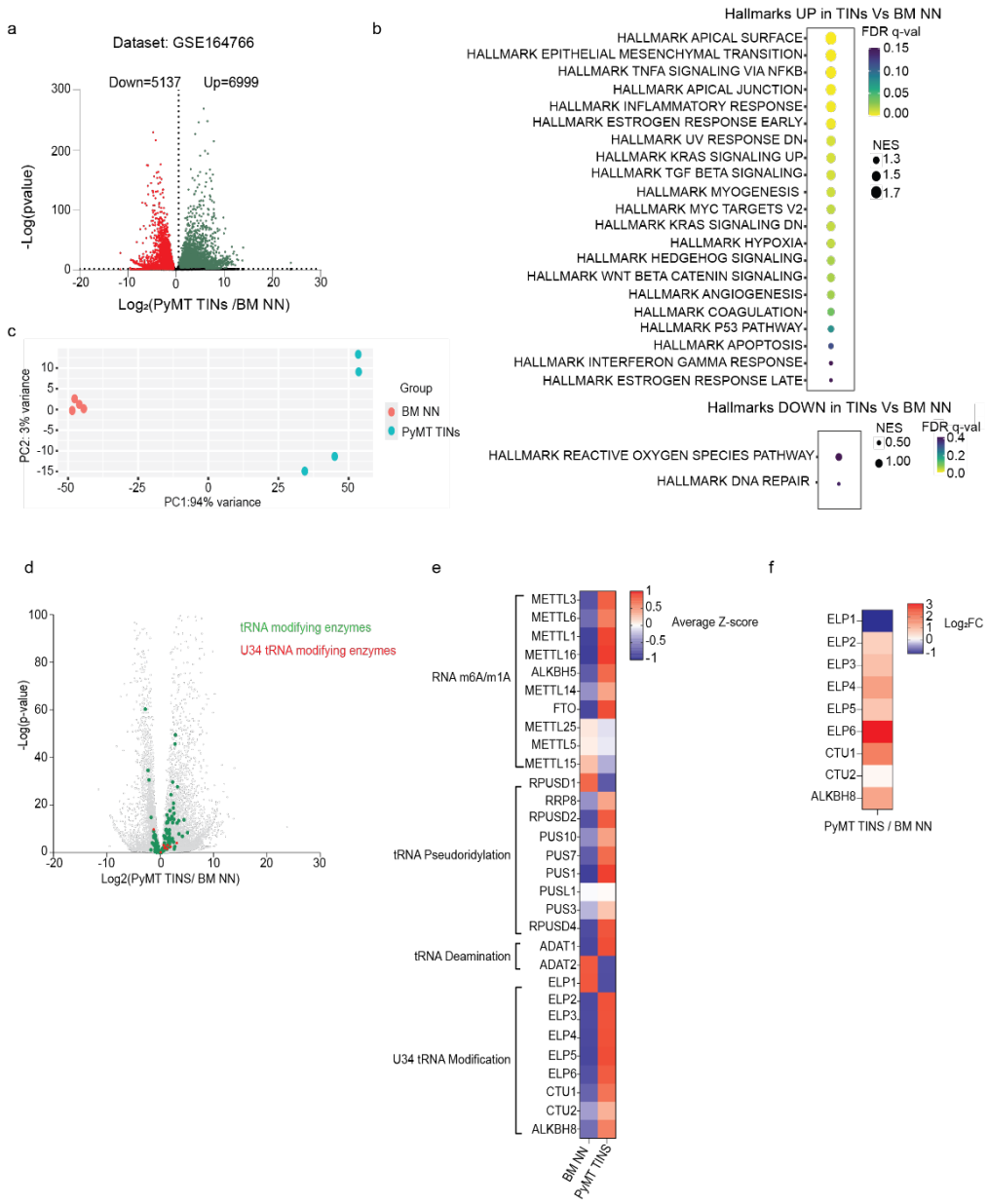

Figure 16: Tumor infiltrating neutrophils exhibit increased expression of tRNA modifying enzymes. a. RNAseq results of PyMT Tumor Infiltrating neutrophils (PyMT TINs) compared to bone marrow normal neutrophils (BM NN) (Dataset extracted from GEO/Accession number GSE164766) using Deseq2 pipeline and Wald statistical test (n=4 per group), b. Gene set enrichment analysis performed on RNAseq data, c. PCA analysis comparing the different samples used in the analyzed dataset. The analysis was performed using Deseq2 pipeline as a quality control step, d. Highlight of the tRNA modifying enzymes distribution in the dataset, e. Heatmap showing the average z-score of 4 tRNA modifying enzymes families in BM normal neutrophils (BM NN) and PyMT TINs, f. Heatmap of the size effect of U34 modifying enzymes in TINs compared to BM NN.

The coordinated upregulation of U34 tRNA modifying enzymes in TINs suggests that this pathway may contribute to the gene expression reprogramming observed upon tumor infiltration. However, whether enhanced U34 dependent modification has functional consequences for neutrophil biology within the tumor microenvironment remained unknown. To directly assess the role of this pathway in vivo, we generated a neutrophil specific knockout mouse model targeting ELP3, a key U34 tRNA modifying enzyme and the catalytic subunit of the elongator complex. This model allows us to investigate its contribution to neutrophil function under steady state conditions and during PyMT-driven breast tumor progression.

II. U34 tRNA modifying enzymes in neutrophils

1. Mouse model

To investigate the role of ELP3 in neutrophils under both physiological and tumor-bearing conditions, we utilized a conditional knockout mouse model ($ELP3^{LoxP/LoxP}$) available in our laboratory. In this model, exon 2 of the Elp3 gene is flanked by loxP sites. Upon expression of CRE recombinase, exon 2 is deleted, resulting in a frameshift and the introduction of a premature stop codon, thereby leading to loss of ELP3 protein expression and function in vivo (Ladang et al., 2015; Laguesse et al., 2015; Delaunay et al., 2016).

To achieve neutrophil specific deletion, we crossed these mice with a CRE-expressing line driven by the S100A8 promoter (also referred to as MRP8-CRE) (Zhao. Et al, Cell metabolism 2023; Nemeth et al., Nature Comm, 2016). Mice carrying both the floxed Elp3 alleles and the MRP8-CRE transgene are referred to as $ELP3^{NEU}$ ($ELP3^{LoxP/LoxP}$ - MRP8-CRE), whereas littermate controls lacking Cre ($ELP3^{LoxP/LoxP}$) are referred to as $ELP3^{CTR}$.

The generated steady state mouse model was crossed with the MMTV-PyMT mice and led to the formation of PyMT mice with the loss of ELP3 in neutrophils (PyMT $ELP3^{NEU}$ and control PyMT $ELP3^{CTR}$ mice are lacking the CRE-recombinase gene).

To validate ELP3 depletion in neutrophils and assess the specificity of the MRP8-Cre model, neutrophils (CD11b+Ly6G+) and monocytes/macrophages (CD11b+Ly6G−) were isolated by cell sorting. Following DNA extraction, PCR amplification was performed using primers 1808 and 1809, designed to

amplify the region spanning the 5′ and 3′ ends of exon 2. The results confirmed the deletion of exon 2 in ELP3-deficient neutrophils, whereas no deletion was detected in the monocyte/macrophage population, supporting the specificity of the recombination in the targeted cell compartment (Figure 17).

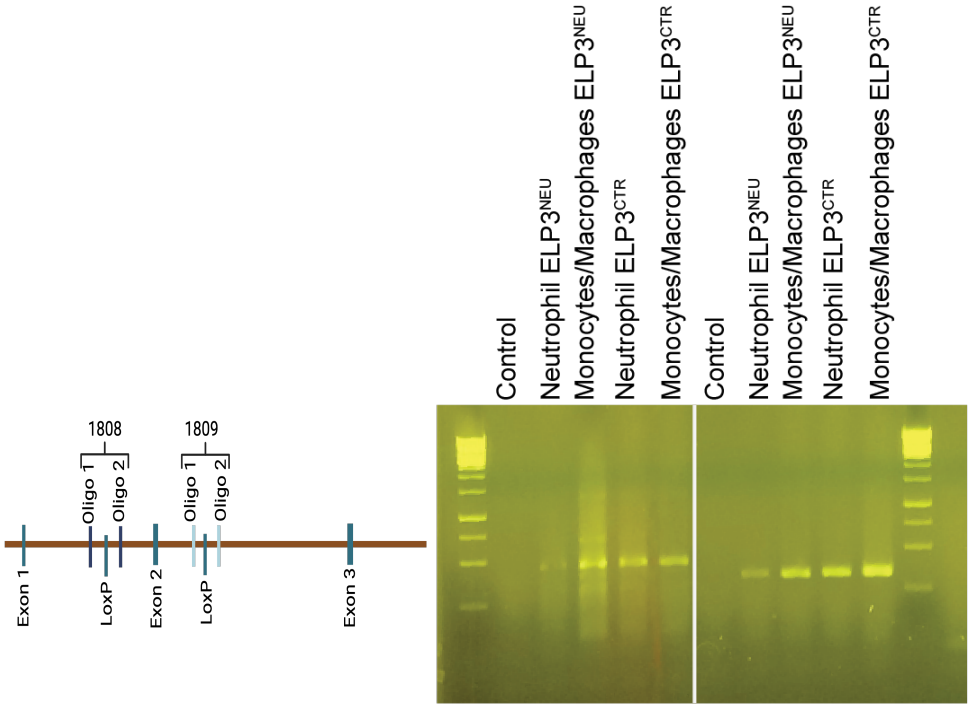

Figure 17: Figure 17: Validation of ELP3 exon 2 deletion in sorted neutrophils and monocytes/macrophages. Agarose gel electrophoresis of PCR products obtained using primer sets 1808 and 1809, designed to amplify the region encompassing exon 2 of the Elp3 gene. For each primer set, lanes correspond to negative PCR control, ELP3NEU neutrophils (CD11b+Ly6G+), monocytes/macrophages (CD11b+Ly6G−) from ELP3NEU mice, wild-type neutrophils (CD11b+Ly6G+), and wild-type monocytes/macrophages (CD11b+Ly6G−). The absence of amplification in ELP3-deficient neutrophils confirms the deletion of exon 2 in the targeted cell population, whereas amplification is maintained in the control populations. Primers used 1808_F: CGTGTTTGCTGCCATCACC, 1808_R: GCACGATTGCCACATCATCC, 1809_F: GCAAACTGACCTAAAGCTACC, 1809_R: TTCCTTCGGTTTCTGTGACC. Using primer 1808, a 172 bp PCR product was detected in the wild-type (WT) allele. Using primer 1809, a 189 bp product was obtained in the WT condition; however, this band was absent in the knockout (KO) samples due to the deletion of the target region normally amplified by this primer pair.

2. Steady-state neutrophil homeostasis is preserved following ELP3 depletion

2.1. Neutrophil expansion

To determine whether neutrophil specific deletion of ELP3 affects neutrophil homeostasis, neutrophil proportions were quantified in bone marrow, blood, spleen, and lung under steady state conditions at 12 weeks. Comparable neutrophil levels were observed between control and knockout mice across all tissues examined, indicating that ELP3 depletion does not alter baseline neutrophil distribution or expansion (Fig 18-a). A slight increase in lung neutrophils was detected in $ELP3^{NEU}$ mice.

To further evaluate the expansion capacity of ELP3-deficient neutrophils in vivo, mice were treated with GM-CSF, a cytokine known to promote neutrophil proliferation and mobilization. GM-CSF administration resulted in the expected increase in neutrophil numbers; however, no significant differences were observed between control and knockout mice. These findings indicate that the depletion of ELP3 does not impair neutrophil responsiveness to proliferative stimuli in vivo (Fig 18-c).

Finally, neutrophils morphology was examined using H&E staining. Our analysis shows that ELP3-depleted neutrophils show normal multilobed nucleus (Fig 18-b), indicating that ELP3 loss does not impact global morphology of neutrophils.

2.2. Neutrophils viability

To assess whether the depletion of ELP3 affects neutrophil survival, neutrophil viability was monitored using Incucyte live cell imaging. Neutrophils were cultured in the presence or absence of G-CSF (200ng/mL), a cytokine known to promote neutrophil survival. As expected, G-CSF supplementation prolonged neutrophil lifespan; however, comparable survival kinetics were observed between control and ELP3 deficient neutrophils under both culture conditions.

These results indicate that ELP3 depletion does not impair neutrophil viability or responsiveness to survival signals in vitro (Fig 18-d).

2.3. ROS production in neutrophils

To evaluate whether ELP3 deletion affects neutrophil activation, reactive oxygen species (ROS) production was assessed in bone marrow neutrophils

isolated from steady-state mice following stimulation with 100 nM PMA. ROS production was quantified by flow cytometry after gating on live neutrophils ($CD45^+$ $CD11b^+$ $Ly6G^+$). PMA stimulation (30 minutes) induced comparable ROS responses in control and ELP3 deficient neutrophils, with no significant differences observed between the two groups.

These findings indicate that ELP3 deletion does not impair neutrophil oxidative burst capacity under steady-state conditions (Fig 18-e).

2.4. Neutrophils migration

To assess whether ELP3 loss affects neutrophil migratory capacity, migration assays were performed using Boyden chambers using 100nM FMLP as a chemoattractant. After 2 hours of incubation at 37°C, comparable numbers of control and ELP3 deficient neutrophils migrated toward FMLP supplemented medium, with no significant differences observed between the two groups (Fig 18-f). A negative control using HBSS only was used and showed no migration at the end of the experiment.

These results indicate that ELP3 depletion does not impair neutrophil chemotactic responses in steady state conditions.

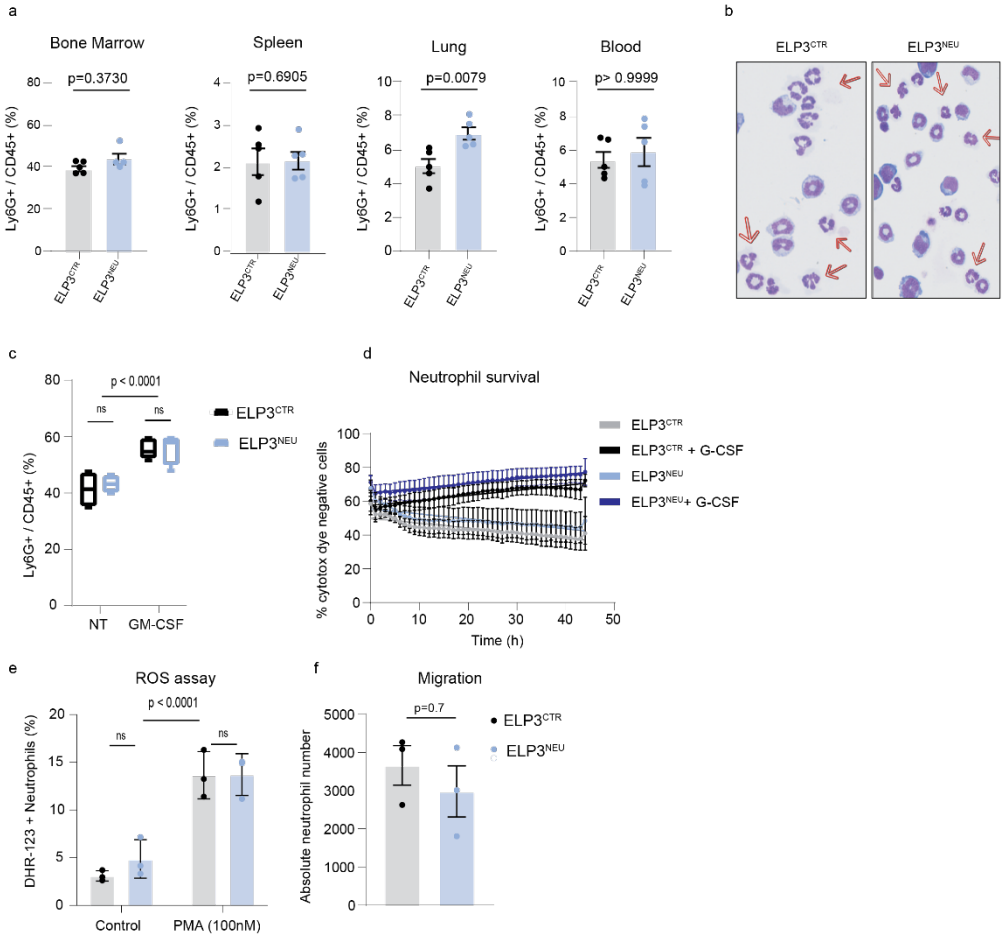

Figure 18: ELP3 is dispensable for steady state neutrophils integrity. a. Neutrophil expansion in BM, spleen, lung and blood of steady state ELP3^{CTR} and ELP3^{NEU} mice at 12 weeks (n=5 , Mann-Whitney test), b. H&E staining showing neutrophil morphology comparison between enriched BM neutrophils from ELP3^{CTR} and ELP3^{NEU} mice, c. Neutrophil expansion in blood upon 5 days of GM-CSF injection in steady state mice (n=4, Mann-Whitney test), d. Neutrophil survival comparison between ELP3^{CTR} and ELP3^{NEU} cultured in the absence or presence of G-CSF and followed over time (100000 Neutrophils/ well were plated and culture medium was supplemented with 500nM of SARTORIUS Red cytotox dye, G-CSF was supplemented at a concentration of 200ng/mL) e. Cellular Reactive oxygen species (ROS) measurement using DHR123 probe in enriched BM neutrophils upon stimulation using PMA (100nM) for 30 minutes (n=3, Mann-Whitney test) , f. Absolute number of ELP3^{CTR} and ELP3^{NEU} migrating neutrophils in Boyden chamber after 2hours of culture and using 100nM FMLP as chemoattractant (n=3, Mann-Whitney test).

Collectively, these findings demonstrate that ELP3 loss in neutrophils does not affect their development, morphology, or canonical effector functions under steady state conditions.

III. Loss of ELP3 in tumor associated neutrophils in PyMT breast cancer model

ELP3 depletion did not affect neutrophil homeostasis under steady-state conditions. Moreover, RNA-seq analysis indicated that bone marrow neutrophils are transcriptionally distinct from tumor-infiltrating neutrophils, highlighting context-dependent reprogramming within the tumor microenvironment. We therefore investigated the impact of neutrophil-specific ELP3 deletion on breast tumor progression using PyMT ELP3^{CTR} and PyMT ELP3^{NEU} mice.

1. Tumor initiation

First, we investigated whether neutrophil specific ELP3 loss affects early tumor development. Mammary gland morphology and tumor initiation were evaluated in PyMT ELP3^{CTR} and PyMT ELP3^{NEU} mice at early time points. Carmine alum staining was performed to visualize the mammary ductal tree and early tumor foci at 4.5 and 6 weeks of age (Fig 19-a).

A comprehensive quantitative assessment of the fourth mammary gland morphology was performed at 4.5 and 6 weeks, including: tumor and ductal tree size, end point, branching, and terminal end bud (TEB) density, and ductal tree length. Eight mammary glands per group were spread onto slides and stained with a carmine solution. Analysis was performed as described in Blacher et al. 2016 using automated digital image processing to minimize manual bias. Our analyses show that no differences were observed between control and ELP3 deficient mice for any of the parameters analyzed, indicating that the loss of ELP3 in neutrophils does not affect PyMT-driven tumor initiation.

2. Tumor progression

Next, in order to determine if ELP3-deleted neutrophils may impact the growth of the primary PyMT breast tumors, we followed tumor growth over time in PyMT ELP3^{CTR} and PyMT ELP3^{NEU} mice.

To do so, tumor burden was evaluated at successive time points between 8 and 14 weeks of age by measuring total tumor weight normalized by mouse body weight (BW) per mouse. Tumor weight was normalized to body weight

to account for variability in animal size and overall body mass between mice. This normalization allows a more accurate comparison of tumor burden across animals by reducing the influence of natural differences in body size, which may arise from litter-to-litter variability.

PyMT ELP3^{NEU} mice exhibited a pronounced delay in primary tumor progression compared to PyMT ELP3^{CTR} group. This difference was maintained over several weeks (Fig 19-b), up to 12 weeks of age onward. From that age onwards, tumor growth in PyMT ELP3^{NEU} mice started to rise and followed a slope comparable to control mice. This indicates that ELP3 loss in neutrophils impacts early tumor growth.

Despite this later convergence in growth kinetics, PyMT ELP3^{NEU} mice reached comparable tumor burden with a delay of more than 6 weeks (at 18 weeks of age) compared to PyMT ELP3^{CTR} control mice (Fig 19-c).

These results show that neutrophil specific ELP3 depletion in neutrophils strongly delays primary tumor progression that is overcome with time, after approximatively 12 weeks of tumor development.

3. Tumor metastasis

The MMTV-PyMT mouse model of breast cancer is characterized by progressive tumor development and spontaneous metastatic dissemination into lungs after approximatively 12 weeks of age (Attala.et al., 2021).

Lung metastasis was assessed in PyMT ELP3^{NEU} mice compared to PyMT ELP3^{CTR} mice using histological approaches.

H&E staining of lung sections was performed to quantify the number and surface area of intrapulmonary metastatic lesions (Fig 19-d).

Interestingly, our data showed a marked reduction in metastatic burden in PyMT ELP3^{NEU} mice compared to PyMT ELP3^{CTR} controls. While metastatic lesions were consistently detected in PyMT ELP3^{CTR} lungs, strong reduction of metastases was observed in PyMT ELP3^{NEU} 12 weeks old mice.

At the ethical endpoint, metastatic lesions were detectable in a subset of PyMT ELP3^{NEU} mice. However, metastatic burden remained reduced compared to PyMT ELP3^{CTR} control mice, with fewer metastatic foci and smaller lesion sizes (Fig 19-d, e).

Of note, the ethical endpoint was reached at approximately 12 weeks of age in PyMT ELP3^{CTR} mice, whereas PyMT ELP3^{NEU} mice remained below the ethical threshold beyond 18 weeks of age.

Notably, a significant proportion of PyMT ELP3^{NEU} mice remained completely metastasis free even at the ethical endpoint.

These findings indicate that ELP3 loss in neutrophils is associated with strong impairment of metastatic progression in the PyMT breast cancer model.

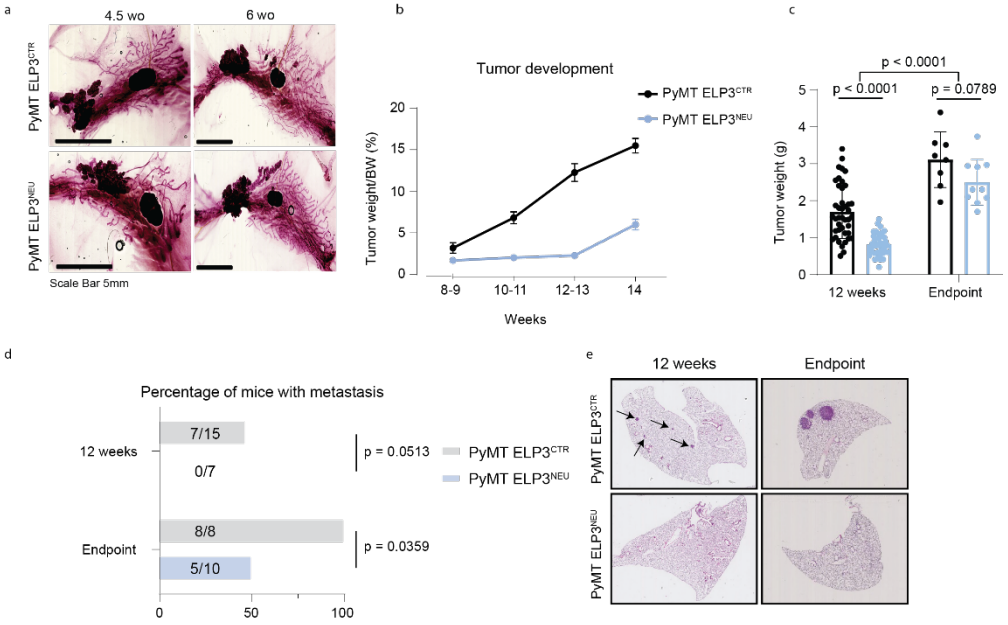

Figure 19: ELP3 loss in neutrophils and its impact on tumor growth and metastasis a. Representative pictures at 4.5 and 6weeks old of the fourth mammary gland showing the initiation of tumor growth, b. Tumor growth curve starting from 8 weeks to 14 weeks of age (n=min 4 per group of age). Tumor progression was monitored by measuring tumor weight and expressing it as a percentage of total body weight, c. Tumor weight at 12 weeks and at endpoint (12 weeks: n=min39 , endpoint: n=min8, Mixed effect model analysis), d. Percentage of mice presenting lung metastasis at 12 weeks and ethical end point (Fischer Test), e. Representative H&E staining of lung metastasis at 12 weeks and endpoint in PyMT ELP3^{CTR} and PyMT ELP3^{NEU} mice

4. Loss of ELP3 in neutrophils induces a delay of stage and impairs vasculature in primary tumors

To refine the characterization of this phenotype, histological analyses were performed to evaluate tumor stage and vascularization. Histopathological evaluation revealed a delay in tumor staging in PyMT ELP3^{NEU} mice compared to PyMT ELP3^{CTR} mice. PyMT ELP3^{NEU} tumors displayed a higher proportion

of mammary intraepithelial neoplasia (MIN), whereas tumors from PyMT ELP3^{CTR} control mice more frequently progressed to advanced carcinoma stages. In addition, tumor foci observed in PyMT ELP3^{NEU} mice were generally smaller than those detected in PyMT ELP3^{CTR}, consistent with the delayed tumor growth observed *in vivo* (Fig 20-a, b, c).

The progression from MIN to carcinoma involves a shift toward increased angiogenesis, a process supported by neutrophils through the secretion of pro-angiogenic factors (Bergers and Benjamin, 2003).

To address this, we sought to investigate whether the vascularization was affected in these tumors, CD31 immunostaining was performed to assess tumor blood vessel density. Quantification of CD31 positive structures revealed a higher level of vascular staining in PyMT ELP3^{CTR} tumors compared to PyMT ELP3^{NEU} tumors, suggesting that tumor vasculature might be impaired in the absence of ELP3 in neutrophils (Fig 20-d).

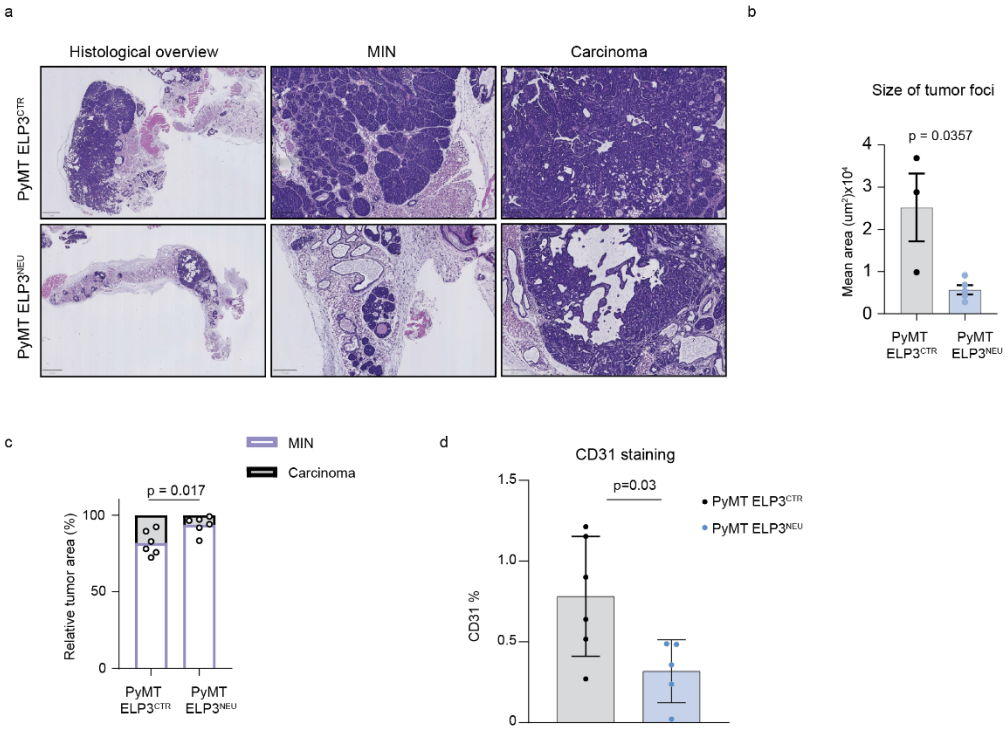

Figure 20: PyMT ELP3^{NEU} tumors show a lower grade of tumor progression and angiogenesis impairment a. Representative H&E tumor histology of PyMT ELP3^{CTR} and PyMT ELP3^{NEU} tumors showing Minimally Invasive Neoplasia (MIN) and carcinoma, b. Tumor size foci (Analysis was performed using Qupath, n=6, Mann-whitney test) c. Relative MIN and Carcinoma (Analysis was performed using Qupath, n=6 , Permanova test), d. CD31 staining for tumor vasculature detection (n=5, Mann Whitney test)

5. ELP3 depletion in neutrophils does not alter the tumor immune landscape

The tumor immune microenvironment plays a central role in shaping tumor progression by influencing the balance between pro- and anti-tumor immune responses. Neutrophils exhibit remarkable functional plasticity as they can suppress T cell activity through the release of immunosuppressive factors and inhibitory signals, or, conversely, promote T cell activation and enhance anti-tumor immunity (Wu. Et al., 2024, Jin. Et al., 2021). To investigate whether PyMT ELP3^{NEU} can modulate the tumor immune microenvironment we performed single cell RNA-sequencing at 10 weeks of age followed by flow cytometry immune profiling to confirm our findings.

5.1. Single cell RNA seq

To investigate the tumor immune microenvironment remodeling hypothesis, single-cell RNA sequencing (scRNA-seq) was performed on both CD45+ enriched fractions and whole tumor samples. Datasets were integrated using the RPCA workflow, and clustering analysis was performed with Seurat v5 using standard suggested parameters. This analysis identified 17 distinct cellular clusters within the tumor microenvironment (Fig 21).

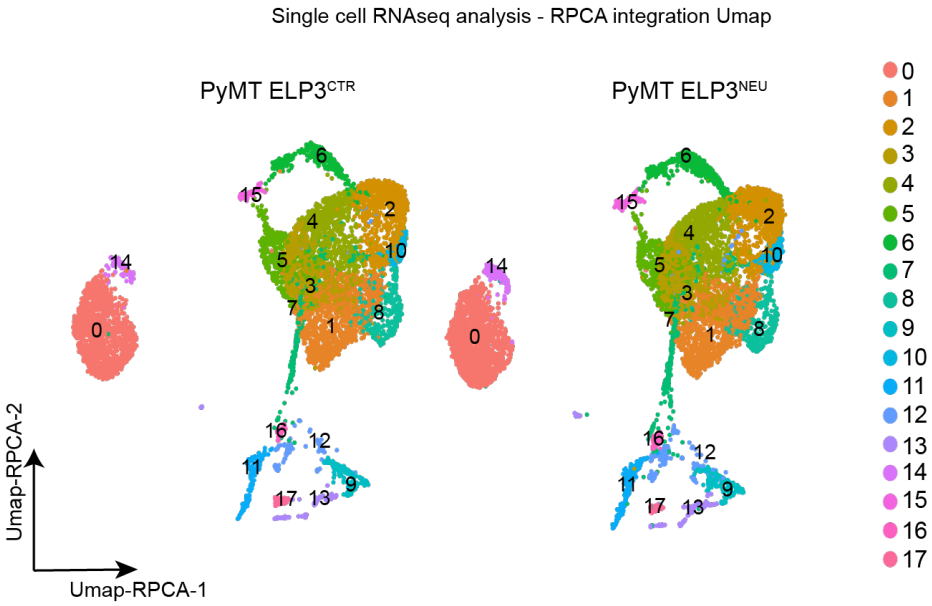

Figure 21: Single cell analysis at 10 Weeks Old – Datasets RPCA integration results (4 tumors were used for the CD45+ enriched dataset and 3 tumors were used for the whole tumor dataset)

Cluster identities were assigned based on the expression of established lineage markers extracted from PangolaoDB (Franzén. Et al., 2019) (Fig 22-a, b), and annotated cell populations were visualized using a simplified UMAP representation (Fig 22-c). The PyMT tumor immune microenvironment was predominantly composed of T cells, representing more than 60% of immune cells, followed by approximately 20% B cells and smaller populations of macrophages/monocytes and NK cells as described in Attalla. Et al., 2021.

Quantification of cell type proportions revealed no significant differences between PyMT ELP3^{CTR} and PyMT ELP3^{NEU} tumors across the major immune populations analyzed (Fig 22-d).

Moreover, differential gene expression analysis was performed within the principal immune cell populations, including T cells, B cells, macrophages, monocytes, and NK cells. Surprisingly, no consistent transcriptional differences were detected between PyMT ELP3^{CTR} and PyMT ELP3^{NEU} tumors in the investigated immune cells (Fig 22-e, f, g, h).

Together, these results indicate that neutrophil-specific deletion of ELP3 does not substantially alter the composition or transcriptional profiles of the major immune populations within the PyMT tumor microenvironment.

Neutrophils were detected in the scRNA-seq dataset. However, this population was represented by a limited number of cells (i.e. 158 neutrophils in total). This limitation restricted the statistical power of downstream analyses. Nevertheless, we performed differential gene expression analysis comparing neutrophils of PyMT ELP3^{CTR} and PyMT ELP3^{NEU} tumors (Fig 22-i).

This analysis identified only two genes (ACOD1 and IFITM1) meeting the significance threshold in the comparison between conditions, while no broader transcriptional changes were detected. The biological relevance of these isolated transcriptional changes remained unclear and was not further investigated due to limited biological material (low number of neutrophils in the tumor).

Of note, structural cell populations, which include epithelial and endothelial cells, showed low transcriptomic quality and were therefore excluded from further analysis.

These findings suggest that the delayed tumor progression observed upon the loss of ELP3 in neutrophils occurs independently of the immune compartment

remodeling and instead point toward a direct effect of ELP3^{NEU} neutrophils on tumor cells.

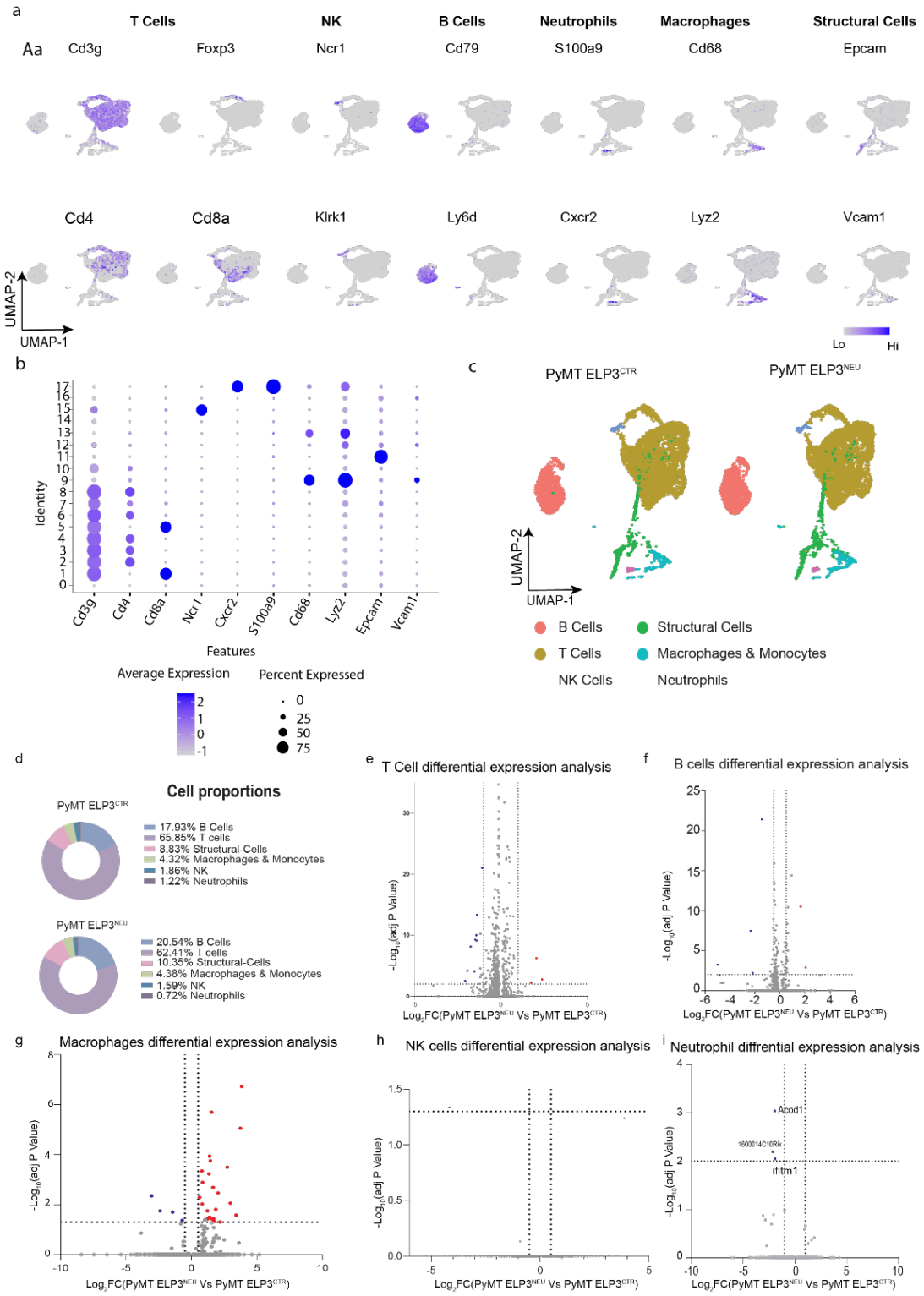
a
T Cells
NK
B Cells
Neutrophils
Macrophages
Structural Cells
Aa
Cd3g
Foxp3
Ncr1
Cd79
S100a9
Cd68
Epcam
Cd4
Cd8a
Klrk1
Ly6d
Cxcr2
Lyz2
Vcam1
UMAP-2
UMAP-1
Lo
Hi
b
Identity
Features
Average Expression
Percent Expressed
c
PyMT ELP3CTR
PyMT ELP3NEU
B Cells
T Cells
NK Cells
Structural Cells
Macrophages & Monocytes
Neutrophils
d
Cell proportions
PyMT ELP3CTR
17.93% B Cells
65.85% T cells
8.83% Structural-Cells
4.32% Macrophages & Monocytes
1.86% NK
1.22% Neutrophils
PyMT ELP3NEU
20.54% B Cells
62.41% T cells
10.35% Structural-Cells
4.38% Macrophages & Monocytes
1.59% NK
0.72% Neutrophils
e
T Cell differential expression analysis
f
B cells differential expression analysis
g
Macrophages differential expression analysis
h
NK cells differential expression analysis
i
Neutrophil diffrential expression analysis
Apod1
1600014C10Rik
ifitm1
-Log10(adj P Value)
Log2FC(PyMT ELP3NEU Vs PyMT ELP3CTR)

Figure 22: Single cell RNA seq analysis of the tumor microenvironment in PyMT ELP3^{CTR} and PyMT ELP3^{NEU} mice at 10WO. a. Feature plot for cluster annotation. Cd3g, Cd4, Cd8a and Foxp3 where used to detect T cells cluster, Ncrc1, Klrk1 were used for NK cells, Cd79 and Ly6d were used for B cells detection, Neutrophils were identified using S100a9 and Cxcr2 expression, Macrophages were detected using Cd68 and Lyz2 expression, Epcam and Vcam1 were used for structural cells, b. Bubble plot showing the same markers for a better identification of the clusters, c. Annotated Umap of the tumor microenvironment of PyMT ELP3 ^{CTR} and PyMT ELP3^{NEU} , d. Cell proportions in each cluster in PyMT ELP3 ^{CTR} and PyMT ELP3^{NEU} , e. T cell differential expression analysis displayed in a volcano plot format, f. B cells differential expression analysis, g. Macrophages differential expression analysis, h. NK cells differential expression analysis, i. Neutrophils differential expression analysis (All the data were generated using Seurat V5 pipeline and following RPCA method integration, n=min3)

Given that T cells represented the most abundant immune compartment detected in the single cell dataset, we further investigated potential differences in T cell functional states between conditions. To this end, module score analyses were performed to evaluate transcriptional programs associated with T cell activation, differentiation, and exhaustion.

UMAP visualization first confirmed a comparable distribution of the major T cell subsets across conditions, including CD4$^+$ T cells, CD8$^+$ T cells and regulatory T cells (Tregs) (Fig 23-a). To assess potential functional differences, several pathway-specific module scores were calculated. Module scores calculate the average expression levels of each pathway on single cell level, subtracted by the aggregated expression of control feature sets. All analyzed features are binned based on averaged expression, and the control features are randomly selected from each bin (Satija. Et al., 2015). The tested pathways included CD4$^+$ T cell activation signatures, T cell receptor (TCR) signaling in CD4$^+$ T cells, naïve and memory T cell programs, exhausted CD4$^+$ T cell signatures, JAK-STAT signaling pathways, as well as granzyme associated signatures and effector programs in CD8$^+$ T cells (Fig 23-b, c, d, e, f, g, h).

Visualization of these module scores across the UMAP revealed similar distributions between conditions, with no apparent changes in the activation or exhaustion states of T cell populations. Although statistical analysis identified significant differences in module scores between groups, the magnitude of these differences was modest and did not correspond to a clear shift in their distribution. These results suggest that neutrophil specific ELP3 deletion does not markedly alter T cell transcriptional programs within the tumor microenvironment but may instead exert only subtle effects on pathway associated gene expression.

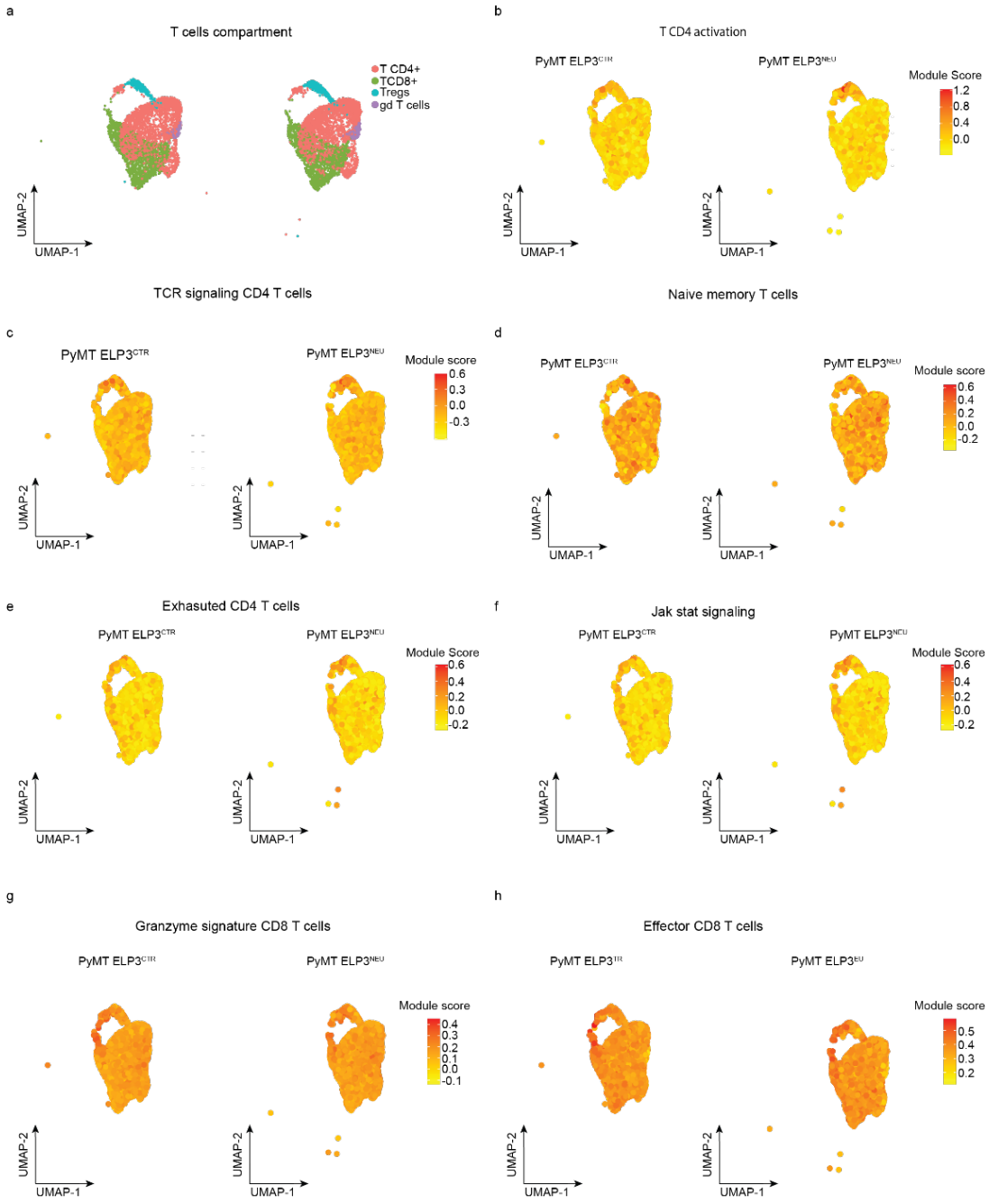

Figure 23: Single-cell transcriptomic analysis of T cell functional states in the tumor microenvironment. a. UMAP of T cells compartment in PyMT ELP3 ^{CTR} and PyMT ELP3^{NEU} tumors, b. Module score projection of TCD4 activation program on UMAP (Median PyMT ELP3^{CTR}= -0.0858 , Median PyMT ELP3^{NEU}= -0.094, p-value=0.00156), c. Module score projection of CD4+ TCR signaling program (Median PyMT ELP3^{CTR}= 0.133, Median PyMT ELP3^{NEU}= 0.1120, p-value=4.048752e-18), d. Module score projection of Naïve Memory T cells signature(Median PyMT ELP3^{CTR}= 0.07, Median PyMT ELP3^{NEU}= 0.08, p-value=0.007), e.

Module score projection of Exhausted CD4+ T cells signature(Median PyMT ELP3^{CTR}= -0.084, Median PyMT ELP3^{NEU}= -0.082, p-value=0.15), f. Module score projection of Jak stat signaling pathway(Median PyMT ELP3^{CTR}= -0.005, Median PyMT ELP3^{NEU}= 0.002, p-value=0.0013), g. Module score projection of granzyme signature in CD8+ Tcells (Median PyMT ELP3^{CTR}= 0.158, Median PyMT ELP3^{NEU}= 0.153, p-value=1.08204e-07), h.Module score projection of effector CD8+ T cells signature(Median PyMT ELP3^{CTR}= 0.36, Median PyMT ELP3^{NEU}= 0.37, p-value= 1.00309e-08),Wilcoxon test was applied for the statistical analysis

In addition to the analysis of T cell-associated signatures, subclustering of the T-cell compartment was performed. As shown in Figure 24-a, the major T-cell populations identified included CD4+ T cells, CD8+ T cells, regulatory T cells (Tregs), and γδ T cells. Further subclustering revealed additional T-cell subsets, which were annotated based on the expression of their characteristic marker genes (Figure 24-b). The relative proportions of the identified T-cell subclusters are presented in Figure 24-c.

One CD4+ T-cell subcluster was characterized by the expression of CD40LG (CD154), a costimulatory molecule transiently expressed upon T-cell activation. CD40LG mediates interactions between activated CD4+ T cells and CD40-expressing antigen-presenting cells and is therefore commonly associated with activated helper T-cell responses (Bullock, 2022). Another CD4+ T-cell subcluster was characterized by the expression of TOX, a transcription factor induced by persistent antigen stimulation and frequently associated with dysfunctional or exhausted T-cell states in tumors. The presence of TOX suggests that these cells have been exposed to chronic stimulation within the tumor microenvironment and may represent an activated or exhaustion-CD4+ T-cell population (Scott *et al.*, 2019).

A third CD4+ T-cell subcluster displayed elevated expression of Dusp10, a dual-specificity phosphatase involved in the negative regulation of MAPK signaling pathways. The expression of Dusp10 suggests active modulation of T-cell activation and inflammatory signaling within this population. In addition, one CD4+ T-cell subcluster was characterized by the expression of Rorc, the lineage-defining transcription factor of Th17 cells, suggesting a Th17-like CD4+ T-cell phenotype within the tumor microenvironment (Dickinson and Keyse, 2006).

Within the CD8+ T-cell compartment, a distinct subcluster expressed high levels of Nkg7, a marker associated with cytotoxic lymphocyte function. Another distinct CD8+ T-cell subcluster was identified and was characterized by the expression of granzyme b together with Eomes.

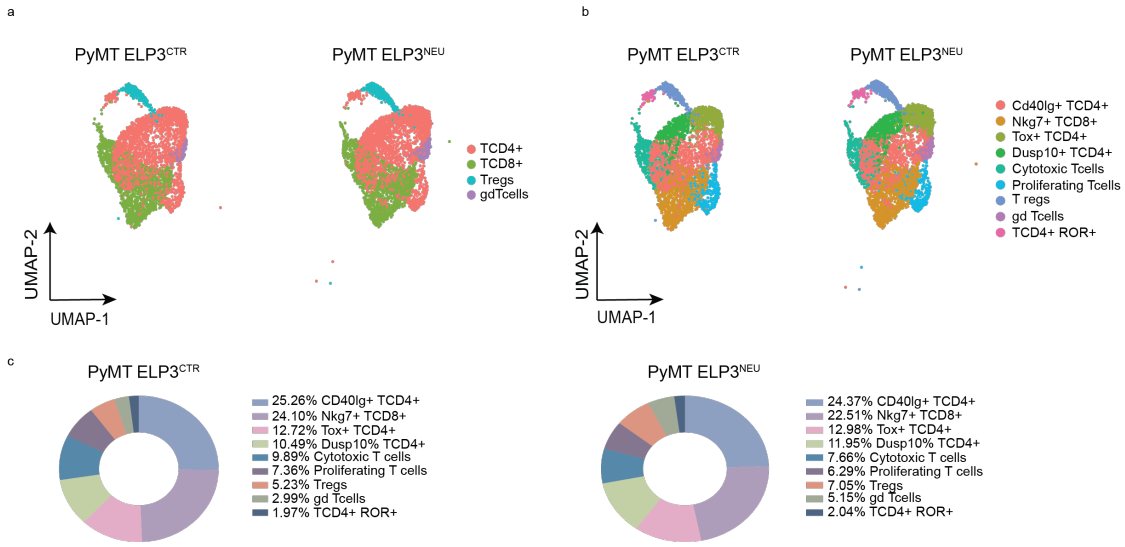

Figure 24: Subclustering analysis of the tumor-infiltrating T-cell compartment. a. Major T cells populations, b. T cells subclustering using Seurat V5 pipeline. Following T cells cluster isolation and Seurat object generation, subclustering is performed using Findclusters function with a 0.5 recommended resolution c. T-cells subclusters proportions

5.2. Flow cytometric analysis of immune populations

To validate the scRNA-seq findings using an independent approach, immune populations within tumors were further characterized by flow cytometry (Fig 25). The abundance of major immune cell populations, including neutrophils (Fig 25-a), $CD4^+$(Fig25-d) T cells (Fig 25-b), $CD8^+$ T cells (Fig 25-c), and NK cells (Fig 25-i), was quantified in PyMT $ELP3^{CTR}$ and PyMT $ELP3^{NEU}$ tumors.

Consistent with the single cell RNA sequencing analysis, no significant difference was observed in the relative abundance of these major immune populations between PyMT $ELP3^{CTR}$ and PyMT $ELP3^{NEU}$ breast tumors.

We next performed a more detailed analysis of T cell activation states. Expression of the activation and differentiation markers CD44 and CD127 was assessed in both $CD4^+$ and $CD8^+$ T cell populations (Fig 25-e, f), revealing comparable activation profiles between the two conditions. The frequency of $FOXP3^+$ regulatory T cells was also similar between control PyMT $ELP3^{NEU}$ tumors (Fig 25-g).

For this analysis the gating strategy used was performed by first selecting lymphocytes (CD45+ and CD3+) (Fig26), $CD4^+$ and $CD8^+$ T cell populations were identified based on CD4 and CD8 expression. Regulatory T cells (Tregs) were defined as $FOXP3^+$ cells within the $CD3^+$ T cell population.

A difference was observed in the proportion of γδ T cells and showed lower rate in the PyMT ELP3^{NEU} tumors compared to PyMT ELP3^{CTR}. However, this variation was not consistent with the scRNA-seq results (Fig 24-c) and was therefore not further investigated (Fig 25-h). In fact, subclustering of the T cell compartment using Seurat V5 pipeline showed an increase in the γδ T cells in PyMT ELP3^{NEU}.

Together, these findings support the conclusion that neutrophil specific depletion of ELP3 does not substantially alter the major immune populations or T cell activation states within the tumor microenvironment. Nevertheless, a decrease in γδ T-cell infiltration was observed, indicating that specific immune subsets may be differentially influenced by ELP3-deficient neutrophils.

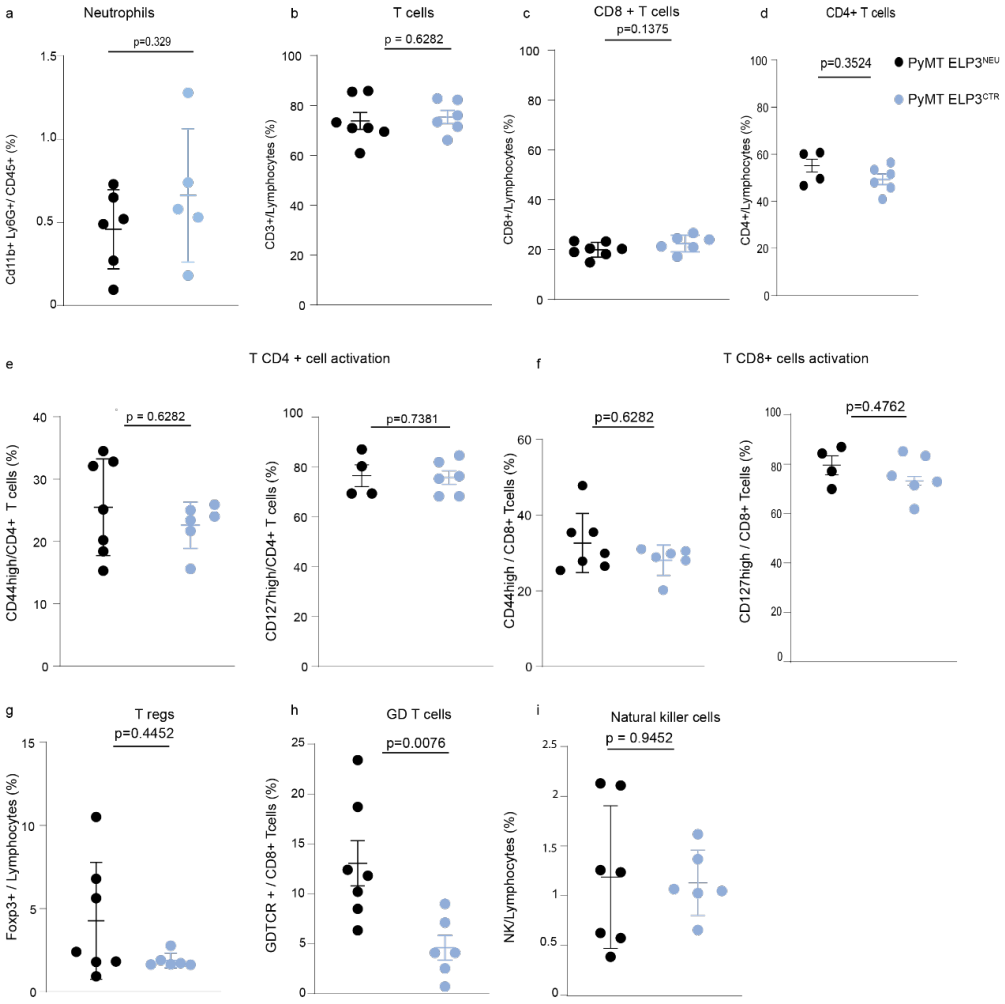

Figure 25:Immune phenotyping at 10 weeks old PyMT ELP3 ^{CTR} and PyMT ELP3^{NEU}. a. Tumor neutrophil (Ly6G+, CD11b+, CD45+) cell proportion, b. Tumor T (CD3+) cells proportion, CD8+ T cells flow cytometry analysis, e. CD4+ T cells activation markers expression; CD44 and CD127, TCD8+ cells activation markers expression; CD44 and CD127, T regs population proportion using Foxp3 staining, h. γδTcells proportion, i. NK cells proportions. For this immune-phenotyping, tumors were processed using DNAse1 and collagenase in the Miltenyi gentle macs and red blood cells were eliminated using red blood cell lysis solution of Miltenyi, (Lymphocytes: Cd11b-, Cd19- and CD3+, n=min4, Mann-Witney test)

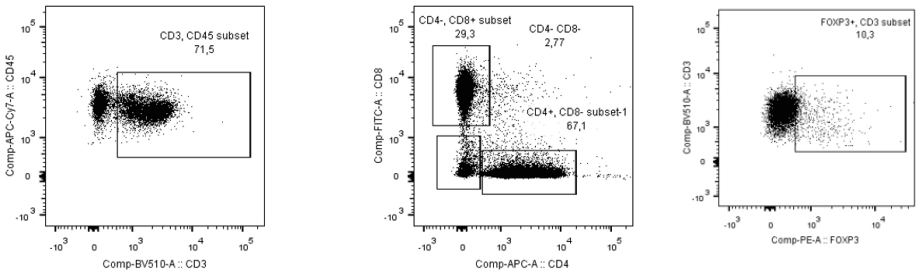

Figure 26: Flow cytometry gating strategy for T cells

6. Neutrophils undergo proteomic remodeling when infiltrating the tumor

Transcriptomic remodeling in tumor associated neutrophils has been extensively characterized, providing important insights into their heterogeneity and functional states within the tumor microenvironment. In contrast, proteomic analyses of these cells remain limited, leaving a significant gap in our understanding of how these transcriptional changes translate into functional protein landscapes. Bridging this gap is essential for a more comprehensive view of neutrophil biology in cancer.

For this purpose, low throughput proteomic analysis was performed on sorted neutrophils isolated from tumors and peripheral blood at 12 weeks old.

Neutrophils were purified by cell sorting following *in vivo* labeling of circulating immune cells using anti CD45 antibody injection, allowing discrimination between tumor infiltrating and blood derived neutrophils.

First, comparative proteomics analysis revealed substantial differences between tumor infiltrating and blood neutrophils in PyMT ELP3^{CTR} mice, indicating proteome remodeling associated with tumor infiltration (Fig 27-a). Numerous proteins were differentially expressed between the two populations, as illustrated by volcano plot analysis (i.e. 297 down-regulated proteins and 1115 up-regulated proteins).

To determine whether these proteomic differences reflected increased global protein synthesis, nascent protein production was measured in vivo using O-propargyl-puromycin (OPP) incorporation at 12 weeks old (Fig 27.e). Comparable OPP incorporation levels were observed in tumor infiltrating or circulating neutrophils, indicating that global protein synthesis rates were not increased in neutrophils upon tumor infiltration.

However, the proteomics data suggests that TINs undergo a selective proteome remodeling which may underlie tumor specific neutrophil function.

To gain functional insights into the observed proteomic changes, GSEA analysis was performed. Several pathways were significantly enriched in tumor infiltrating neutrophils compared to circulating neutrophils. Among the upregulated pathways, oxidative phosphorylation, fatty acid metabolism, and adipogenesis were prominently enriched (Fig 27-b). These pathways are closely linked to mitochondrial metabolism, suggesting a shift toward enhanced mitochondrial associated functions in tumor infiltrating neutrophils.

To further investigate the importance of mitochondrial involvement in tumor infiltrating neutrophils, mitochondrial associated pathways were extracted from the MitoCarta database and used to generate dedicated gene signatures. MitoCarta is an inventory database compiled using mass spectrometry analyses of mitochondria isolated from 14 different tissues (Rath *et al.,* 2021). Enrichment analysis demonstrated an upregulation of mitochondrial pathways in tumor infiltrating neutrophils compared to circulating neutrophils (Fig 27-d).

Supporting proteomics findings, mitochondrial reactive oxygen species (ROS) production was assessed by flow cytometry using MitoSOX Red staining. Tumor infiltrating neutrophils exhibited increased mitochondrial ROS levels compared to circulating neutrophils (Fig 27-f), consistent with enhanced mitochondrial activity upon tumor infiltration.

Together, these results indicate that tumor infiltration is associated with extensive mitochondrial related proteomic remodeling and activity in neutrophils.

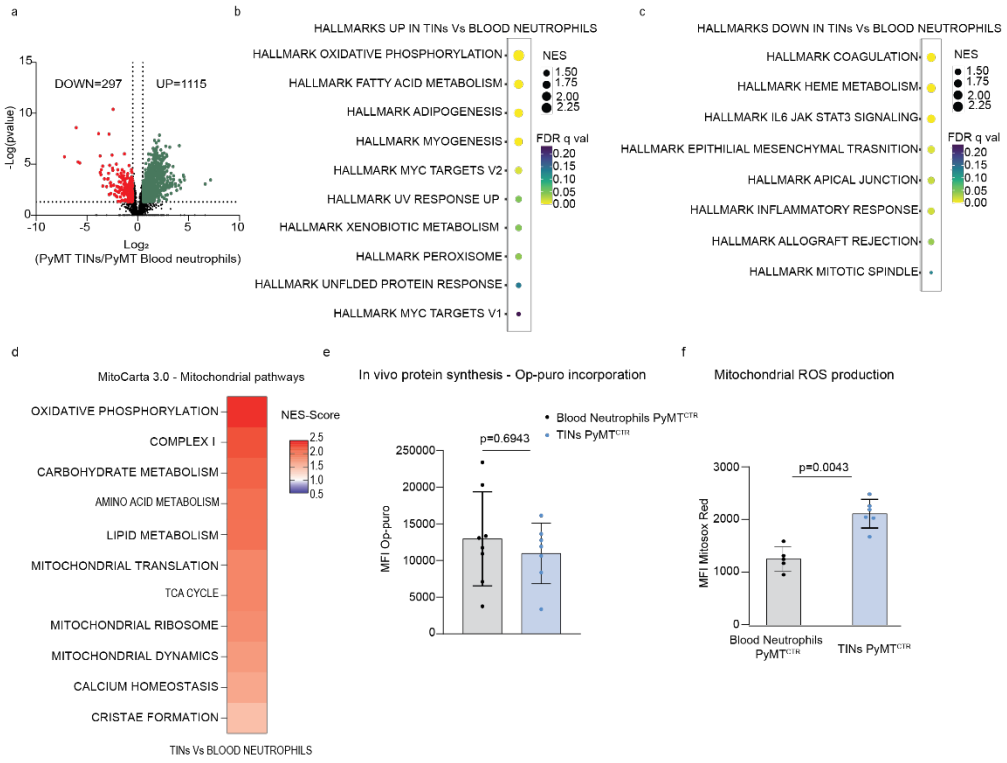

Figure 27: Proteomics analysis and protein synthesis flow cytometry analysis on PyMT Tumor infiltrating neutrophils and blood neutrophils at 12 weeks a. Volcano plot of TINs compared to blood neutrophils (n=min 5, Analysis generated using Perseus, T test), b. Gene set enrichment analysis - All upregulated hallmarks in TINs Vs Blood neutrophils, c. GSEA - All downregulated hallmarks in TINs Vs Blood neutrophils, d. Mitochondrial pathways enrichment in TINs Vs Blood Neutrophils, e. In vivo protein synthesis in blood and tumor neutrophils measurement using Op-puro incorporation (n=min6, Mann-Whitney test), f. Mitochondrial ROS measurement using mitosox red in blood and tumor neutrophils. (n=min 5, Mann-Whitney test)

7. Proteomic remodeling of ELP3 depleted neutrophils upon tumor infiltration

To characterize proteomic changes associated upon the loss of ELP3, we compared first, tumor infiltrating neutrophils to circulating blood neutrophils isolated from PyMT ELP3^{NEU} mice. Differential protein abundance was first visualized using a volcano plot, highlighting extensive proteome remodeling between the two neutrophil populations. Analysis performed using perseus shows the upregulation of 635 proteins and the downregulation of 482 proteins (Fig 28-a).

To further identify biological pathways associated with tumor infiltration, gene set enrichment analysis (GSEA) was performed on the proteomics dataset (Fig 28-b, c). This analysis revealed significant enrichment of multiple

metabolic pathways in tumor infiltrating neutrophils similarly to PyMT ELP3^{CTR}. Among the most upregulated hallmarks were oxidative phosphorylation, fatty acid metabolism, and adipogenesis. Conversely, several pathways related to other cellular processes were downregulated.

Together, these results indicate that neutrophils undergo substantial metabolic remodeling upon tumor infiltration, characterized by an increased representation of mitochondrial and lipid associated pathways.

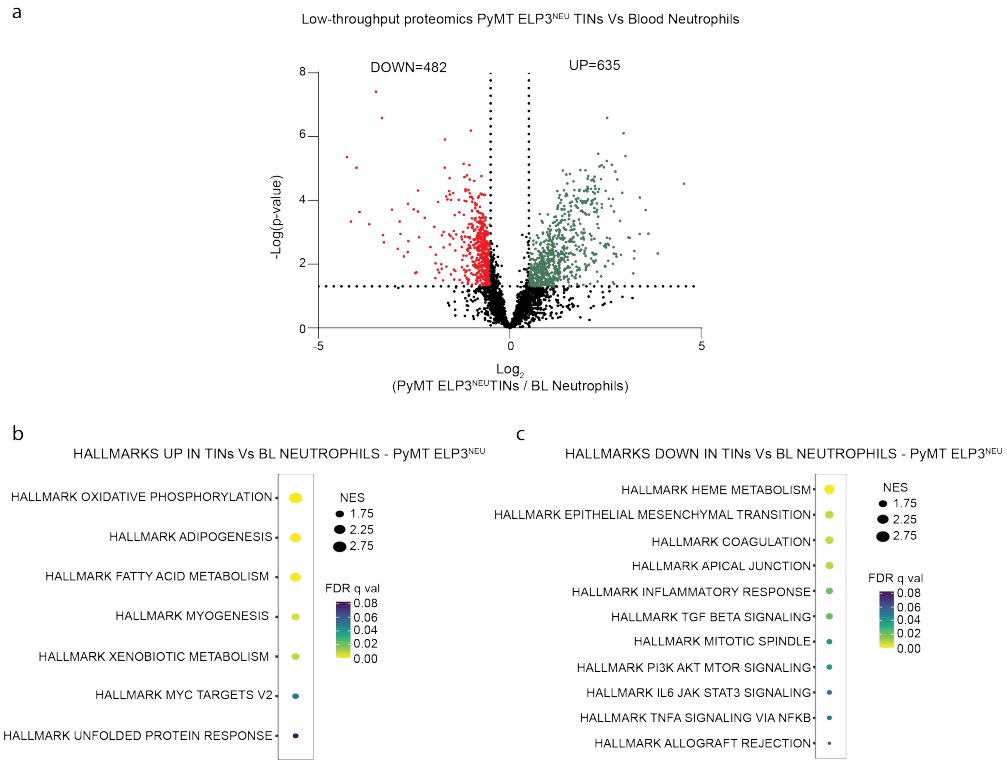

Figure 28:Proteomic remodeling of tumor infiltrating neutrophils in PyMT ELP3^{NEU} mice. a. Volcano plot of TINs compared to blood neutrophils (n=min 5, Analysis generated using Perseus, T test), b. GSEA - All upregulated hallmarks in TINs Vs Blood neutrophils, c. GSEA - All downregulated hallmarks in TINs Vs Blood neutrophils

8. Proteomic analysis reveals mitochondrial pathway alterations in ELP3-deficient TINs

To further investigate the impact of ELP3 depletion on proteome remodeling in tumor-infiltrating neutrophils, the same proteomic workflow was applied to neutrophils isolated from PyMT ELP3^{NEU} mice in comparison with PyMT ELP3^{CTR}. Proteomics profiles were generated for both circulating neutrophils and tumor infiltrating neutrophils.

Comparative analysis of circulating neutrophils revealed no significant proteomic differences between PyMT ELP3^{CTR} and PyMT ELP3^{NEU} mice (Fig 29-a), indicating that ELP3 depletion does not substantially alter the proteome of circulating neutrophils.

In contrast, proteomic comparison of tumor infiltrating neutrophils identified differences between ELP3^{CTR} and ELP3^{NEU} mice. Approximately 3,000 proteins were detected, among which 34 proteins were significantly upregulated, and 25 proteins were significantly downregulated in ELP3 deficient tumor infiltrating neutrophils (Fig 29-c).

Gene Set Enrichment Analysis performed on the full proteomics dataset did not reveal strong pathway enrichment. However, oxidative phosphorylation emerged as the only significantly downregulated pathway in ELP3 deficient tumor infiltrating neutrophils compared to controls (Fig 29-b).

To further investigate mitochondrial involvement, mitochondrial associated pathways derived from the MitoCarta database were analyzed. Enrichment analysis revealed a downregulation of mitochondrial pathways in ELP3 deficient compared to control TINs (Fig 29-d).

Heatmap visualization confirmed that most mitochondrial associated pathways were reduced in ELP3 deficient tumor infiltrating neutrophils.

To determine whether these proteomic differences resulted from altered global protein synthesis, nascent protein production was measured in vivo using O-propargyl-puromycin (OPP) incorporation. Comparable OPP incorporation levels were observed between PyMT ELP3^{CTR} and PyMT ELP3^{NEU}

neutrophils, indicating that ELP3 deletion does not reduce global protein synthesis (Fig 29-e).

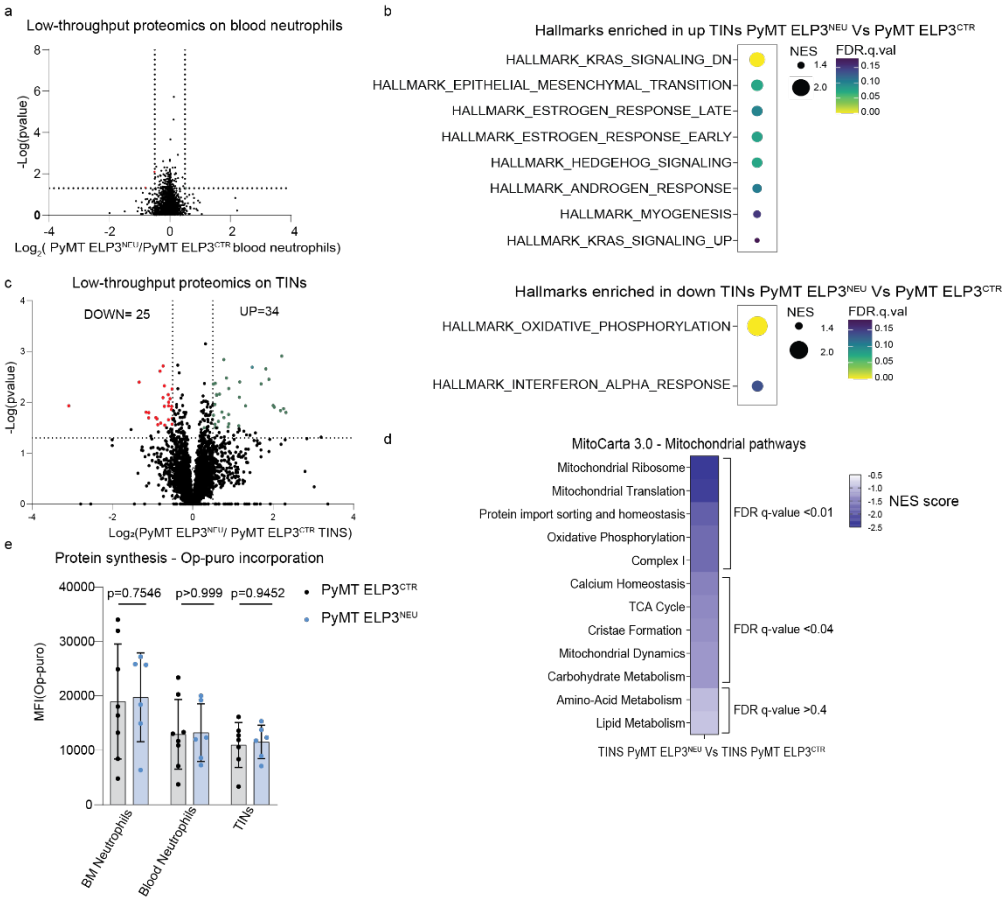

Figure 29:Proteomics analysis and protein synthesis comparison between PyMT ELP3^{CTR} and PyMT ELP3^{NEU} tumor associated neutrophils at 12 weeks. a. Blood PyMT ELP3^{CTR} and PyMT ELP3^{NEU} neutrophils proteomics analysis results, b. GSEA all hallmarks analysis between TINs PyMT ELP3^{CTR} and PyMT ELP3^{NEU}, c. TINs PyMT ELP3^{CTR} and PyMT ELP3^{NEU} comparison (n=min5, Results generated on Perseus, T-test), d. Mitochondrial pathways (extracted from MitoCarta repository) enrichment in TINs PyMT ELP3^{CTR} and PyMT ELP3^{NEU}, e. In vivo protein synthesis using Op-puro incorporation. A single dose of 1 mg OP-Puro was administered intraperitoneally, and mice were sacrificed 1-hour post-injection. (n=min6, Mann-Whitney test)

As presented earlier comparative proteomics analysis of TINs from PyMT ELP3^{CTR} and PyMT ELP3^{NEU} mice revealed a limited number of significantly modulated proteins. Heatmap visualization of these differentially expressed proteins highlighted modest changes between conditions (Fig 30), with no evidence of widespread proteomic remodeling. These results suggest that ELP3 deletion induces only subtle alterations in the proteomic landscape of

TINs.

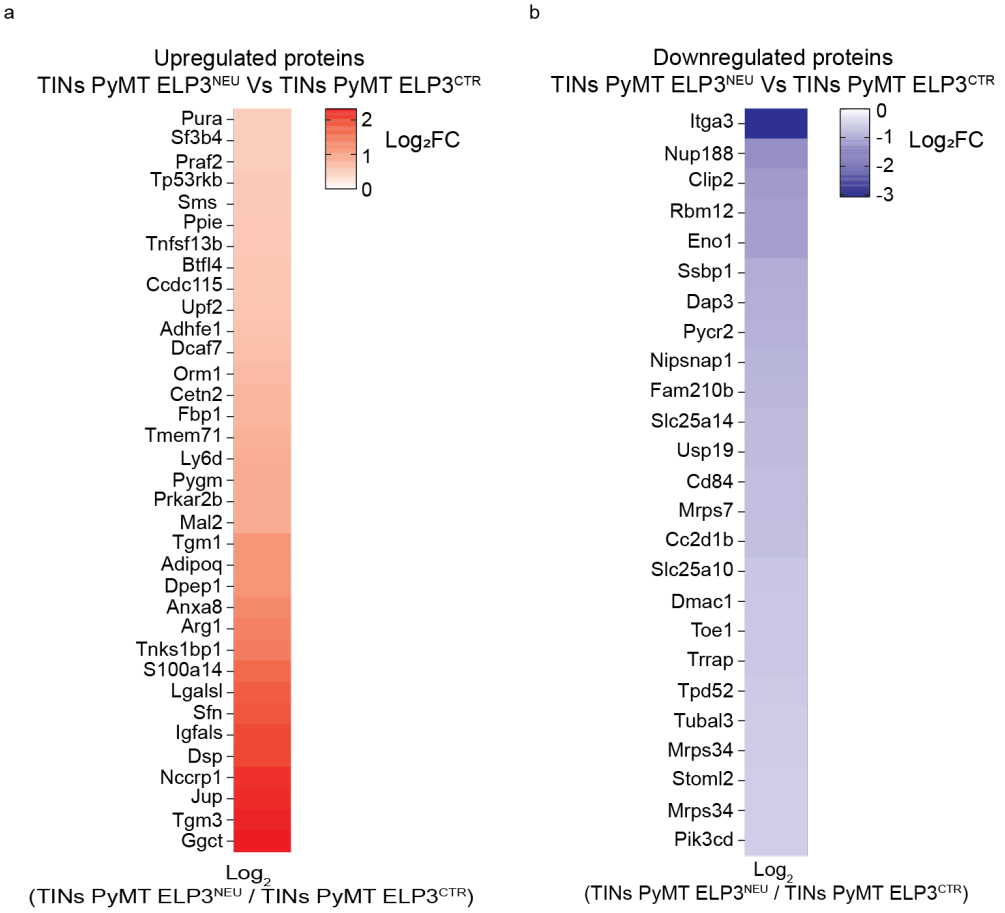

Figure 30: Modulated proteins in Tumor infiltrating neutrophils PyMT ELP3^{CTR} and PyMT ELP3^{NEU} a. Upregulated proteins in TINS PyMT ELP3^{NEU} Compared tp PyMT ELP3^{CTR}, b. Downregulated proteins in TINS PyMT ELP3^{NEU} compared to PyMT ELP3^{CTR}

9. ELP3 depletion alters mitochondrial structure and metabolism in neutrophils

Our proteomics data indicate that mitochondrial pathways are impacted upon the loss of ELP3 in neutrophils. We next sought to investigate the impact of ELP3 in mitochondrial structure and metabolism in neutrophils.

Because tumor infiltrating neutrophils were recovered in limited numbers, we used bone marrow derived neutrophils from ELP3^{CTR} and ELP3^{NEU} mice to investigate the possible role of ELP3 in regulating mitochondrial functions and neutrophil metabolism remodeling.

First, we assessed mitochondrial ultrastructure, bone marrow neutrophils ELP3^{CTR} and ELP3^{NEU} mice were analyzed by electron microscopy (Fig 31-a, b).

Quantitative analysis revealed that ELP3^{NEU} neutrophils contained fewer mitochondria per cell compared to ELP3^{CTR} neutrophils (Fig. 31-c), and that a higher proportion of the detected mitochondria lacked cristae (Fig. 31-d).

Electron microscopy revealed also that ~30% of ELP3^{NEU} neutrophils contained autophagosomes, compared to fewer than 0.5% of ELP3^{CTR} neutrophils (Fig 31-e).

These findings indicate that ELP3 deletion is associated with altered mitochondrial content and increased autophagosome formation in neutrophils.

Next, we investigated metabolic changes upon the loss of ELP3 in neutrophils. We performed LC-MS on bone marrow neutrophils derived from ELP3^{CTR} and ELP3^{NEU} mice. By targeted approach we detected 63 metabolites. Only 10 metabolites the threshold for statistical significance and are represented in figure 31-f. Among the most prominent changes, α-ketoglutarate levels were decreased, suggesting alterations in pathways linked to glutamine metabolism. In addition, reduced levels of fructose-6-phosphate and glucose-6-phosphate were observed, indicating possible alterations in glycolytic or pentose phosphate pathway intermediates.

Together, these results indicate that ELP3 deletion is associated with metabolic alterations in neutrophils in steady state conditions.

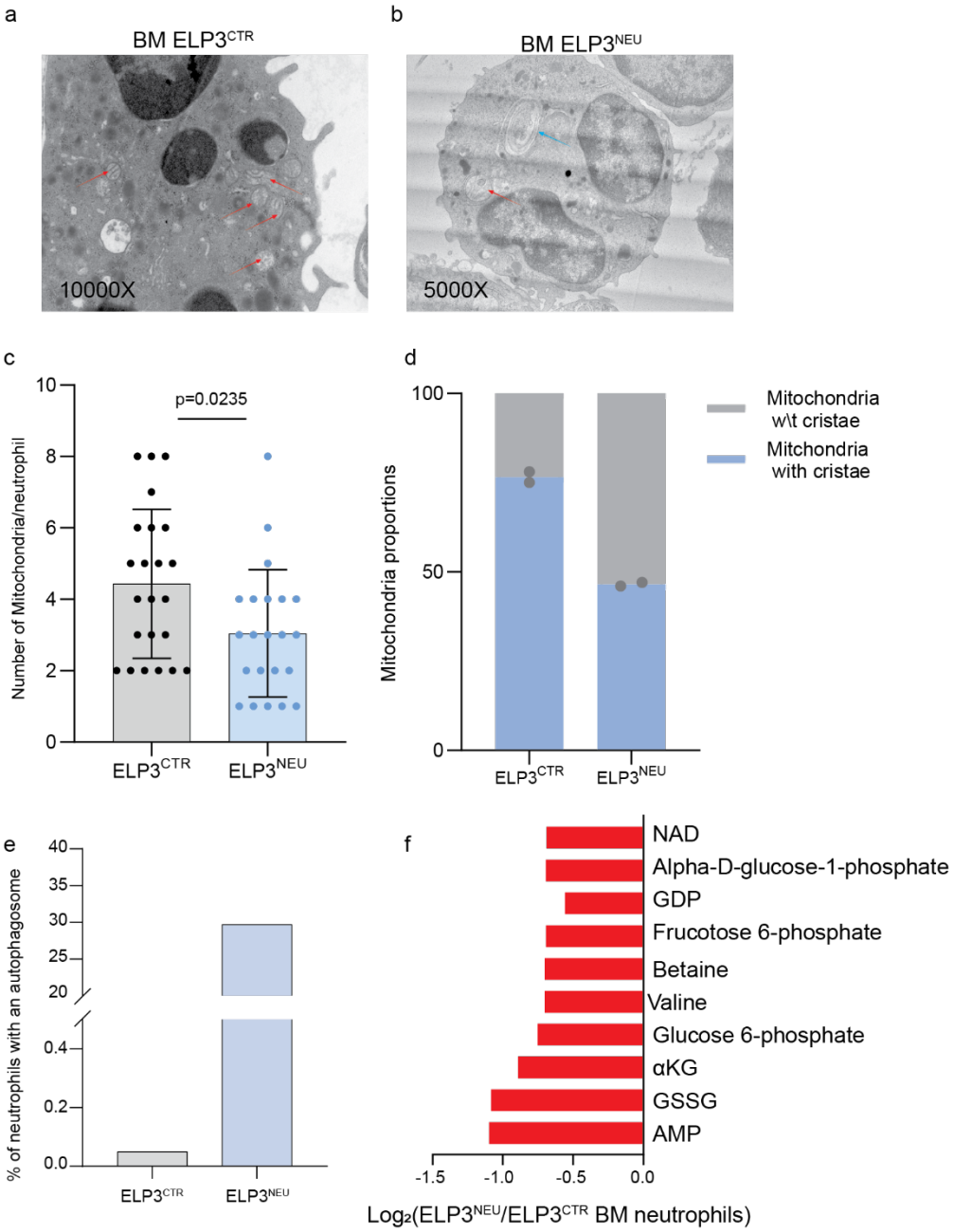

Figure 31: Electron microscopy and Metabolomics analysis on Bone marrow ELP3^{CTR} and ELP3^{NEU} mice neutrophils at 12 weeks. a. Electron microscopy on enriched bone marrow ELP3^{CTR} neutrophils, b. Electron microscopy on bone marrow ELP3^{NEU} neutrophils, c. Quantification of the number of mitochondria per neutrophil (n=2 mice and min23 neutrophils were analyzed, Mann-Witney test), d. Mitochondria with and without cristae proportions per group, e. Autophagosomes proportion in ELP3^{CTR} and ELP3^{NEU} neutrophils f. Metabolomics analysis on bone marrow neutrophils: Significantly regulated metabolites(-Log10 (pvalue) >1.3) Log2FC in ELP3^{NEU} neutrophils compared to ELP3^{CTR} neutrophils (n=4, Mann-Whitney test)

To understand whether ELP3 deletion alters neutrophil bioenergetic function, oxygen consumption rate (OCR) and extracellular acidification rate (ECAR) were measured using Seahorse extracellular flux analysis. Measurements were performed under multiple substrate conditions, including glucose-containing medium, glucose free medium supplemented with pyruvate and glutamine, and glutamine only conditions.

Across all conditions tested, OCR and ECAR profiles were comparable between control and ELP3 deficient neutrophils. Although ELP3 deficient neutrophils displayed a trend toward slightly higher basal OCR, this difference did not reach statistical significance (Fig 32).

These results indicate that ELP3 deletion does not produce a detectable change in mitochondrial respiration or glycolytic activity in normal neutrophils under the assay conditions used.

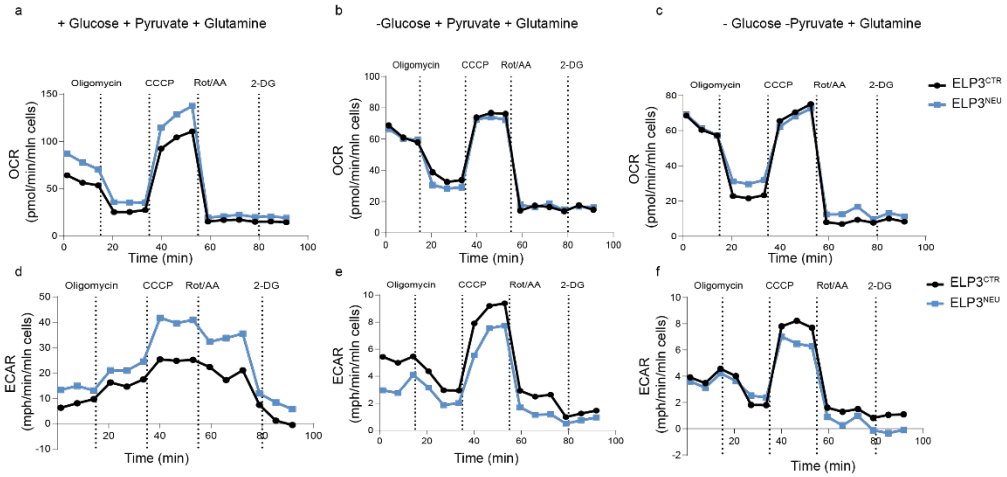

Figure 32: OCR and ECAR measurement of 12 weeks ELP3^{CTR} and ELP3^{NEU} steady state bone marrow neutrophils. a, b, c OCR measurement respectively in Glucose, Pyruvate and Glutamine, Pyruvate and Glutamine and Glutamine only supplemented medium, d, e, f. ECAR measurement respectively in Glucose, Pyruvate and Glutamine, Pyruvate and Glutamine and Glutamine only supplemented medium. Seahorse metabolic analysis was performed using 200,000 neutrophils per well (n = 5 technical replicates per condition, mice N= min 7). OCR and ECAR were measured following sequential injections of oligomycin, CCCP, rotenone plus antimycin A, and 2-DG.

Given the downregulation of mitochondrial pathways observed in our proteomic analysis, we next sought to assess mitochondrial function in PyMT ELP3^{CTR} and PyMT ELP3^{NEU} neutrophils at 12 weeks of age. To this end, we measured mitochondrial reactive oxygen species (mtROS) production and evaluated mitochondrial membrane potential using TMRM. These assays provide functional readouts of mitochondrial activity and integrity, allowing us

to determine whether the observed proteomic changes are associated with altered mitochondrial performance.

Mitochondrial superoxide was quantified by flow cytometry using MitoSOX Red staining (Fig 33-a). In the different tested organs, tumor associated neutrophils from PyMT ELP3^{CTR} and PyMT ELP3^{NEU} mice displayed comparable MitoSOX fluorescence, indicating no detectable difference in mitochondrial ROS levels between genotypes. On the other hand, our results show that only tumor infiltrating neutrophils upregulate their mitochondrial ROS.

To investigate the activity of the electron transport chain (ETC) we used the TMRM (Tetramethylrhodamine, methyl ester) dye to measure the mitochondrial membrane potential.

Quantification of TMRM fluorescence (Fig 33-b) revealed comparable mitochondrial membrane potential between PyMT ELP3^{CTR} and PyMT ELP3^{NEU} neutrophils. Significant differences were only observed between blood neutrophils. However, no differences were detected between blood and TINs indicating that tumor infiltration does not upregulate mitochondrial membrane potential.

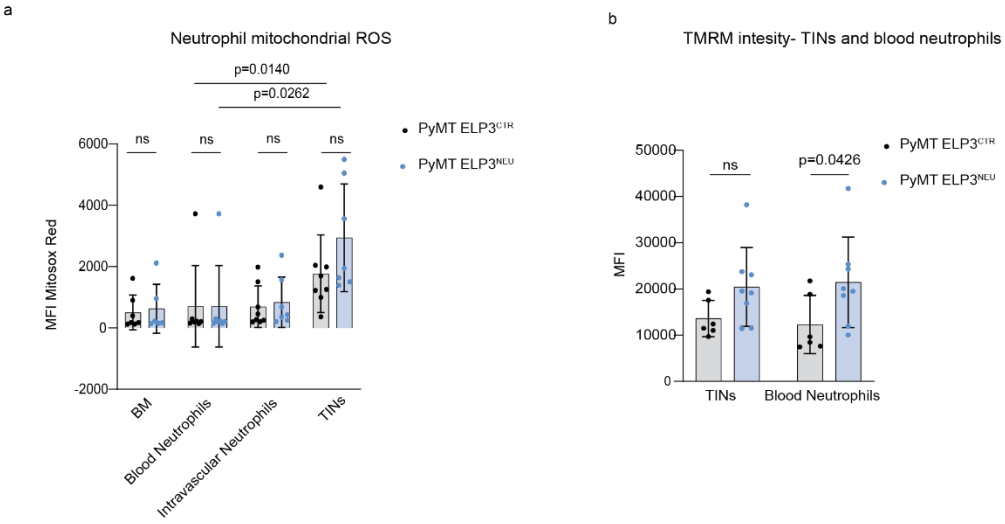

Figure 33: Mitochondrial ROS and membrane potential in Tumor associated neutrophils a. Mitochondrial ROS measurement in tumor associated neutrophils in PyMT ELP3^{CTR} and PyMT ELP3^{NEU} mice. MitoSOX Red fluorescence was quantified as mean fluorescence intensity (MFI) to assess mitochondrial superoxide levels (n=8, Mann Whitney test), b. Mitochondrial membrane differential potential measurement using TMRM staining in TINs and blood neutrophils and quantified as MFI by flow-cytometry (n=8, Mann Whitney test)

This data suggests that ELP3 dependent mitochondrial proteomic remodeling in tumor infiltrating neutrophils is not accompanied by a measurable change in mitochondrial ROS production or inner mitochondrial membrane potential.

10. Investigation of ELP3 depleted neutrophils roles in vasculature regulation

Given the delayed tumor progression and the reduced CD31 staining observed in PyMT ELP3^{NEU} tumors, we next investigated whether ELP3 deficient neutrophils could directly affect angiogenesis-related functions. Several neutrophil effector mechanisms previously implicated in tumor vascular remodeling were therefore examined.

First, total cellular reactive oxygen species (ROS) production was measured in tumor infiltrating neutrophils (TINs) and compared with other neutrophil populations associated with the tumor bearing mice, including bone marrow, circulating blood, and intravascular neutrophils isolated from PyMT mice. No differences in ROS production were detected between PyMT ELP3^{CTR} and PyMT ELP3^{NEU} neutrophils (Fig 34-a).

We next evaluated additional neutrophil associated factors involved in angiogenesis.

In the 4T1 breast cancer model, arginase I was induced in myeloid-derived suppressor cells during anti-VEGFR-2 therapy, and arginase inhibition using DC101 antibody reduced lung metastasis, showing that ARG1 can participate in the broader angiogenesis/immune-suppression network (Secondini *et al.*, 2017).

MMP-9 (matrix metalloproteinase-9) is a zinc-dependent endopeptidase that plays a key role in tumor angiogenesis. By degrading components of the basement membrane and extracellular matrix, MMP-9 facilitates endothelial cell migration and proliferation, thereby promoting the formation of new blood vessels. Consequently, alterations in MMP-9 secretion or activity may directly influence tumor vascularization and disease progression. In addition to its extracellular matrix remodeling functions, MMP-9 has been reported to regulate VEGF bioavailability and signaling. Indeed, MMP-9 depletion has been shown to impair VEGF–VEGF receptor interactions, further highlighting its importance in angiogenic processes (Nozawa, Chiu and Hanahan, 2006b).

Arginase-1 expression was assessed by intracellular staining (Fig 34-b), and MMP9 production was analyzed both by ELISA (Fig 34-c) in neutrophil culture

supernatants and by Western blot analysis performed on enriched neutrophils protein extract (Fig 34-d). In all cases, ELP3^{NEU} neutrophils displayed levels comparable to those observed in control neutrophils.

Together, these results indicate that the angiogenesis defect observed in PyMT ELP3^{NEU} tumors is not explained by major alterations in ROS production, arginase-1 expression, or MMP9 secretion in neutrophils.

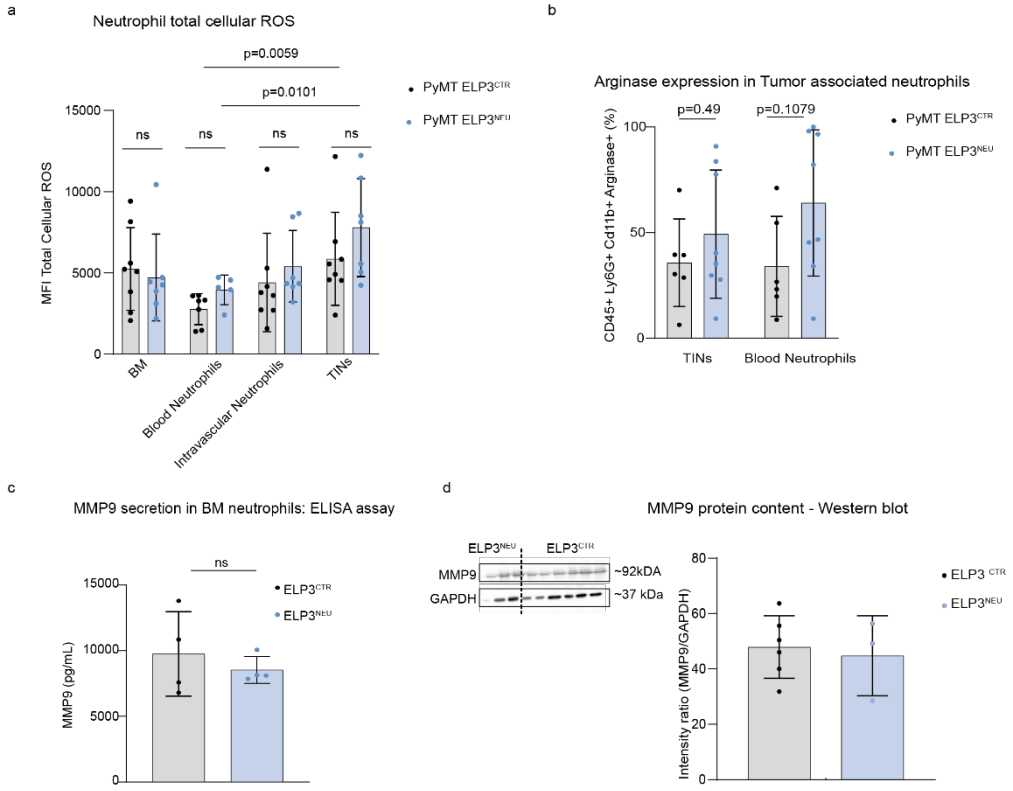

Figure 34: Functional assessment of pro-angiogenic activities in neutrophils. a. Neutrophil total ROS measurement using DHR123 probe and flow-cytometry (n=min6, Mann-Whitney test), b. Arginase expression in TINs and Blood neutrophils (n=min5, Mann-Whitney test), c: MMP9 secretion analysis by enriched bone marrow neutrophils from steady state mice cultured in serum free medium for 2 hours (ELISA assay, n=4, Mann-Whitney test), d. MMP9 protein content normalized on GAPDH levels of enriched bone marrow neutrophils (Western Blot, n=min4, Mann-Whitney test)

11. Comparison of transcriptomic and proteomic profiles in ELP3 deficient tumor infiltrating neutrophils

Because neutrophils were underrepresented in the scRNA-seq dataset, differential expression analysis at the transcript level had limited power. Nevertheless, we assessed the concordance between transcriptional and

proteomic changes in tumor infiltrating neutrophils. We compared Log2 fold changes measured by scRNA-seq and proteomics for ELP3 deficient versus control TINs.

This analysis revealed low concordance between transcript and protein changes, as reflected by weak correlation coefficients (Spearman ρ = 0.05054 and Pearson r = 0.1067) (Fig 35-a).

To further characterize this discordance, genes were stratified based on their expression changes at both levels. A subset of genes (73 proteins) displayed reduced protein expression ($log_2FC < -0.5$) while transcripts levels remained unchanged or even increased ($log_2FC > -0.5$) (Fig. 33-b, blue). Conversely, another group (65 proteins) showed decreased or unchanged transcript levels ($log_2FC < 0.5$) but increased protein abundance ($log_2FC > 0.5$) (Fig. 35-b, red).

To determine whether these discordant profiles were associated with specific biological functions, Gene Ontology cellular component analysis was performed on both groups. Upregulated proteins with unchanged or decreased transcript levels were mainly associated with the extrinsic component of the membrane. In contrast, downregulated proteins with unchanged or increased transcript levels were predominantly linked to mitochondrial compartments and ribosomal subunits (Fig.35-c, d).

To investigate whether translational regulation could contribute to the observed discrepancies, we performed a codon enrichment analysis focusing on U34 tRNA modification (i.e. AAA, CAA, and GAA) following Z-score calculation method detailed in Rosu *et al.*, 2021. This analysis revealed only limited enrichment, with 5 out of 68 genes in the upregulated protein group and 3 out of 73 genes in the downregulated protein group showing increased U34 codon frequency. These results suggest that codon usage bias is restricted to a small subset of transcripts and does not represent a global feature of the dataset.

On the other hand, the main U34 codon enriched downregulated proteins captured through this analysis were MRPS30, ABHD12 and STOML2. These genes are linked to mitochondria and lipid signaling.

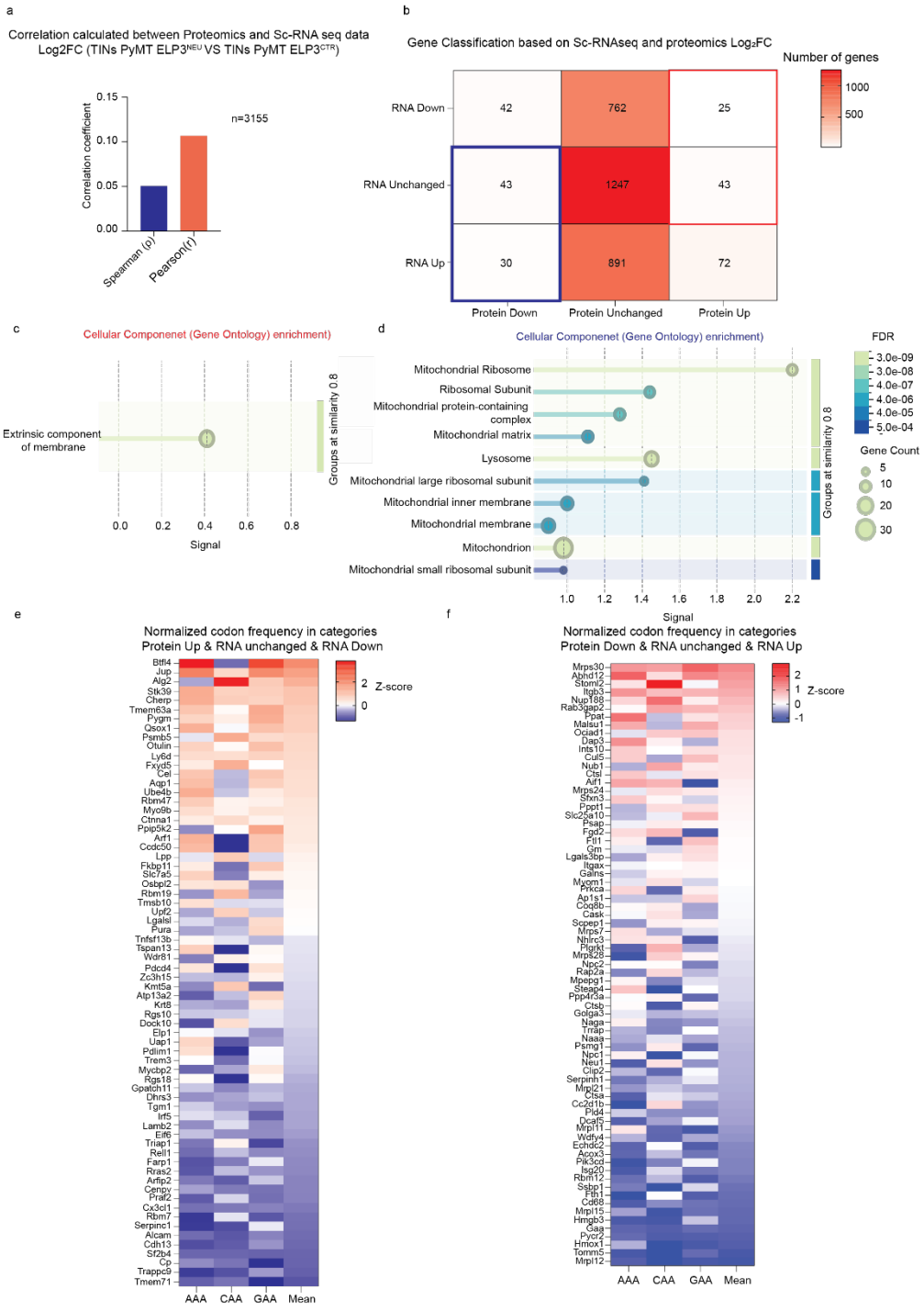

Figure 35:Integrated transcriptomics and proteomics analysis in PyMT ELP3^{CTR} and PyMT ELP3^{NEU} TINs. a. Person and Spearman correlation coefficient between Log$_2$FC (TINs PyMT ELP3^{NEU}/TINs PyMT ELP3^{CTR}) extracted from single cell RNAseq and Log$_2$FC (TINs PyMT ELP3^{NEU}/TINs PyMT ELP3^{CTR}) extracted from proteomics, b. Gene categories based on levels

of expression in sc-RNAseq and proteomics, c. Cellular component STRING analysis performed on genes categories highlighted in red in b., d. Cellular component STRING analysis performed on genes categories highlighted in blue in b., e. Normalized codon frequency performed in genes highlighted in red in b., f. Normalized codon frequency performed in genes highlighted in blue in b (no p-value filtering was used during this analysis)

Conclusions

This work aimed to investigate the role of U34 tRNA modifying enzymes in neutrophil biology within the context of breast cancer, with a particular focus on their contribution to tumor progression and metastasis. By combining transcriptomic analyses, conditional mouse models, functional assays, and proteomic approaches, this study provides new insights into the mechanisms underlying tumor infiltrating neutrophil (TIN) reprogramming and identifies a potential contribution of post-transcriptional regulation to neutrophil function in the tumor microenvironment.

Consistent with published work (SF NG. et al., 2024, Wu.et al., 2024, Timaxian. Et al, 2021), our initial analyses demonstrated that neutrophils undergo extensive transcriptional reprogramming upon tumor infiltration. RNA-seq analysis of a publicly available dataset of tumor associated neutrophils revealed large scale gene expression changes, including enrichment of inflammatory pathways such as TNFα/NF-κB signaling. These findings are consistent with the current understanding that neutrophils adapt to the tumor microenvironment and acquire distinct functional states (i.e. UV response, Inflammatory response, TNF-α signaling …) shaped by cytokines, hypoxia, and local cellular interactions. In this context, the identification of a coordinated upregulation of tRNA modifying enzymes, and particularly U34 dependent enzymes, suggested that neutrophil adaptation may also involve modulation of the translational machinery.

To address this hypothesis, we generated a neutrophil specific ELP3 knockout model. Under steady state conditions, ELP3 depletion did not affect neutrophil homeostasis, viability, migration, ROS production, or responsiveness to proliferative stimuli. These results indicate that ELP3 is dispensable for normal neutrophil functions and suggest that its role is likely context dependent, becoming relevant under specific environmental constraints such as tumor infiltration.

In contrast, in the MMTV-PyMT breast cancer model, ELP3 depletion in neutrophils resulted in a pronounced delay in primary tumor progression and a strong reduction in metastatic dissemination to the lungs. Histopathological analyses further revealed a delay in tumor stage progression, with an increased proportion of early lesions and reduced transition to carcinoma in ELP3 deficient mice. In addition, reduced CD31 staining suggested impaired tumor vascularization. Together, these findings identify ELP3 dependent

neutrophil functions as contributors to tumor progression, tumor blood vasculature formation, and metastasis.

Surprisingly, these phenotypic effects were not associated with major alterations in the tumor immune microenvironment. Both single-cell RNA sequencing and flow cytometry analyses showed overall comparable immune cell composition and T cell activation states between control and PyMT ELP3^{NEU} mice. These observations suggest that the tumor phenotype is unlikely to be driven by changes in adaptive immune responses and instead points toward neutrophil intrinsic mechanisms.

Proteomic analyses provided insights into these mechanisms. Comparison between tumor infiltrating and circulating neutrophils revealed a marked enrichment of mitochondrial pathways, including oxidative phosphorylation and fatty acid metabolism, indicating that neutrophils undergo metabolic reprogramming upon tumor infiltration. Notably, this mitochondrial signature was impaired in ELP3 deficient TINs when compared to control neutrophils. These results suggest that ELP3 contributes to the establishment or maintenance of mitochondrial associated programs in this context.

Further analyses revealed alterations in mitochondrial content and metabolite levels in ELP3 deficient neutrophils, supporting a link between ELP3 activity and neutrophil metabolism. However, functional assays assessing mitochondrial respiration, membrane potential, and ROS production did not reveal major differences, indicating that these alterations may be subtle, context-dependent, or not fully captured under the experimental conditions used.

Interestingly, the blood vasculature defect observed in ELP3 deficient tumors was not explained by changes in classical neutrophil pro-angiogenic functions, including ROS production, arginase-1 expression, and MMP9 secretion. This suggests that neutrophils may regulate tumor vascularization through alternative mechanisms, potentially linked to metabolic or translational changes. These results also suggest that neutrophil effector functions such as MMP9 secretion may be modulated by the tumor microenvironment. Although no differences were observed under steady state or in vitro conditions, it remains possible that MMP9 release or degranulation dynamics are differentially regulated within the tumor context.

Finally, integration of transcriptomic and proteomic datasets revealed a limited concordance between mRNA and protein levels in ELP3 deficient neutrophils, highlighting a potential role for post transcriptional regulation. Notably,

proteins reduced independently of their mRNA levels were enriched for mitochondrial and ribosomal components, supporting the hypothesis that translational control contributes to the observed phenotype. However, codon usage analysis did not reveal strong enrichment of U34 sensitive codons, suggesting that ELP3 dependent effects are not solely explained by global codon bias and may involve additional regulatory mechanisms.

Discussion

Discussion

Neutrophils have long been considered predominantly glycolytic cells under steady-state conditions; however, increasing evidence indicates that their metabolism can be extensively reprogrammed in response to environmental cues. In the tumor microenvironment, characterized by hypoxia, nutrient limitation, and high metabolic competition, neutrophils undergo a profound metabolic adaptation. Recent studies have shown that tumor-associated neutrophils can engage alternative metabolic pathways, including mitochondrial oxidative metabolism, lipid utilization, and amino acid catabolism, to sustain their functions under stress conditions (Huang et al., 2025). In line with this concept, our proteomic analysis revealed that tumor infiltrating neutrophils display a distinct metabolic signature compared to circulating neutrophils, with enrichment of pathways related to oxidative phosphorylation, fatty acid metabolism, and adipogenesis. These findings support the idea that neutrophils adapt their metabolic programs upon tumor infiltration.

Importantly, our data provide direct evidence of this metabolic remodeling at the proteomic level in tumor infiltrating neutrophils, extending previous observations made in alternative compartments. For instance, tumor elicited neutrophils with immature phenotypes have been shown to rely on mitochondrial metabolism to sustain ROS production and promote tumor progression in murine models; however, these cells were primarily isolated from the spleen rather than directly from the tumor site. In contrast, our analysis demonstrates that neutrophils infiltrating the tumor itself undergo a similar mitochondrial reprogramming, highlighting the relevance of this adaptation within the tumor microenvironment (Rice *et al.*, 2018).

Consistent with the proteomic data, we observed an increase in mitochondrial ROS production in tumor infiltrating neutrophils, further supporting enhanced mitochondrial activity upon tumor infiltration. In addition, the enrichment of lipid metabolism pathways aligns with previous reports showing that neutrophils accumulate lipids within the tumor microenvironment, which can support their pro-tumoral functions and metabolic flexibility (Gao *et al.*, 2026). Altogether, these findings indicate that tumor infiltrating neutrophils shift toward a mitochondria-associated metabolic state, likely enabling them to sustain their activity and adapt to the metabolic constraints of the tumor microenvironment.

In addition to metabolic reprogramming, our analyses suggest that tumor infiltrating neutrophils may also undergo adaptations at the level of

translational regulation. By interrogating publicly available RNA-seq datasets of PyMT TINs compared to bone marrow normal neutrophils, we identified a coordinated upregulation of tRNA modifying enzymes in TINs, with a particular enrichment of enzymes involved in U34-dependent tRNA modification. This observation points toward a potential remodeling of the translational machinery in neutrophils upon tumor infiltration.

While neutrophil plasticity has largely been described at the transcriptional level, these findings suggest that post-transcriptional mechanisms may also contribute to their functional adaptation within the tumor microenvironment. tRNA modifications, and particularly U34 tRNA modifications, have been shown to regulate codon dependent translation efficiency and protein synthesis in response to cellular stress. In this context, the coordinated upregulation of U34 associated enzymes in tumor infiltrating neutrophils raises the possibility that translational control may represent an additional layer of regulation shaping neutrophil responses in tumors.

To investigate the functional relevance of U34 tRNA modification in neutrophils, we generated conditional mouse models with neutrophil specific deletion of ELP3 using a well-established CRE-LoxP system driven by the MRP8 (S100A8) promoter. These models allowed us to assess the role of ELP3 under both steady state conditions and in the context of tumor development in the MMTV-PyMT model.

The MRP8-Cre system is a well-established and widely used model for investigating gene function in neutrophils in vivo, as its expression is predominantly restricted to the neutrophil compartment. To validate the specificity of ELP3 deletion in our model, PCR analyses were performed on FACS-sorted neutrophils and monocytes/macrophages. These experiments confirmed recombination within the targeted cell population. Additional validation at the protein level using Western blot analysis is planned to further assess the efficiency of ELP3 depletion.

Furthermore, the available literature provides little evidence supporting significant MRP8-Cre activity in epithelial cells. Nevertheless, given the genetic instability and transcriptional deregulation characteristic of tumor cells, ectopic Cre activity cannot be completely excluded. Therefore, future studies will include additional validation of ELP3 deletion in sorted tumor cells (CD45−EpCAM+) to further confirm the cell-type specificity of the model.

Regarding the tumor model, the MMTV-PyMT model was selected because it faithfully recapitulates several key histological and molecular features of

human breast cancer progression. First described in 1992, expression of the polyomavirus middle T antigen under the control of the MMTV promoter drives rapid mammary tumorigenesis, with lesions progressing from hyperplasia at approximately 4 weeks of age to multifocal adenocarcinomas and spontaneous lung metastases. Molecularly, the PyMT model closely resembles the luminal B subtype of breast cancer and undergoes progressive changes during tumor evolution, including the loss of estrogen receptor (ER) and progesterone receptor (PR) expression and increased expression of ErbB2 and Cyclin D1. These characteristics are associated with more aggressive disease and poor clinical outcome in patients. Notably, loss of ER expression is frequently observed in endocrine therapy-resistant and recurrent breast cancers, further supporting the clinical relevance of this model for studying advanced disease (Attalla *et al.*, 2021).

In addition to recapitulating breast cancer progression, the MMTV-PyMT model has been extensively used to investigate the role of neutrophils during tumor development and metastasis. Previous studies have demonstrated an accumulation of neutrophils in the pre-metastatic lung during metastatic progression, supporting their involvement in disease dissemination. Although neutrophils represent a relatively small proportion of the immune infiltrate within primary PyMT tumors, their abundance is markedly increased compared with healthy mammary tissue. Indeed, analyses comparing healthy mammary glands and PyMT tumors revealed that neutrophils account for less than 1% of CD45+ immune cells in normal tissue, whereas their frequency exceeds 5% in advanced tumors. Therefore, while neutrophils are not the dominant immune population in this model, their recruitment is significantly enhanced during tumor progression and may have important functional consequences. Furthermore, emerging evidence indicates that neutrophils exert context-dependent and sometimes opposing functions in breast cancer, highlighting the importance of studying these cells in physiologically relevant models that reproduce the natural evolution of the disease (Zhao *et al.*, 2023).

Functional characterization under steady state conditions revealed that ELP3 is largely dispensable for neutrophil homeostasis. Indeed, ELP3 deficient neutrophils displayed normal development, viability, migratory capacity, and ROS production, indicating that the loss of ELP3 does not impair canonical neutrophil functions under physiological conditions.

These findings contrast with previous reports describing a critical role for ELP3 in hematopoietic compartments. Deletion of ELP3 in hematopoietic populations has been shown to induce bone marrow failure, impaired stem

cell function, and increased cell death, partly through activation of stress responses such as ATF4 signaling, and p53-dependent checkpoints (Rosu *et al.,* 2021). The absence of such defects in our model likely reflects the cell type specificity of ELP3 deletion and suggests that mature neutrophils may be less dependent on ELP3 activity for maintaining baseline functions.

Altogether, these results indicate that ELP3 is not required for neutrophil homeostasis under steady state conditions and support the idea that its function may become relevant in specific environmental contexts, such as the tumor microenvironment.

Strikingly, neutrophil specific deletion of ELP3 resulted in a pronounced delay in primary tumor progression in the MMTV-PyMT model without any impact on tumor initiation. ELP3-deficient mice exhibited reduced tumor growth kinetics and a clear delay in tumor stage progression, characterized by a reduced transition toward carcinoma. These findings indicate that ELP3-dependent neutrophil functions contribute to primary tumor development.

This finding differs from previous studies reporting that neutrophil depletion does not affect primary tumor growth in breast cancer models. Neutrophil targeting through antibody-mediated depletion, genetic ablation, or G-CSF deficiency has been shown to impair metastatic dissemination without altering primary tumor size, proliferation, apoptosis, or vascularization (Wculek and Malanchi, 2015). These studies have led to the prevailing view that neutrophils primarily contribute to tumor progression at the metastatic stage, notably through the establishment of the pre-metastatic niche.

In contrast, our findings suggest that modulation of neutrophil function, rather than their complete depletion, can influence primary tumor progression. This indicates that ELP3 dependent pathways may regulate specific pro-tumoral activities of neutrophils within the tumor microenvironment.

Neutrophil specific deletion of ELP3 resulted in a strong impairment of metastatic dissemination in the MMTV-PyMT model. While lung metastases were consistently observed in control mice, PyMT ELP3^{NEU} mice displayed marked inhibition of lung metastasis. At advanced stages, metastases could be detected in a subset of ELP3-deficient mice; however, these remained limited in number and size, and a proportion of mice remained metastasis free even at the ethical endpoint.

To determine whether this phenotype could be linked to alterations in neutrophil effector mechanisms, we assessed NET formation in primary

tumors. MPO and H3Cit staining did not reveal detectable differences between PyMT ELP3^{CTR} and PyMT ELP3^{NEU} mice. In addition, in vitro NETosis assays performed under steady state conditions showed comparable NET release between ELP3-deficient and control neutrophils (Data not shown). Together, these results suggest that the impaired metastatic dissemination is unlikely to be explained by changes in NET formation.

The absence of significant differences in NETosis observed using slide-based staining approaches may be partially explained by the relatively low abundance of neutrophils within the tumor microenvironment. Given the limited number of cells available for analysis, subtle differences in NET formation may be difficult to detect using microscopy-based methods. In this context, flow cytometry may represent a more sensitive and quantitative approach for assessing NETosis. Indeed, a study published in 2017 demonstrated that NET formation can be effectively quantified by flow cytometry using SYTOX Green to detect extracellular DNA, either alone or in combination with neutrophil markers such as myeloperoxidase (MPO) (Masuda *et al.*, 2017). Such approaches may improve the detection of modest changes in NETosis and provide a more robust assessment of neutrophil function in tumor-bearing mice.

Our data support a model in which the reduction in metastasis is primarily a consequence of delayed primary tumor progression. In line with this, histological analyses revealed impaired tumor vascularization in PyMT ELP3^{NEU} tumors, as indicated by reduced CD31 staining. These findings suggest that ELP3 deficient TINs may disrupt tumor blood vasculature formation thus, delay tumor progression and reduce metastatic dissemination.

To investigate the hypothesis that the vascular phenotype observed in PyMT ELP3^{NEU} tumors may result from altered neutrophil-mediated angiogenic signaling, we performed secretome analysis on bone marrow-derived neutrophils and specifically assessed MMP9 secretion. While MMP9 was readily detected, VEGF was not measurable under the experimental conditions used. However, recent evidence suggests that neutrophils can promote angiogenesis in breast cancer through direct interactions with epithelial and tumor cells, leading to the induction of VEGF production (Camargo *et al.*, 2025). Therefore, the absence of detectable VEGF secretion from neutrophils cultured alone does not exclude a role for ELP3 in regulating angiogenic signaling. Future experiments employing co-culture systems combining ELP3-deficient neutrophils with PyMT cells will be necessary to determine whether ELP3 deletion impairs VEGF production through cell-cell

interactions within the tumor microenvironment. In addition, other neutrophil-derived pro-angiogenic mediators should be investigated, including BV8 (PROK2), which has been implicated in myeloid cell dependent angiogenesis, and tumor progression (Shojaei *et al.*, 2007). Of note, MMP9 should be further evaluated by gelatin zymography, as this technique distinguishes between the inactive and active forms of the enzyme, thereby providing a more accurate assessment of its biological activity.

A broader characterization of the angiogenic secretome may therefore provide a more comprehensive understanding of the mechanisms underlying the vascular phenotype observed in PyMT ELP3^{NEU} tumors.

In parallel, we investigated the immune tumor microenvironment (TME) remodeling. In fact, the TME in the MMTV-PyMT model has been extensively described as predominantly immunosuppressive, with progressive accumulation of tumor-associated macrophages, regulatory T cells, and myeloid-derived suppressor cells, while T cells remain present but functionally constrained (Attalla et al., 2020). In this context, we sought to determine whether neutrophil-specific deletion of ELP3 could modulate the immune landscape of the tumor microenvironment. To address this, we performed single-cell RNA sequencing alongside flow cytometry analyses to assess both immune cell composition and functional states.

Our analyses revealed no major differences between control and ELP3 deficient tumors. The relative proportions of major immune populations, including CD4$^+$ and CD8$^+$ T cells, B cells, macrophages, and NK cells, remained comparable across conditions. Furthermore, detailed evaluation of T cell functional states, including activation, differentiation, and exhaustion programs such as JAK–STAT signaling and CD4$^+$/CD8$^+$ activation pathways, did not reveal substantial differences. Although minor variations were observed, these did not correspond to a clear shift in T cell activity or distribution.

Interestingly, flow cytometric analysis revealed a reduction in the proportion of γδ T cells in PyMT ELP3^{NEU} tumors. Although the mechanisms underlying the interaction between neutrophils and γδ T cells remain poorly understood, emerging evidence suggests the existence of a functional crosstalk between these two cell populations in cancer. In breast cancer, γδ T cells have been shown to promote the recruitment and expansion of neutrophils through a G-CSF-dependent mechanism, leading to the accumulation of immunosuppressive neutrophils that support tumor progression (Coffelt *et al.*,

2015). More recently, a study published in Nature Cancer (2025) demonstrated that, in HR+HER2− breast cancer, IL-17-producing γδ T cells contribute to therapeutic resistance and promote tumor progression through the activation of macrophages (Petroni *et al.*, 2025). Therefore, the reduced frequency of γδ T cells observed in PyMT ELP3^{NEU} tumors may contribute to the protective phenotype observed in this model by limiting the establishment of a pro-tumorigenic immune microenvironment.

Interestingly, single-cell RNA-sequencing analysis did not confirm this reduction and instead suggested a higher proportion of γδ T cells. This discrepancy may reflect the intrinsic limitations of single-cell transcriptomic approaches, which are not designed to provide quantitative measurements of cell abundance and may be influenced by sampling and processing biases. Additional studies are therefore required to clarify the impact of ELP3-depleted neutrophils on γδ T-cell biology. Functional characterization of γδ T cells through the assessment of IL-17 production may help determine whether their pro-tumorigenic activity is altered in PyMT ELP3^{NEU} tumors.

Notably, neutrophils represented a minor fraction of the tumor immune compartment, accounting for approximately 1–2% of immune cells. Despite this low abundance, modulation of neutrophil function through ELP3 deletion resulted in significant effects on tumor progression and metastasis. Altogether, these findings indicate that the observed phenotype is unlikely to be driven by changes in the global immune landscape and instead support a neutrophil intrinsic mechanism acting within the tumor microenvironment.

Our proteomic analyses indicate that ELP3 contributes to the metabolic adaptation of neutrophils within the tumor microenvironment. While circulating neutrophils from ELP3-deficient and control mice displayed highly similar proteomic profiles, clear differences emerged upon tumor infiltration. PyMT ELP3^{NEU} TINs showed a downregulation of mitochondrial pathways, including oxidative phosphorylation, suggesting that ELP3 is required for the establishment or maintenance of mitochondrial programs specifically within the tumor context. This observation highlights the importance of the tumor microenvironment in revealing ELP3 dependent functions in neutrophils.

Comparison between PyMT ELP3^{CTR} and PyMT ELP3^{NEU} TINs revealed the downregulation of several mitochondrial proteins. Two main transporters were downregulated upon the loss of ELP3 in TINs. SL25A14 is a downregulated transporter in ELP3 depleted TINs and plays a role in transferring sulfate, sulfite, thiosulfate and phosphate thus maintaining oxidative balance and ATP production.

On the other hand, a second transporter was downregulated upon the loss of ELP3. SLC25A10 is a main transporter of dicarboxylate (Malate, Succinate and Malonate) and a main transporter of substrates to sustain metabolic pathways such as fatty acid metabolism, gluconeogenesis and sulfur metabolism. In prostate cancer, SLC25A10 showed an increased expression correlated with cancer aggressiveness and progression by inhibiting ferroptosis through p62/KEAP1/Nrf2-linked mechanism (Yu *et al.*, 2025). These findings raise the hypothesis of perturbated metabolism within the tumor additionally to a possible ferroptosis induced cell death of PyMT ELP3^{NEU} TINs.

Consistent with these findings, ultrastructural analysis revealed a reduction in mitochondrial content in ELP3 deficient neutrophils. In addition, metabolomic profiling identified decreased levels of key metabolic intermediates, including α-ketoglutarate, as well as fructose-6-phosphate and glucose-6-phosphate. These alterations suggest potential impairments in central metabolic pathways, notably the tricarboxylic acid (TCA) cycle and glycolysis associated pathways, including the pentose phosphate pathway (PPP).

These observations are particularly relevant considering recent studies highlighting the importance of metabolic flexibility in neutrophil function. It has been shown that, upon activation, neutrophils rapidly redirect glucose flux toward the oxidative pentose phosphate pathway to sustain NADPH production and support ROS generation, with this metabolic switch occurring within minutes and being tightly linked to oxidative burst capacity (Britt *et al.,* 2022). In this context, reduced availability of G6P and F6P in ELP3-deficient neutrophils may indicate an impaired capacity to engage the PPP, potentially affecting ROS related functions under specific conditions.

Furthermore, our findings are consistent with previous reports describing a role for ELP3 in regulating cellular metabolism. In macrophages, ELP3 has been shown to support metabolic programs associated with M2 profile, and its deletion leads to reduced levels of α-ketoglutarate and glycolytic intermediates, suggesting a broader role for ELP3 in controlling metabolic pathways (Chen *et al.,* 2022). Altogether, these data support a model in which ELP3 contributes to the metabolic adaptation of neutrophils within the tumor microenvironment, potentially through the regulation of mitochondrial function and key metabolic pathways.

Despite the metabolic alterations suggested by proteomic and metabolomic analyses, functional assays did not reveal major bioenergetic defects in ELP3-deficient neutrophils. Measurements of oxygen consumption rate (OCR) and

extracellular acidification rate (ECAR) performed on bone marrow derived neutrophils under multiple substrate conditions did not show significant differences between control and ELP3 depleted neutrophils extracted from steady state mice. Similarly, mitochondrial membrane potential and mitochondrial ROS levels remained comparable between $ELP3^{CTR}$ and $ELP3^{NEU}$ neutrophils in tumor bearing conditions.

These observations suggest that ELP3 loss might not induce a global collapse of mitochondrial function but rather leads to more subtle alterations. This is consistent with our proteomic data showing that, although mitochondrial pathways are reduced in ELP3-deficient TINs compared to controls, these pathways remain elevated when compared to circulating neutrophils, indicating that mitochondrial activity is not abolished but potentially partially impaired.

It is important to note that OCR and ECAR measurements were performed under standard culture conditions and therefore may not fully recapitulate the metabolic constraints encountered within the tumor microenvironment. Consequently, these results should be interpreted with caution, as potential metabolic alterations associated with ELP3 deficiency may only become apparent under conditions mimicking the hypoxic, acidic, and inflammatory environment of the tumor.

Importantly, these results highlight the context dependent nature of ELP3 function. Seahorse analyses were performed on bone marrow neutrophils, which may not fully recapitulate the phenotype of TINs. Indeed, previous studies have demonstrated that metabolically active neutrophil subsets with enhanced mitochondrial function, such as c-Kit^{+} tumor elicited neutrophils, are enriched in tumor bearing conditions and differ from steady state populations (Rice *et al.*, 2018). In this regard, the use of bone marrow neutrophils represents a limitation, as these cells likely do not fully capture the metabolic adaptations occurring within the tumor microenvironment.

On the other hand, the same study reported that the oxidative burst occurs rapidly following neutrophil stimulation, with oxygen consumption rates peaking within approximately 10 minutes after PMA exposure. The authors further showed that this response is transient and rapidly dissipates thereafter. These findings suggest that the DHR123-based assay used in our study may not optimally capture the peak oxidative burst response. Indeed, the interval required for probe incubation, surface staining, washing steps, and flow cytometric acquisition may exceed the duration of maximal ROS production, potentially resulting in an underestimation of the oxidative burst signal.

Consequently, the absence of significant differences in our FACS readouts should be interpreted with caution, as technical limitations may have masked transient changes in neutrophil ROS production.

In addition, PMA is a potent pharmacological activator of protein kinase C (PKC) that induces a strong and non-physiological oxidative burst in neutrophils. As such, PMA stimulation may be too robust to reveal subtle differences in ROS production resulting from ELP3 deficiency. The intense activation of NADPH oxidase elicited by PMA may override more nuanced regulatory mechanisms and thereby mask genotype-dependent effects. To better reflect the tumor microenvironment, future studies should employ more physiologically relevant stimuli, including G-CSF, TNF-α, IFN-γ, or acidic culture conditions that mimic tumor-associated pH alterations. These approaches may provide a more accurate assessment of the contribution of ELP3 to neutrophil ROS production under conditions relevant to breast cancer progression.

Furthermore, the low abundance of neutrophils within tumors (approximately 1–2% of immune cells) and the limited number of cells recovered after sorting (~5,000 cells per tumor) restricted our ability to perform functional metabolic assays directly on tumor infiltrating neutrophils. Altogether, these findings suggest that ELP3-dependent metabolic alterations are subtle and likely emerge specifically within the tumor microenvironment, rather than being detectable under steady state or in vitro conditions.

In line with the possibility of a subtle metabolic rewiring, additional molecular observations provide tentative support for alterations in TCA cycle associated pathways. Although single-cell RNA sequencing was limited by low neutrophil representation and reduced analytical depth, we observed a decrease in ACOD1 expression in PyMT ELP3^{NEU} neutrophils.

ACOD1 encodes aconitate decarboxylase 1, a key enzyme that converts cis-aconitate into itaconate, a metabolite derived from the TCA cycle with important immunometabolism functions. Recent work has shown that ACOD1 is strongly upregulated in tumor infiltrating neutrophils, where itaconate production contributes to metabolic adaptation, supports neutrophil fitness within the tumor microenvironment and protects against ferroptosis in an NRF2 dependent manner (Zhao et al., 2023). In this context, reduced ACOD1 expression in ELP3 deficient neutrophils may suggest a perturbation in adaptation and viability within the tumor microenvironment.

Interestingly, our two independent datasets: Proteomics and sc-RNAseq converged on genes linked to redox homeostasis and ferroptosis resistance, with ACOD1 downregulated at the transcript level and SLC25A10 reduced at the proteomic level in PyMT ELP3^{NEU} TINs. Both molecules have been implicated in NRF2 associated antioxidant responses, suggesting that ELP3 loss may impair protective pathways against oxidative stress and ferroptosis (Zhao *et al.*, 2023; Yu *et al.*, 2025).

While this observation remains exploratory, it is consistent with our metabolomic data showing reduced α-ketoglutarate levels, further supporting the hypothesis that ELP3 loss may affect TCA cycle linked metabolic processes. Altogether, these findings raise the possibility that ELP3 contributes to the regulation of neutrophil immunometabolism within tumors, although direct functional validation will be required to establish this link.

To further investigate whether the effects of ELP3 loss could be explained by codon-dependent translation, we compared transcriptomic and proteomic changes in tumor infiltrating neutrophils. This analysis revealed a low correlation between mRNA and protein levels, suggesting the presence of post-transcriptional regulatory mechanisms. Notably, proteins associated with mitochondrial function and ribosomal components were preferentially affected at the proteomic level, despite limited corresponding changes at the transcript level.

However, codon usage analysis focusing on U34-sensitive codons (AAA, CAA, GAA) did not reveal strong enrichment within the differentially regulated protein subsets. These findings indicate that the effects of ELP3 depletion are unlikely to be explained by a global codon bias mechanism. Instead, they suggest that ELP3 may regulate gene expression through more selective processes, potentially involving context dependent translation, modulation of protein stability, or regulation of specific subsets of transcripts rather than broad codon driven effects.

Despite the clear impact of ELP3 deficient neutrophils on tumor progression and tumor blood vasculature development, the underlying mechanisms remain unresolved. Functional analyses did not reveal significant differences in key neutrophil effector functions commonly associated with vascular remodeling, including total ROS production, arginase-1 expression, and MMP9 secretion.

It is important to note that ROS production is a highly dynamic process, and previous studies have shown that oxidative burst responses occur rapidly,

within minutes of stimulation (Britt *et al.*, 2022). Therefore, it is possible that transient or localized ROS signals were not fully captured under the experimental conditions used, particularly given the constraints of ex vivo measurements and flow cytometry-based readouts. In this context, alternative approaches such as real-time metabolic assays measuring OCR upon stimulation may provide additional insights.

Altogether, these results suggest that the primary tumor development phenotype observed in vivo is not driven by major alterations in canonical neutrophil effector functions. Instead, they raise the possibility that ELP3 deficient neutrophils may regulate angiogenesis through more subtle or context dependent mechanisms, such as localized degranulation, spatially restricted factor release, or metabolic signaling within the tumor microenvironment.

This study presents several limitations that should be considered when interpreting the results. From a technical perspective, the low abundance of neutrophils within tumors limited downstream analyses, particularly in the single-cell RNA sequencing dataset, where the small number of captured neutrophils reduced the power to detect subtle transcriptional changes. In addition, the short lifespan of neutrophils and the limited cell yield obtained after tumor dissociation further constrained the range of experiments that could be performed.

At the mechanistic level, direct assessment of translational regulation could not be achieved. Polysome profiling and direct translation assays were not successfully implemented, preventing a definitive evaluation of codon dependent translation. While our data suggest the involvement of post-transcriptional mechanisms, the precise contribution of U34 dependent translation remains to be fully established.

An additional approach to further investigate the role of ELP3 in neutrophil biology would be the use of the human promyelocytic leukemia cell line PLB-985. Upon differentiation using established protocols, including culture in the presence of Nutridoma for six days, PLB-985 cells acquire neutrophil-like characteristics and functional properties. This model provides a readily available and scalable source of neutrophil-like cells, overcoming the limitations associated with the isolation of primary neutrophils and enabling experiments that require large cell numbers. Consequently, PLB-985-derived neutrophils could represent a valuable tool for future mechanistic studies investigating the impact of ELP3 depletion on neutrophil functions and characteristics (Bhakta *et al.*, 2024).

In addition, Human peripheral blood neutrophils provide a readily accessible model to investigate neutrophil responses under controlled experimental conditions. However, tumor-associated neutrophils (TANs) undergo extensive transcriptional, translational, and metabolic reprogramming within the tumor microenvironment, resulting in phenotypes that are not fully recapitulated ex vivo.

Given our observations linking U34 tRNA modifications to neutrophil plasticity, we are currently investigating conditions that promote the expression of U34-modifying enzymes and tRNA remodeling in human blood neutrophils. Our objective is to identify tumor-associated signals capable of inducing TAN-like features and to establish an ex vivo model for studying the contribution of translational reprogramming to neutrophil adaptation in cancer.

From a functional standpoint, metabolic assays were primarily conducted ex vivo using bone marrow derived neutrophils. These conditions may not fully recapitulate the tumor microenvironment and attempts to mimic tumor conditions using conditioned media did not reproduce the in vivo phenotype, highlighting the context dependent nature of neutrophil adaptation. In addition, although metabolomic analyses suggested alterations in key intermediates such as α-ketoglutarate and glucose-6-phosphate, further targeted quantification of metabolites including NADPH, α-ketoglutarate, and G6P will be required to validate and refine these findings.

Overall, although the results consistently support a role for ELP3 in neutrophil function during tumor progression, the underlying mechanisms remain partially unresolved and require further investigation.

Altogether, although ferroptosis was not directly assessed in this study, the convergence of metabolic alterations observed in ELP3 deficient neutrophils including changes in TCA cycle intermediates and the potential modulation of ACOD1 expression and SLC25A10 who are 2 proteins implicated in ferroptosis raises the possibility that ferroptosis related pathways may be affected. This hypothesis remains speculative and will require dedicated validation in the TINs. This work highlighted also the metabolic rewiring of TINs as a critical aspect of their pro-tumoral activity and identifies neutrophil metabolism as a potential therapeutic vulnerability that could be exploited to limit tumor progression.

Supplementary materials

MFI TMRM FACs results

Blood neutrophils PyMT ELP3^{CTR}	TINs PyMT ELP3^{CTR}	Blood neutrophils PyMTELP3^{NEU}	TINs PyMTELP3^{NEU}
9632	12400	19477	16876
18854	17578	20079	19524
21742	19391	41736	38212
8445	11027	11883	11394
7611	11490	24330	23733
7457	9681	25293	23062
		10028	11485
		18581	19148

Mitosox Facs results

BM PyMT ELP3^{NEU}	BM PyMT ELP3^{CTR}	Blood neutrophils PyMT ELP3^{CTR}	TINs PyMT ELP3^{CTR}	Blood neutrophils PyMT ELP3^{NEU}	TINs PyMT ELP3^{NEU}
222	1618	3723	4594	311	1946
168	396	196	1259	179	1636
157	900	207	1991	174	1506
142	178	224	2044	401	1389
958	178	140	996		3561
2115	122	298	1699		5497
	130	156	1225		5050
			362		

MFI Total cellular ROS FACs data

BM PyMT ELP3^{NEU}	BM PyMT ELP3^{CTR}	Blood neutrophils PyMT ELP3^{CTR}	TINs PyMT ELP3^{CTR}	Blood neutrophils PyMT ELP3^{NEU}	TINs PyMT ELP3^{NEU}

3886	5233	3622	4922	4556	4246
4263	3839	3279	4547	2420	8117
2193	5604	3590	4585	4730	8503
3118	5087	1474	5553	3967	5051
10443	2560	1410	2405	4106	10848
4719	2071	3326	6932		12226
4452	9420	2762	12163		5566
	8152		5839		
	3622				

Arginase 1: % of population CD45+ Ly6G+ CD11b+ Arginase1+

Blood neutrophils PyMT ELP3^{CTR}	TINs PyMT ELP3^{CTR}	Blood neutrophils PyMTELP3^{NEU}	TINs PyMTELP3^{NEU}
54.6	39.5	100	90.9
8.79	6.35	96.6	40.3
71.1	70.1	98	9.27
23.2	39.4	46.7	35.2
19.8	30.4	34.1	29.7
26.7	28.7	82.1	83.7
		45.4	77.5
		9.27	27.8

Migration assay

BM PyMT ELP3^{CTR}	BM PyMT ELP3^{NEU}
4090.633	1805.88
4267.686	4125.481
2626.962	3009.437

Total cellular ROS : % of the population CD45+ Ly6G+ CD11b+ DHR123 +

BM PyMT ELP3^{CTR}	BM PyMT ELP3^{NEU}
16.3	15.05
11.4	14.9
13.25	11.18

Protein synthesis assay OPP

BM PyMT ELP3^{NEU}	BM PyMT ELP3^{CTR}	Blood neutrophils PyMT ELP3^{CTR}	TINs PyMT ELP3^{CTR}	Blood neutrophils PyMT ELP3^{NEU}	TINs PyMT ELP3^{NEU}

27227	18057	10929	10631	12362	7112
25851	13234	7108	13626	12011	13782
14943	8463	13063	16135	8605	11768
6370	31970	11732	11914	7299	8947
25713	34005	3758	3363	19210	15350
18405	24900	20298	12751	20018	12334
	16433	13340	8370		
	4810	23378			

Immune profiling :

Neutrophils

PyMT ELP3^{CTR}	PyMT ELP3^{NEU}
0.52	0.58
0.65	0.53
0.49	1.28
0.27	0.18
0.094	0.74
0.73	

T cells : Live+ CD45+ CD3+

PyMT ELP3^{CTR}	PyMT ELP3^{NEU}
85.5	71.5
73.2	76
85.8	82.3
71	82.8
	73.4
	66.1

Live+ CD45+ CD3+ CD8+

PyMT ELP3^{CTR}	PyMT ELP3^{NEU}
20.448	20.9495
23.427	24.5156
18.1536	21.28
23.2518	26.6652
	24.012
	17.1199

Live+ CD45+CD3+CD4+

PyMT ELP3^{CTR}	PyMT ELP3^{NEU}
46.576	47.9765
60.1065	45.7282
49.5564	51.528
60.6606	53.4127
	56.4696
	40.8498

CD44+ CD8+

PyMT ELP3^{CTR}	PyMT ELP3^{NEU}
29.9	31
26.5	30.5
35.4	29.8
35.5	28
	28.9
	20.2

CD127+ CD8+

PyMT ELP3^{CTR}	PyMT ELP3^{NEU}
86.9	75.2
69.9	72.9
77.1	83.3
84.3	71.4
	85.1
	61.8

CD44+ CD4+

PyMT ELP3^{CTR}	PyMT ELP3^{NEU}
18.4	25
15.3	25.9
25.1	23.4
32.8	21.7
	24
	15.6

CD127+ CD4+

PyMT ELP3^{CTR}	PyMT ELP3^{NEU}
87.1	76.3
69.4	75.3
69.4	84.6

80.3	68.3
	82
	68.3

NK

PyMT ELP3^{CTR}	PyMT ELP3^{NEU}
1.26	1.03
2.11	1.37
0.63	1.07
2.13	1.05
	1.62
	0.66

γδTC8+

PyMT ELP3^{CTR}	PyMT ELP3^{NEU}
8.48	4.08
12.4	2.51
18.7	7.1
11.8	8.99
	4.08
	0.69
	0.06

T regulatory

PyMT ELP3^{CTR}	PyMT ELP3^{NEU}
5.615813	2.767466
6.78732	1.706006
1.779636	1.64637
1.812732	1.629966
2.393751	1.884168
10.51339	1.619144
0.926106	

Survival of BM neutrophils ELP3^{CTR} and ELP3^{NEU}

Time (h)	WT - G-CSF			WT + G-CSF			KO - G-CSF			KO + G-CSF		
0	45.88571	62.21006	67.57777	48.0714	64.72001	67.86018	58.22647	71.76625	73.29866	63.27806	74.03722	76.27417
1	48.94295	60.95755	46.71855	48.9818	65.89602	49.19241	57.08523	69.73816	54.08753	62.70616	74.46514	56.59641
2	49.20651	57.38321	50.3172	50.38626	66.01102	52.60713	55.95363	65.88418	56.34699	62.27998	74.45231	59.02397
3	49.41976	55.44007	51.85286	50.88194	66.00453	54.16756	53.12712	63.97149	57.62669	61.0556	74.76942	61.15599
4	46.41981	54.69477	51.5824	49.80802	67.03194	54.85452	49.70335	63.45399	56.65884	58.49308	75.14171	61.27428
5	45.38258	54.10165	50.01224	50.77083	67.29103	55.01076	46.26608	63.68988	54.65189	58.14952	75.88913	62.41771
6	42.95139	53.68165	46.86522	52.44133	68.00043	55.18917	43.54274	62.89362	50.68272	59.06708	76.73893	62.7566
7	41.96575	53.38298	43.61536	54.00847	68.38793	54.69707	42.73707	63.02731	47.72336	58.44458	77.32801	62.33411
8	41.18522	53.63828	41.61526	53.88132	69.77983	54.58583	42.07292	63.26002	46.27573	58.92136	77.97119	62.45344
9	40.74197	53.60964	39.70814	54.87753	70.50392	54.35389	40.08054	63.53064	44.18496	58.51931	78.07407	62.61361
10	40.3479	54.23414	39.01455	55.17468	70.34823	54.17827	40.03472	63.83682	43.39532	58.72422	78.94406	62.89664
11	40.65773	54.00811	38.14035	56.37687	71.03886	54.41426	40.00709	64.01051	42.75731	59.48979	79.31333	63.62546
12	39.56795	54.097	37.76062	56.41443	71.30408	54.58705	39.52308	63.73427	42.00245	58.66415	80.28865	63.75694
13	40.37833	54.49295	37.48133	57.1543	71.9091	54.99301	39.59138	63.80378	41.72553	58.99647	80.29408	64.17183
14	39.49484	54.55065	37.19223	58.02655	72.3838	55.40444	40.13271	64.63629	41.89098	59.50302	80.95168	64.48492
15	39.64687	53.98776	37.22	58.59994	73.06617	55.60626	40.08289	64.54939	41.44124	59.76717	81.06717	65.16042
16	39.24123	54.69297	37.14542	58.46554	73.44735	56.208	39.72529	64.09369	40.73778	59.62659	81.31263	65.71747
17	39.05794	53.04237	36.67422	59.26173	72.83051	56.44623	40.70886	63.17994	40.74758	60.48013	80.83277	66.44975
18	39.69789	53.21626	36.46546	60.28521	73.35736	57.27005	40.11541	63.83067	40.41729	61.44598	81.5317	66.7084
19	39.53552	53.92523	36.41113	61.23687	73.77637	57.51871	40.14589	64.51039	40.40978	61.42132	81.59126	67.58407
20	39.03123	54.14765	36.12974	61.84108	73.94418	57.56326	40.87883	64.37758	39.98823	62.33879	82.1189	67.99873
21	39.55726	53.91413	35.95724	61.90725	74.30596	58.4734	40.44395	64.18656	39.74031	62.45714	82.18168	68.5073

22	39.2351	54.01788	36.15104	61.81986	74.474	58.97314	39.64457	64.60055	39.88693	62.96901	82.61481	68.73233
23	39.07085	53.81502	35.82769	63.19967	74.98832	59.81155	39.8431	64.36067	39.48052	63.0285	82.68076	69.08799
24	39.21933	53.98779	35.91655	63.54576	74.81882	59.82076	38.88931	64.01507	39.09226	64.24932	82.67164	69.43843
25	38.23884	53.13229	35.58324	63.81784	75.2517	60.49626	39.33787	63.97082	38.50998	64.59478	83.42587	69.37128
26	36.90144	53.53261	35.64677	63.65531	75.34622	60.94227	38.23541	64.62844	38.48861	63.77978	83.32867	69.8162
27	37.54287	53.09656	33.12967	64.96613	75.58034	58.72916	39.20487	64.31768	36.21556	65.42402	83.6351	68.60272
28	37.4527	52.85942	35.02319	64.91106	75.43393	60.27781	38.87964	64.34856	37.82944	65.3171	83.92878	70.08903
29	37.47725	53.06938	34.56059	65.83247	75.77824	61.14911	39.47286	64.17956	37.32788	66.13865	83.9839	70.72524
30	36.22872	52.64034	35.00702	65.80313	75.67713	61.71478	38.70455	63.59442	37.82711	67.10769	84.07872	71.14259
31	36.10097	52.28639	34.40454	66.51346	75.80685	61.66478	37.86011	63.53863	37.71451	67.03464	84.20903	71.54723
32	35.66944	52.4375	33.56917	66.16046	76.0154	61.46501	37.48843	63.77009	36.70837	67.07772	84.27884	71.4454
33	35.94926	52.38594	33.53074	67.37779	76.16009	61.4604	38.03775	63.73348	36.80801	67.30234	84.15081	71.56026
34	35.1629	52.65081	33.49205	66.99021	76.54698	61.35508	37.64302	63.68881	37.09606	67.11961	84.21527	71.89583
35	34.07494	52.69447	32.70291	67.03954	76.51803	61.11146	36.71984	63.5613	36.00914	68.03028	84.41969	71.81387
36	33.88691	52.1212	32.75865	67.67794	76.04721	60.66741	37.05728	63.21897	35.74154	67.83958	84.50342	71.94017
37	34.12159	52.10577	32.21349	68.1366	76.22083	59.96464	37.41035	63.23482	36.48041	68.24969	84.54602	72.4022
38	33.40357	52.39542	32.15239	67.77685	76.12472	59.19012	36.48993	63.40334	35.25853	68.58051	84.58733	71.85638
39	33.27579	52.11252	32.38676	68.01235	76.11677	59.31644	36.00571	63.80993	35.65809	68.57921	84.78766	72.41755
40	32.57906	51.64726	31.99005	68.36204	75.68947	58.33181	35.69971	62.61223	36.01323	68.68933	84.85269	72.16553
41	32.67657	51.96337	30.77744	68.68644	76.05582	57.52888	35.73195	63.34636	35.4774	69.60222	85.25723	72.33566
42	31.72861	51.07932	30.67414	68.68106	76.07875	56.51218	34.71387	62.55303	35.21163	69.62491	85.3728	72.58038
43	31.59172	51.60289	30.41588	69.14665	76.07474	55.49754	35.66169	62.87393	35.04384	68.93694	85.43386	72.82756

Bibliography

Anastasiadi, Z. *et al.* (2017) “Breast cancer in young women: an overview,” *Updates in Surgery*, 69(3), pp. 313–317. Available at: https://doi.org/10.1007/s13304-017-0424-1.

Añazco-Guenkova, A.M. *et al.* (2024) “The impact of tRNA modifications on translation in cancer: identifying novel therapeutic avenues,” *NAR Cancer*, 6(1), p. zcae012. Available at: https://doi.org/10.1093/narcan/zcae012.

Andzinski, L. *et al.* (2016) “Type I IFNs induce anti-tumor polarization of tumor associated neutrophils in mice and human,” *International Journal of Cancer*, 138(8), pp. 1982–1993. Available at: https://doi.org/10.1002/ijc.29945.

Attalla, S. *et al.* (2021) “Insights from transgenic mouse models of PyMT-induced breast cancer: recapitulating human breast cancer progression in vivo,” *Oncogene*, 40(3), pp. 475–491. Available at: https://doi.org/10.1038/s41388-020-01560-0.

Barroso-Sousa, R. *et al.* (2020) “Prevalence and mutational determinants of high tumor mutation burden in breast cancer,” *Annals of Oncology*, 31(3), pp. 387–394. Available at: https://doi.org/10.1016/j.annonc.2019.11.010.

Belambri, S.A. *et al.* (2018) “NADPH oxidase activation in neutrophils: Role of the phosphorylation of its subunits,” *European Journal of Clinical Investigation*, 48(S2), p. e12951. Available at: https://doi.org/10.1111/eci.12951.

Berg, M.D. and Brandl, C.J. (2020) “Transfer RNAs: diversity in form and function,” *RNA Biology*, 18(3), pp. 316–339. Available at: https://doi.org/10.1080/15476286.2020.1809197.

Bergers, G. and Benjamin, L.E. (2003) “Tumorigenesis and the angiogenic switch,” *Nature Reviews Cancer*, 3(6), pp. 401–410. Available at: https://doi.org/10.1038/nrc1093.

Bhakta, S.B. *et al.* (2024) “Neutrophil-like cells derived from the HL-60 cell-line as a genetically-tractable model for neutrophil degranulation,” *PLOS ONE*, 19(2), p. e0297758. Available at: https://doi.org/10.1371/journal.pone.0297758.

Boye, E. and Grallert, B. (2020) “eIF2α phosphorylation and the regulation of translation,” *Current Genetics*, 66(2), pp. 293–297. Available at: https://doi.org/10.1007/s00294-019-01026-1.

Brambilla, M. *et al.* (2025) “Neutrophil extracellular traps in cancer: immune modulation, therapy resistance, and the dilemma of targeting,” *Cell Death & Disease*, 16(1), p. 882. Available at: https://doi.org/10.1038/s41419-025-08218-3.

Brito Querido, J., Díaz-López, I. and Ramakrishnan, V. (2024) “The molecular basis of translation initiation and its regulation in eukaryotes,” *Nature Reviews Molecular Cell Biology*, 25(3), pp. 168–186. Available at: https://doi.org/10.1038/s41580-023-00624-9.

Britt, E.C. *et al.* (2022) “Switching to the cyclic pentose phosphate pathway powers the oxidative burst in activated neutrophils,” *Nature Metabolism*, 4(3), pp. 389–403. Available at: https://doi.org/10.1038/s42255-022-00550-8.

Britt, E.C. *et al.* (2024) “Activation induces shift in nutrient utilization that differentially impacts cell functions in human neutrophils,” *Proceedings of the National Academy of Sciences of the United States of America*, 121(39), p. e2321212121. Available at: https://doi.org/10.1073/pnas.2321212121.

Bullock, T.N.J. (2022) “CD40 stimulation as a molecular adjuvant for cancer vaccines and other immunotherapies,” *Cellular & Molecular Immunology*, 19(1), pp. 14–22. Available at: https://doi.org/10.1038/s41423-021-00734-4.

Buszka, K. *et al.* (2025) “Dual Nature of Neutrophil Extracellular Traps (NETs)-From Cancer’s Ally to Therapeutic Target,” *Cells*, 14(15), p. 1200. Available at: https://doi.org/10.3390/cells14151200.

Camargo, S. *et al.* (2025) “Neutrophils physically interact with tumor cells to form a signaling niche promoting breast cancer aggressiveness,” *Nature Cancer*, 6(3), pp. 540–558. Available at: https://doi.org/10.1038/s43018-025-00924-3.

Carlos Silvestre-Roig, Andres Hidalgo, and Oliver Soehnlein (2016) “Neutrophil heterogeneity: implications for homeostasis and pathogenesis,” *Blood* [Preprint].

Christie, M. and Igreja, C. (2023) “eIF4E-homologous protein (4EHP): a multifarious cap-binding protein,” *The FEBS journal*, 290(2), pp. 266–285. Available at: https://doi.org/10.1111/febs.16275.

Coffelt, S.B. *et al.* (2015) “IL-17-producing γδ T cells and neutrophils conspire to promote breast cancer metastasis,” *Nature*, 522(7556), pp. 345–348. Available at: https://doi.org/10.1038/nature14282.

Coffelt, S.B., Wellenstein, M.D. and de Visser, K.E. (2016) “Neutrophils in cancer: neutral no more,” *Nature Reviews Cancer*, 16(7), pp. 431–446. Available at: https://doi.org/10.1038/nrc.2016.52.

Cooper, G.M. (2000) “Translation of mRNA,” *The Cell: A Molecular Approach. 2nd edition*. Sinauer Associates. Available at: https://www.ncbi.nlm.nih.gov/books/NBK9849/ (Accessed: April 10, 2026).

Creppe, C. *et al.* (2009) “Elongator controls the migration and differentiation of cortical neurons through acetylation of alpha-tubulin,” *Cell*, 136(3), pp. 551–564. Available at: https://doi.org/10.1016/j.cell.2008.11.043.

Crick, F. (1970) “Central Dogma of Molecular Biology,” *Nature*, 227(5258), pp. 561–563. Available at: https://doi.org/10.1038/227561a0.

Dickinson, R.J. and Keyse, S.M. (2006) “Diverse physiological functions for dual-specificity MAP kinase phosphatases,” *Journal of Cell Science*, 119(22), pp. 4607–4615. Available at: https://doi.org/10.1242/jcs.03266.

Dvir, K., Giordano, S. and Leone, J.P. (2024) “Immunotherapy in Breast Cancer,” *International Journal of Molecular Sciences*, 25(14), p. 7517. Available at: https://doi.org/10.3390/ijms25147517.

Fabbri, L. *et al.* (2021) “The plasticity of mRNA translation during cancer progression and therapy resistance,” *Nature Reviews Cancer*, 21(9), pp. 558–577. Available at: https://doi.org/10.1038/s41568-021-00380-y.

Gao, J. *et al.* (2026) “Restricting lipid accumulation in tumor-infiltrating neutrophils mediates caloric restriction-induced anti-cancer effects,” *Cell Metabolism*, 38(3), pp. 598-615.e7. Available at: https://doi.org/10.1016/j.cmet.2025.11.007.

Geering, B. and Simon, H.-U. (2011) “Peculiarities of cell death mechanisms in neutrophils,” *Cell Death & Differentiation*, 18(9), pp. 1457–1469. Available at: https://doi.org/10.1038/cdd.2011.75.

Gierlikowska, B. *et al.* (2021) “Phagocytosis, Degranulation and Extracellular Traps Release by Neutrophils—The Current Knowledge, Pharmacological Modulation and Future Prospects,” *Frontiers in Pharmacology*, 12. Available at: https://doi.org/10.3389/fphar.2021.666732.

Han, S.-H. *et al.* (2022) “Expression of HLA class I is associated with immune cell infiltration and patient outcome in breast cancer,” *Scientific Reports*, 12, p. 20367. Available at: https://doi.org/10.1038/s41598-022-24890-3.

Ho, J.J.D. *et al.* (2020) “A network of RNA-binding proteins controls translation efficiency to activate anaerobic metabolism,” *Nature Communications*, 11(1), p. 2677. Available at: https://doi.org/10.1038/s41467-020-16504-1.

Ioannis, K. *et al.* (2021) “G-CSF in tumors: aggressiveness, tumor microenvironment and immune cell regulation,” *Cytokine*, 142, p. 155479. Available at: https://doi.org/10.1016/j.cyto.2021.155479.

Jaillon, S. *et al.* (2020) “Neutrophil diversity and plasticity in tumour progression and therapy,” *Nature Reviews Cancer*, 20(9), pp. 485–503. Available at: https://doi.org/10.1038/s41568-020-0281-y.

Jeon, J.-H. *et al.* (2020) “Current Understanding on the Metabolism of Neutrophils,” *Immune Network*, 20(6). Available at: https://doi.org/10.4110/in.2020.20.e46.

Kakumoto, A. *et al.* (2024) “Prognostic impact of tumor-associated neutrophils in breast cancer,” *International Journal of Clinical and Experimental Pathology*, 17(3), pp. 51–62. Available at: https://doi.org/10.62347/JQDQ1527.

Kolaczkowska, E. and Kubes, P. (2013) “Neutrophil recruitment and function in health and inflammation,” *Nature Reviews Immunology*, 13(3), pp. 159–175. Available at: https://doi.org/10.1038/nri3399.

Kong, J. and Lasko, P. (2012) “Translational control in cellular and developmental processes,” *Nature Reviews Genetics*, 13(6), pp. 383–394. Available at: https://doi.org/10.1038/nrg3184.

Ladang, A. *et al.* (2015) “Elp3 drives Wnt-dependent tumor initiation and regeneration in the intestine,” *The Journal of Experimental Medicine*, 212(12), pp. 2057–2075. Available at: https://doi.org/10.1084/jem.20142288.

Laguesse, S. *et al.* (2015) “A Dynamic Unfolded Protein Response Contributes to the Control of Cortical Neurogenesis,” *Developmental Cell*, 35(5), pp. 553–567. Available at: https://doi.org/10.1016/j.devcel.2015.11.005.

Lause, J., Berens, P. and Kobak, D. (2021) “Analytic Pearson residuals for normalization of single-cell RNA-seq UMI data,” *Genome Biology*, 22(1), p. 258. Available at: https://doi.org/10.1186/s13059-021-02451-7.

Lawrence, S.M., Corriden, R. and Nizet, V. (2018) “The Ontogeny of a Neutrophil: Mechanisms of Granulopoiesis and Homeostasis,” *Microbiology and Molecular Biology Reviews : MMBR*, 82(1), pp. e00057-17. Available at: https://doi.org/10.1128/MMBR.00057-17.

Lee, H.J. *et al.* (2016) “Differential expression of major histocompatibility complex class I in subtypes of breast cancer is associated with estrogen receptor and interferon signaling,” *Oncotarget*, 7(21), pp. 30119–30132. Available at: https://doi.org/10.18632/oncotarget.8798.

Li, T. *et al.* (2026) “CXCR2-Dependent Infiltration of Tumor-Associated Neutrophils Is Linked to Enhanced CD8+ T Cell Effector Function and Reduced Lung Metastasis in 4T1 Breast Cancer,” *International Journal of Molecular Sciences*, 27(7), p. 3143. Available at: https://doi.org/10.3390/ijms27073143.

Liang, Y. *et al.* (2023) “The emerging roles of metabolism in the crosstalk between breast cancer cells and tumor-associated macrophages,” *International Journal of Biological Sciences*, 19(15), pp. 4915–4930. Available at: https://doi.org/10.7150/ijbs.86039.

Lin, S. *et al.* (2017) “Lactate-activated macrophages induced aerobic glycolysis and epithelial-mesenchymal transition in breast cancer by regulation of CCL5-CCR5 axis: a positive metabolic feedback loop,” *Oncotarget*, 8(66), pp. 110426–110443. Available at: https://doi.org/10.18632/oncotarget.22786.

Lin, S. and Kuang, M. (2024) “RNA modification-mediated mRNA translation regulation in liver cancer: mechanisms and clinical perspectives,” *Nature Reviews Gastroenterology & Hepatology*, 21(4), pp. 267–281. Available at: https://doi.org/10.1038/s41575-023-00884-y.

Margraf, A., Ley, K. and Zarbock, A. (2019) “Neutrophil Recruitment: From Model Systems to Tissue-Specific Patterns,” *Trends in Immunology*, 40(7), pp. 613–634. Available at: https://doi.org/10.1016/j.it.2019.04.010.

Martínez-Reyes, I. and Chandel, N.S. (2020) “Mitochondrial TCA cycle metabolites control physiology and disease,” *Nature Communications*, 11(1), p. 102. Available at: https://doi.org/10.1038/s41467-019-13668-3.

Masuda, S. *et al.* (2017) “Measurement of NET formation in vitro and in vivo by flow cytometry,” *Cytometry Part A*, 91(8), pp. 822–829. Available at: https://doi.org/10.1002/cyto.a.23169.

Matlung, H.L. *et al.* (2018) “Neutrophils Kill Antibody-Opsonized Cancer Cells by Trogoptosis,” *Cell Reports*, 23(13), pp. 3946-3959.e6. Available at: https://doi.org/10.1016/j.celrep.2018.05.082.

Metzemaekers, M., Gouwy, M. and Proost, P. (2020) “Neutrophil chemoattractant receptors in health and disease: double-edged swords,”

Cellular and Molecular Immunology, 17(5), pp. 433–450. Available at: https://doi.org/10.1038/s41423-020-0412-0.

Morita, M. *et al.* (2012) “A Novel 4EHP-GIGYF2 Translational Repressor Complex Is Essential for Mammalian Development,” *Molecular and Cellular Biology*, 32(17), pp. 3585–3593. Available at: https://doi.org/10.1128/MCB.00455-12.

Moura, T. *et al.* (2025) “Breast Cancer and Tumor Microenvironment: The Crucial Role of Immune Cells,” *Current Oncology*, 32(3), p. 143. Available at: https://doi.org/10.3390/curroncol32030143.

Mu, X. *et al.* (2018) “Tumor-derived lactate induces M2 macrophage polarization via the activation of the ERK/STAT3 signaling pathway in breast cancer,” *Cell Cycle*, 17(4), pp. 428–438. Available at: https://doi.org/10.1080/15384101.2018.1444305.

Muller, W.A. (2011) “Mechanisms of Leukocyte Transendothelial Migration,” *Annual Review of Pathology: Mechanisms of Disease*, 6(1), pp. 323–344. Available at: https://doi.org/10.1146/annurev-pathol-011110-130224.

Nandagopal, N. and Roux, P.P. (2015) “Regulation of global and specific mRNA translation by the mTOR signaling pathway,” *Translation*, 3(1), p. e983402. Available at: https://doi.org/10.4161/21690731.2014.983402.

Ng, M.S.F. *et al.* (2024) “Deterministic reprogramming of neutrophils within tumors,” *Science*, 383(6679), p. eadf6493. Available at: https://doi.org/10.1126/science.adf6493.

Nguyen, G.T., Green, E.R. and Mecsas, J. (2017) “Neutrophils to the ROScue: Mechanisms of NADPH Oxidase Activation and Bacterial Resistance,” *Frontiers in Cellular and Infection Microbiology*, 7. Available at: https://doi.org/10.3389/fcimb.2017.00373.

Nozawa, H., Chiu, C. and Hanahan, D. (2006a) “Infiltrating neutrophils mediate the initial angiogenic switch in a mouse model of multistage carcinogenesis,” *Proceedings of the National Academy of Sciences of the United States of America*, 103(33), pp. 12493–12498. Available at: https://doi.org/10.1073/pnas.0601807103.

Nozawa, H., Chiu, C. and Hanahan, D. (2006b) “Infiltrating neutrophils mediate the initial angiogenic switch in a mouse model of multistage carcinogenesis,” *Proceedings of the National Academy of Sciences*, 103(33), pp. 12493–12498. Available at: https://doi.org/10.1073/pnas.0601807103.

Onkar, S.S. *et al.* (2023) “The Great Immune Escape: Understanding the Divergent Immune Response in Breast Cancer Subtypes,” *Cancer Discovery*, 13(1), pp. 23–40. Available at: https://doi.org/10.1158/2159-8290.CD-22-0475.

Orrantia-Borunda, E. *et al.* (2022) “Subtypes of Breast Cancer,” in H.N. Mayrovitz (ed.) *Breast Cancer*. Brisbane (AU): Exon Publications. Available at: http://www.ncbi.nlm.nih.gov/books/NBK583808/ (Accessed: January 22, 2026).

Othman, A., Sekheri, M. and Filep, J.G. (2022) “Roles of neutrophil granule proteins in orchestrating inflammation and immunity,” *The Febs Journal*, 289(14), pp. 3932–3953. Available at: https://doi.org/10.1111/febs.15803.

Ozel, I. *et al.* (2022) “The Good, the Bad, and the Ugly: Neutrophils, Angiogenesis, and Cancer,” *Cancers*, 14(3), p. 536. Available at: https://doi.org/10.3390/cancers14030536.

Panopoulos, A.D. and Watowich, S.S. (2008) “GRANULOCYTE COLONY-STIMULATING FACTOR: MOLECULAR MECHANISMS OF ACTION DURING STEADY STATE AND ‘EMERGENCY’ HEMATOPOIESIS,” *Cytokine*, 42(3), pp. 277–288. Available at: https://doi.org/10.1016/j.cyto.2008.03.002.

Parker, J.S. *et al.* (2009) “Supervised Risk Predictor of Breast Cancer Based on Intrinsic Subtypes,” *Journal of Clinical Oncology*, 27(8), pp. 1160–1167. Available at: https://doi.org/10.1200/JCO.2008.18.1370.

Petri, B. and Sanz, M.-J. (2018) “Neutrophil chemotaxis,” *Cell and Tissue Research*, 371(3), pp. 425–436. Available at: https://doi.org/10.1007/s00441-017-2776-8.

Petroni, G. *et al.* (2025) “IL-17A-secreting γδ T cells promote resistance to CDK4/CDK6 inhibitors in HR+HER2− breast cancer via CX3CR1+ macrophages,” *Nature Cancer*, 6(10), pp. 1656–1675. Available at: https://doi.org/10.1038/s43018-025-01007-z.

Pillay, J. *et al.* (2010) “In vivo labeling with 2H2O reveals a human neutrophil lifespan of 5.4 days,” *Blood*, 116(4), pp. 625–627. Available at: https://doi.org/10.1182/blood-2010-01-259028.

Pylaeva, E. *et al.* (2019) “NAMPT signaling is critical for the proangiogenic activity of tumor-associated neutrophils,” *International Journal of Cancer*, 144(1), pp. 136–149. Available at: https://doi.org/10.1002/ijc.31808.

Ramessur, A. *et al.* (2023) “Circulating neutrophils from patients with early breast cancer have distinct subtype-dependent phenotypes,” *Breast cancer research: BCR*, 25(1), p. 125. Available at: https://doi.org/10.1186/s13058-023-01707-3.

Rapino, F. *et al.* (2017) “tRNA Modification: Is Cancer Having a Wobble?,” *Trends in Cancer*, 3(4), pp. 249–252. Available at: https://doi.org/10.1016/j.trecan.2017.02.004.

Rapino, F. *et al.* (2018) “Codon-specific translation reprogramming promotes resistance to targeted therapy,” *Nature*, 558(7711), pp. 605–609. Available at: https://doi.org/10.1038/s41586-018-0243-7.

Rapino, F. *et al.* (2021) “Wobble tRNA modification and hydrophilic amino acid patterns dictate protein fate,” *Nature Communications*, 12(1), p. 2170. Available at: https://doi.org/10.1038/s41467-021-22254-5.

Ravindran, M., Khan, M.A. and Palaniyar, N. (2019) “Neutrophil Extracellular Trap Formation: Physiology, Pathology, and Pharmacology,” *Biomolecules*, 9(8), p. 365. Available at: https://doi.org/10.3390/biom9080365.

Reiding, K.R. *et al.* (2021) “Neutrophil azurophilic granule glycoproteins are distinctively decorated by atypical pauci- and phosphomannose glycans,” *Communications Biology*, 4(1), p. 1012. Available at: https://doi.org/10.1038/s42003-021-02555-7.

Rice, C.M. *et al.* (2018) “Tumour-elicited neutrophils engage mitochondrial metabolism to circumvent nutrient limitations and maintain immune suppression,” *Nature Communications*, 9(1), p. 5099. Available at: https://doi.org/10.1038/s41467-018-07505-2.

Rivalta, A. *et al.* (2025) “Ribosomes: from conserved origin to functional/medical mobility and heterogeneity,” *Philosophical Transactions of the Royal Society B: Biological Sciences*, 380(1921), p. 20230393. Available at: https://doi.org/10.1098/rstb.2023.0393.

Rosu, A. *et al.* (2021) “Loss of tRNA-modifying enzyme Elp3 activates a p53-dependent antitumor checkpoint in hematopoiesis,” *The Journal of Experimental Medicine*, 218(3), p. e20200662. Available at: https://doi.org/10.1084/jem.20200662.

Scott, A.C. *et al.* (2019) “TOX is a critical regulator of tumour-specific T cell differentiation,” *Nature*, 571(7764), pp. 270–274. Available at: https://doi.org/10.1038/s41586-019-1324-y.

Secondini, C. *et al.* (2017) “Arginase inhibition suppresses lung metastasis in the 4T1 breast cancer model independently of the immunomodulatory and anti-metastatic effects of VEGFR-2 blockade,” *Oncoimmunology*, 6(6), p. e1316437. Available at: https://doi.org/10.1080/2162402X.2017.1316437.

Shojaei, F. *et al.* (2007) “Bv8 regulates myeloid-cell-dependent tumour angiogenesis,” *Nature*, 450(7171), pp. 825–831. Available at: https://doi.org/10.1038/nature06348.

Silvestre-Roig, C., Hidalgo, A. and Soehnlein, O. (2016) “Neutrophil heterogeneity: implications for homeostasis and pathogenesis,” *Blood*, 127(18), pp. 2173–2181. Available at: https://doi.org/10.1182/blood-2016-01-688887.

Structure of a Ribonucleic Acid (1965). Available at: https://doi.org/10.1126/science.147.3664.1462.

Suzuki, T. (2021) “The expanding world of tRNA modifications and their disease relevance,” *Nature Reviews Molecular Cell Biology*, 22(6), pp. 375–392. Available at: https://doi.org/10.1038/s41580-021-00342-0.

TeSlaa, T. *et al.* (2023) “The pentose phosphate pathway in health and disease,” *Nature Metabolism*, 5(8), pp. 1275–1289. Available at: https://doi.org/10.1038/s42255-023-00863-2.

Timaxian, C. *et al.* (2021) “Pivotal Role for Cxcr2 in Regulating Tumor-Associated Neutrophil in Breast Cancer,” *Cancers*, 13(11), p. 2584. Available at: https://doi.org/10.3390/cancers13112584.

Topisirovic, I. *et al.* (2011) “Cap and cap-binding proteins in the control of gene expression,” *WIREs RNA*, 2(2), pp. 277–298. Available at: https://doi.org/10.1002/wrna.52.

Translation: DNA to mRNA to Protein | Learn Science at Scitable (no date). Available at: https://www.nature.com/scitable/topicpage/translation-dna-to-mrna-to-protein-393/ (Accessed: January 29, 2026).

Veenith, T. *et al.* (2022) “High generation of reactive oxygen species from neutrophils in patients with severe COVID-19,” *Scientific Reports*, 12(1), p. 10484. Available at: https://doi.org/10.1038/s41598-022-13825-7.

Vono, M. *et al.* (2017) “Neutrophils acquire the capacity for antigen presentation to memory CD4+ T cells in vitro and ex vivo,” *Blood*, 129(14), pp. 1991–2001. Available at: https://doi.org/10.1182/blood-2016-10-744441.

Wagner, J. *et al.* (2019) “A Single-Cell Atlas of the Tumor and Immune Ecosystem of Human Breast Cancer,” *Cell*, 177(5), pp. 1330-1345.e18. Available at: https://doi.org/10.1016/j.cell.2019.03.005.

Wculek, S.K. and Malanchi, I. (2015) “Neutrophils support lung colonization of metastasis-initiating breast cancer cells,” *Nature*, 528(7582), pp. 413–417. Available at: https://doi.org/10.1038/nature16140.

Weill, L. *et al.* (2012) “Translational control by changes in poly(A) tail length: recycling mRNAs,” *Nature Structural & Molecular Biology*, 19(6), pp. 577–585. Available at: https://doi.org/10.1038/nsmb.2311.

Wek, R.C. (2018) “Role of eIF2α Kinases in Translational Control and Adaptation to Cellular Stress,” *Cold Spring Harbor Perspectives in Biology*, 10(7), p. a032870. Available at: https://doi.org/10.1101/cshperspect.a032870.

Williams, M. *et al.* (2011) “Emerging mechanisms of neutrophil recruitment across endothelium,” *Trends in immunology*, 32(10), pp. 461–469. Available at: https://doi.org/10.1016/j.it.2011.06.009.

Woodcock, H.V. *et al.* (2019) “The mTORC1/4E-BP1 axis represents a critical signaling node during fibrogenesis,” *Nature Communications*, 10(1), p. 6. Available at: https://doi.org/10.1038/s41467-018-07858-8.

Wu, Y. *et al.* (2024) “Neutrophil profiling illuminates anti-tumor antigen-presenting potency,” *Cell*, 187(6), pp. 1422-1439.e24. Available at: https://doi.org/10.1016/j.cell.2024.02.005.

Yu, G. *et al.* (2025) “Mitochondrial SLC25A10 promotes prostate cancer progression by inhibiting ferritinophagy,” *Cell Death Discovery*, 11(1), p. 242. Available at: https://doi.org/10.1038/s41420-025-02528-3.

Zhang, F. *et al.* (2024) “Neutrophil diversity and function in health and disease,” *Signal Transduction and Targeted Therapy*, 9(1), p. 343. Available at: https://doi.org/10.1038/s41392-024-02049-y.

Zhao, Y. *et al.* (2023) “Neutrophils resist ferroptosis and promote breast cancer metastasis through aconitate decarboxylase 1,” *Cell Metabolism*, 35(10), pp. 1688-1703.e10. Available at: https://doi.org/10.1016/j.cmet.2023.09.004.